RELATIVISTIC EFFECTS IN EXTRAGALACTIC RADIO SOURCES

Thesis by

Arieh Königl

In Partial Fulfillment of the Requirements
for the Degree of
Doctor of Philosophy

California Institute of Technology
Pasadena, California

1980

(Submitted May 20, 1980)

ACKNOWLEDGMENTS

My thanks are due, first and foremost, to my advisor Roger Blandford. Roger has been for me both an inspiring teacher and a true friend. I learned from him a great deal of physics and much about the nature of good research. From my early days as his student, he treated me as an "equal", and did not hesitate to "bombard" me with an almost continuous stream of original and sometimes provocative ideas. I learned that it is permissible and even desirable to let my imagination run wild, but that a lot of scrutiny and hard labor is required to accompany the delivery of an incipient idea. I was encouraged to ask questions, which Roger would invariably answer with patience and good humor, but I was also encouraged to pursue my independent research and carve my own paths. Of particular educational value to me were our collaborative projects. These were sometimes carried out in Roger's house, where I enjoyed the hospitality of his family. I also should not fail to mention the continuous encouragement and moral support that I received from him. All in all, being a student under Roger's tutelage has been a very gratifying and enjoyable experience.

I also owe many thanks to Kip Thorne for his kind attitude towards me and for much help and good advice, and to Marshall Cohen, who took an early interest in my work and offered me help and encouragement.

It was in Kip's friendly and stimulating Theoretical Astrophysics group that I found a haven during my graduate years. I thank all my friends and colleagues in the group, particularly

Carl Caves, Bill DeCampli, Rich Flammang and David Payne, as well as our computer "whiz" Yekta Gürsel and our able "administrators" JoAnn Boyd and Ruthie Parchen. Special thanks are also due to Jan Rasmussen and the other members of the Kellogg staff who typed my papers for their careful and dedicated work, and to Pamela DePriest from the Graduate Office for her kind cooperation.

During my stay at Caltech I was supported at various times by an Earl C. Anthony fellowship, Physics Department teaching assistantships, and graduate research assistantships provided by the National Science Foundation (through Kip's and Roger's grants). I acknowledge all these sources of financial help.

Last but not least, I thank my friends in the "outside world", particularly Kerry John, Kathleen Kavanagh and Jim Roberts, for sharing with me some of my difficult moments, as well as the happy ones.

ABSTRACT

This thesis deals with the interpretation of compact extragalactic radio sources in the context of the twin-beam model with a particular emphasis on the role of special-relativistic kinematical and dynamical effects. Various such effects are investigated, both in a general manner and in application to specific observed phenomena. Among the observed phenomena which are interpreted in this way are:

i) Apparent superluminal flux variations, i.e., variations which occur on timescales short compared with the light travel time across the apparent source. It is shown that this and other spectral effects could be attributed to relativistic expansion of the source, and that objections raised against the relativistic interpretation (Terrell 1977) are model-dependent and do not apply in general.

ii) Apparent superluminal separation of source components. It is shown that in a relativistic jet model where the radio emission originates both from the quasi-steady jet itself and from behind shock waves which travel with relativistic speeds in the jet, the source could display apparent superluminal expansion in which the moving component (associated with a shock) and the stationary component (associated with the optically-thick core of the jet) would have comparable, Doppler-boosted fluxes. The shocks could either propagate in the jet or arise behind dense clouds which are accelerated by the supersonic flow. The origin as well as the kinematical and radiative properties of the clouds are discussed, and it is proposed that the bright knots observed in

certain jets, such as the jet in M87, could in fact correspond to dense accelerated clouds.

iii) Rapid swings in the observed polarization position angle. It is shown that synchrotron sources which accelerate to (or decelerate from) relativistic speeds could display rapid swings in the observed polarization position angle of up to 180° as a result of the relativistic aberration effect. This mechanism is suggested for the large swing observed in the BL Lac object AO 0235+164 (Ledden and Aller 1978).

It is argued that the majority of bright compact sources are observed along lines of sight making small ($\lesssim 10^{\circ}$) angles to the jet velocity. On the basis of this hypothesis, a unified interpretation of compact, variable radio sources and of extended double radio sources is presented. More generally, it is suggested that active galactic nuclei may have two types of emission: an isotropic, fairly steady, unpolarized optical continuum, and a beamed, variable, strongly polarized synchrotron component associated with a relativistic jet. The sequence: radio-quiet quasars, radio-loud quasars, and blazars (i.e., optically-violent variable quasars and BL Lac objects) would then correspond to similar sources which are viewed at progressively decreasing angles to their jet axes. Model synchrotron and inverse-Compton spectra for resolved jets and for unresolved inhomogeneous jets are calculated, taking into account the effect of synchrotron - radiation losses, and applied to the interpretation of the spectra of BL Lac objects. The possible contribution of beamed sources to the diffuse x-ray and γ-ray background is also

discussed.

In addition, the steady two-dimensional flow of an ideal compressible fluid is studied in the context of special-relativistic gas dynamics. The Newtonian equations for potential flow are generalized, and it is found that they can have the same form in the Newtonian and the relativistic regimes if their parameters are defined in the local rest-frame of the fluid. The Mach number thus defined is shown to have the same properties as its Newtonian analog. The Newtonian equations for oblique plane shock waves are similarly generalized in certain cases (which include, in particular, the extreme-relativistic limit). Several applications of these results, particularly to the study of relativistic jets, are suggested.

TABLE OF CONTENTS

PAPER 3

PAPER 4

PAPER 5

INTRODUCTION

Radio observations of extragalactic sources have advanced dramatically in recent years following the construction of powerful radio telescopes and the improvement in interferometric observation techniques. Large arrays of radio telescopes are now being employed simultaneously, often over very long intercontinental baselines, to produce high-resolution maps of even the more distant sources. One of the most striking discoveries to have come out of these observations is that of radio jets - elongated, narrow components which emanate from a central compact core, often in two opposite directions, and extend toward the distant outer radio lobes. The jets can be extremely thin and straight, and in some sources are detected on length scales ranging from a few parsecs to over a megaparsec (see, e.g., the attached radio maps of NGC6251, reproduced from Waggett, Warner, and Baldwin 1977, and from Readhead, Cohen, and Blandford 1978). The discovery of jets was regarded as evidence in favor of the "twin-beam" model - proposed by Blandford and Rees (1974), following earlier work by Rees (1971), Scheuer (1974), and others - according to which the extended radio lobes are supplied continuously with energy, mass and momentum from a central "power-house" by means of two well-collimated beams of plasma. (However, some alternative models, reviewed, e.g., by De Young (1976), may not yet be completely ruled out.) The initial motivation for the twin-beam model was provided by the morphology of the outer radio lobes, which often are situated symmetrically about a central compact component and show collinear structure, and by

the large energy content ($\sim 10^{56}$-10^{61} ergs) inferred for the extended radio-emitting regions, which in conjunction with the observed luminosities ($\sim 10^{40}$-10^{46} ergs s^{-1}) indicates a continuous supply of energy over an extended ($\sim 10^{8}$ years) period of time. Additional motivation for the model came from spectral measurements of the bright emission regions ("hot spots") found in the outermost parts of the most luminous double sources. These measurements reveal power-law radio spectra which show no break below 100 GHz. In general, the power-law spectra and the occasionally high degree of linear polarization measured in the radio lobes are interpreted as evidence for optically-thin incoherent synchrotron emission produced by a power-law distribution of relativistic electrons radiating in a $\sim 10^{-3}$-10^{-6} Gauss magnetic field. The fact that the spectrum of the "hot spots" does not cut off below 100 GHz then implies that the radiative lifetime of the source is relatively short, in some cases even shorter than the light travel time from the central component. This indicates that the radiating relativistic electrons must be continuously reaccelerated. In the twin-beam model the jets are produced as a relativistic fluid of plasma and magnetic field near a massive accreting object (e.g., a black hole of mass $\gtrsim 10^{8}$ $M_{\odot}$) residing in the center of a quasar or an active galactic nucleus, and imbedded in a cloud of relatively cool and dense gas. The light relativistic fluid is thought to emerge in two opposite directions along the rotation axis of the central object and to be collimated by the confining cloud, forming de Laval nozzles in which the flow becomes supersonic. The

details of the formation process are as yet unknown and remain a challenging research problem; however, there is evidence that in several sources the radio axis is correlated with the rotation axis of the associated galaxy and that at least some jets are highly supersonic, tending to support the general picture. The collimation of the beams is assumed to be achieved within a few parsecs from the central "power-house", and they then move into the surrounding medium, creating cavities which may become visible as radio jets if some of the bulk kinetic energy is dissipated and converted into synchrotron radiation. In this picture, the "hot spots" are identified with shock waves formed when the beams impinge on the external medium, and in which particle acceleration and magnetic field amplification can take place. "Head-tail" sources also find a natural explanation in this model (e.g., Begelman, Blandford, and Rees 1979). These sources are characterized by a bright radio "head", coincident with a visible galaxy, which is trailed by two fainter "tails" extending over hundreds of kiloparsecs (see, e.g., the attached radio map of NGC1265, reproduced from Owen, Burns, and Rudnick 1978), and tend to occur in clusters. They may be interpreted as jets which are swept back as a result of the motion of the galaxy through the relatively dense intracluster medium. Recent measurements of the polarization position angle in jets indicate that the magnetic field vector is generally aligned along the jet axis close to the galactic nucleus, but becomes perpendicular to the axis at larger distances (see, e.g., the attached radio map of NGC315, reproduced from Fomalont et al. 1980, in which

the line segments represent linear polarization vectors which are thought to be roughly perpendicular to the magnetic field vectors). These measurements, too, are consistent with the predictions of the beam model for highly supersonic jets which move ballistically and in which the flux of the convected magnetic field is conserved.

The jets in the twin-beam model are assumed to be discharged with relativistic speeds. The arguments given for relativistic bulk motions in compact extragalactic sources were initially indirect. Estimates based on synchrotron-radiation theory (e.g., Burbidge, Jones, and O'Dell 1974) indicate that in many sources the energy density of relativistic electrons exceeds the magnetic energy density, implying that relativistic expansion is to be expected unless the density of thermal plasma in the source is sufficiently high. The density of thermal plasma is generally estimated from measurements of the polarization position angle at different frequencies, which are interpreted in terms of the Faraday effect. From the small values of Faraday rotation indicated in most sources it is inferred that the ratio of thermal plasma to relativistic plasma is in fact much smaller than unity (e.g., Jones and O'Dell 1977). Relativistic expansion speeds were suggested also as a means of alleviating the so-called "inverse-Compton catastrophe". As was first pointed out by Hoyle, Burbidge and Sargent (1966), if the short timescales for flux variability measured in many sources are interpreted in the context of synchrotron-radiation theory, then the inferred radiation energy density is larger than the magnetic energy

density, implying very high energy requirements in the source. However, as Rees (1967) has shown, the actual size of the source may be much larger than the size inferred from the observed variability timescale if relativistic expansion is present, in which case the problem is less acute. The inferred "catastrophe" is particularly severe in sources which display high variability at low frequencies, and it is now believed that relativistic motion is the most likely mechanism for explaining it away (e.g., Condon et al. 1979). The model proposed by Rees (1967) could also account for apparent superluminal flux variations, i.e., variations which occur on timescales short compared to the light travel time across the apparent source. The discovery that strong compact radio sources often show apparent superluminal separation velocities of source components (e.g., Cohen et al. 1979) has subsequently provided a more direct evidence for relativistic bulk motions. In fact, most of the plausible interpretations of this phenomenon require relativistic velocities in the source (e.g., Blandford, McKee, and Rees 1977). High-resolution very-long-baseline interferometric observations reveal that these sources have a core-jet morphology - a one-sided jet projecting from a compact nucleus (see, e.g., the attached radio maps of NGC6251 and NGC315)-which may also be interpreted as pointing out to relativistic motion of the emitting material (e.g., Readhead et al. 1978). According to this interpretation, the twin-beam model still applies, but the emission from the counter-jet is beamed away from the observer because of the relativistic Doppler effect. Despite the accumulating evidence

for relativistic motion close to the nucleus, there are however indications in a few jets that at sufficiently large distances the velocity is nonrelativistic. This is inferred from an analysis of the dynamical interaction of the jets with the surrounding medium (e.g., Begelman, Rees, and Blandford 1979) or with nearby galaxies (e.g., Blandford and Icke 1978). If closer to the nucleus these jets were relativistic, then the implied deceleration would be accompanied by a dissipation of large amounts of kinetic energy, for which there appears to be no evidence. The question of the actual velocities of jets is thus still not entirely settled.

The discovery of jets and of apparent superluminal effects in compact extragalactic radio sources has opened up new areas of research in high-energy astrophysics. These include the application of relativistic kinematics and dynamics to the interpretation of the various apparent superluminal phenomena, the application of relativistic hydrodynamics and magnetohydrodynamics to the study of observed jet morphologies, and the investigation of emission and particle-acceleration mechanisms in luminous extragalactic sources. These areas of research are all the more exciting as they bear directly on some of the most puzzling questions of modern astronomy, having to do with the nature of quasars and of the energy source in active galactic nuclei. The work described in this thesis involves some of these areas of research, and is directly concerned with the interpretation of compact extragalactic radio sources and with the study of the physical processes which may be taking place in them. It is

organized in the form of five separate papers, each of which is self-contained, but all of which are related by the common underlying theme. As an aid to the reader, I now give a brief description of each paper, together with a summary of the main results.

The first paper, entitled "Flux Variations in Relativistically Expanding Spherical Radio Sources", was published in The Astrophysical Journal (Vol. 225, p. 732, 1978). It was motivated by an objection raised against the relativistic-expansion interpretation of apparent superluminal flux variations. According to this objection, such expansion would not lead to observed pulses which are short compared with the light travel time across the apparent source. In the paper it is shown that the arguments against the relativistic interpretation are model-dependent and do not apply in general. A specific example is discussed in detail and used to show that some additional observed effects, which were previously interpreted in a nonrelativistic context, could also be attributed to relativistic expansion of the source. The main purpose of this paper, however, is to clarify in principle the effect of relativistic expansion on apparent flux variability.

The second paper (in collaboration with R. Blandford; published in Astrophysical Letters, Vol. 20, p. 15, 1979) presents a model for the bright emission knots in the jet of the galaxy M87. Similar knots have been detected also in other jets, and Rees (1978) suggested that they could be attributed to the steepening of nonlinear sound waves propagating in the jet. In

this paper it is proposed that the knots correspond to dense clouds which are accelerated by a supersonic jet, and that the emission arises in strong bow shocks which form behind the accelerated clouds.

The interpretation of compact radio sources in the context of the relativistic-jet model is discussed in the third paper, also written in collaboration with R. Blandford, which was published in The Astrophysical Journal (Vol. 232, p. 34, 1979). In this paper it is proposed that the emission in the jet has both a steady component, associated with the stationary flow pattern, and a variable component, associated with shock waves which travel in the jet. It is shown that in a relativistic jet the moving shock and the stationary optically-thick core of the jet could appear to separate with a superluminal velocity. In this case both of the separating components would have comparable, Doppler-boosted fluxes, so that a common difficulty encountered in previous "relativistic" interpretations, namely, that one component would be much brighter than the other, is no longer present. Specific models for the dynamical and radiative properties of the jet and of individual shocks are presented. The shocks could be associated with propagating nonlinear waves or with accelerated dense clouds of the type proposed for the knots in the M87 jet. This paper also considers various additional consequences of relativistic motion; in particular, it is pointed out that a synchrotron source accelerating to (or decelerating from) relativistic speeds could display a large and rapid swing in the observed polarization position angle of the kind already

detected in some compact sources. In addition, it is postulated that quasars in general may have a beamed emission component, associated with relativistic jets, as well as an isotropic component responsible for photoionizing the emission-line gas. In this picture, bright compact sources are the ones which are observed along lines of sight which make small angles to the jet velocity. This hypothesis leads to a unified interpretation of core-halo and of extended double radio sources, and provides an explanation of the relationship between radio-quiet quasars, radio-loud quasars, optically-violent variable quasars and BL Lac objects. (Some of these ideas have been suggested independently by Scheuer and Readhead (1979).)

The application of this model to the interpretation of x-ray and γ-ray observations of quasars and BL Lac objects is discussed in the fourth paper, which will shortly be submitted for publication in The Astrophysical Journal. In this paper, model synchrotron and inverse-Compton spectra are calculated for both a resolved jet and for an unresolved inhomogeneous jet, taking into account the effect of synchrotron-radiation losses. On the basis of this model it is concluded that various observed features in the spectra of BL Lac objects, which according to the beaming hypothesis are sources observed at very small angles to the jet axis, could in fact be attributed to emission from unresolved relativistic jets. The class properties of beamed x-ray sources and the contribution of relativistic jets to the diffuse x-ray and γ-ray background are also considered in this paper.

The work described so far dealt mainly with the kinematical

and radiative properties of beamed sources. The fifth paper, entitled "Relativistic Gas Dynamics in Two Dimensions" (scheduled for publication in the May 1980 issue of The Physics of Fluids), turns to some dynamical aspects of relativistic flow. This is essentially a general theoretical paper, which demonstrates that the Newtonian theory of steady two-dimensional flow of an ideal compressible fluid has in many cases a simple relativistic generalization. In particular, it is shown that the generalized expressions can often be written in the Newtonian form, and that it is then possible to study specific flow problems using the methods of Newtonian gas dynamics. As is pointed out in the paper, this theory could find applications in nuclear physics and cosmology, as well as in high-energy astrophysics. A specific example of oblique-shock refraction at the interface between a relativistic and a nonrelativistic medium, which may be relevant in the context of radio jets, is considered. Another application in this context is to the calculation of the flow pattern in a supersonic relativistic jet which moves from one region into another region of lower ambient pressure. The calculation can be effected using the method of characteristics discussed in the paper. The resulting flow pattern involves alternating compression and rarefaction waves, and could provide an alternative interpretation of the bright emission knots observed in radio jets, as well as of the "gaps" in emission which are found in some sources in the vicinity of the nucleus (see, e.g., the attached radio map of 3C449, reproduced from Perley, Willis, and Scott 1979).

Our understanding of extragalactic radio sources is still incomplete. Although the twin-beam model appears to be successful in interpreting the general features of these sources, the nature of the jets and their dynamical interaction with the surrounding medium are as yet not fully understood. For example, it is not yet clear whether the flow is stable, what are the values of its characteristic parameters, such as the Mach number and the Reynolds number, or what is the dynamical role played by the convected magnetic field. The details of the formation and collimation of the jets are also still unknown. Likewise, there does not yet exist a comprehensive model which would incorporate the various apparent superluminal effects into a single, unified picture. The nature of the particle-acceleration mechanisms is another general problem which remains to be solved. However, steadily improving observations in different regions of the spectrum continue to provide valuable clues to the resolution of these questions, and are already supplying important constraints which any viable model would have to satisfy. Further insight into the hydrodynamics of jets could be gained from extensive numerical calculations and from laboratory experiments involving high Mach-number flows in wind tunnels, both of which are already under way. The prospects for continued progress in our understanding of these fascinating objects thus appear to be quite bright.

REFERENCES

Begelman, M.C., Rees, M.J., and Blandford, R.D. 1979, Nature, 279, 770.

Blandford, R.D., and Icke, V. 1978, M.N.R.A.S., 185, 527.

Blandford, R.D., McKee, C.F., and Rees, M.J. 1977, Nature, 267, 211.

Blandford, R.D., and Rees, M.J. 1974, M.N.R.A.S., 169, 395.

Burbidge, G.R., Jones, T.W., and O'Dell, S.L. 1974, Ap.J., 193, 43.

Cohen, M.H., Pearson, T.J., Readhead, A.C.S. Seielstad, G.A., Simon, R.S., and Walker, R.C. 1979, Ap.J., 231, 293.

Condon, J.J., Ledden, J.E., O'Dell, S.L., and Dennison, B. 1979, A.J., 84, 1.

De Young, D.S. 1976, Ann. Rev. Astr. Ap., 15, 175.

Fomalont, E.B., Bridle, A.H., Willis, A.G., and Perley, R.A. 1980, Ap.J. (in press).

Hoyle, F., Burbidge, G.R., and Sargent, W.L.W. 1966, Nature, 209, 751.

Jones, T.W., and O'Dell, S.L. 1977, Astr. Ap., 61, 291.

Owen, F.N., Burns, J.O., and Rudnick, L. 1978, Ap.J. (Letters), 226, L119.

Perley, R.A., Willis, A.G., and Scott, J.S. 1979, Nature, 281, 437.

Readhead, A.C.S., Cohen, M.H., and Blandford, R.D. 1978, Nature, 272, 131.

Readhead, A.C.S., Cohen, M.H., Pearson, T.J., and Wilkinson, P.N. 1978, Nature, 276, 768.

Rees, M.J. 1967, M.N.R.A.S., 135, 345.

_____. 1971, Nature, 229, 312.

_____. 1978, M.N.R.A.S., 184, 61.

Scheuer, P.A.G. 1974, M.N.R.A.S., 166, 513.

Scheuer, P.A.G., and Readhead, A.C.S. 1979, Nature, 277, 182.

Waggett, P.C., Warner, P.J., and Baldwin, J.E. 1977, M.N.R.A.S., 181, 465.

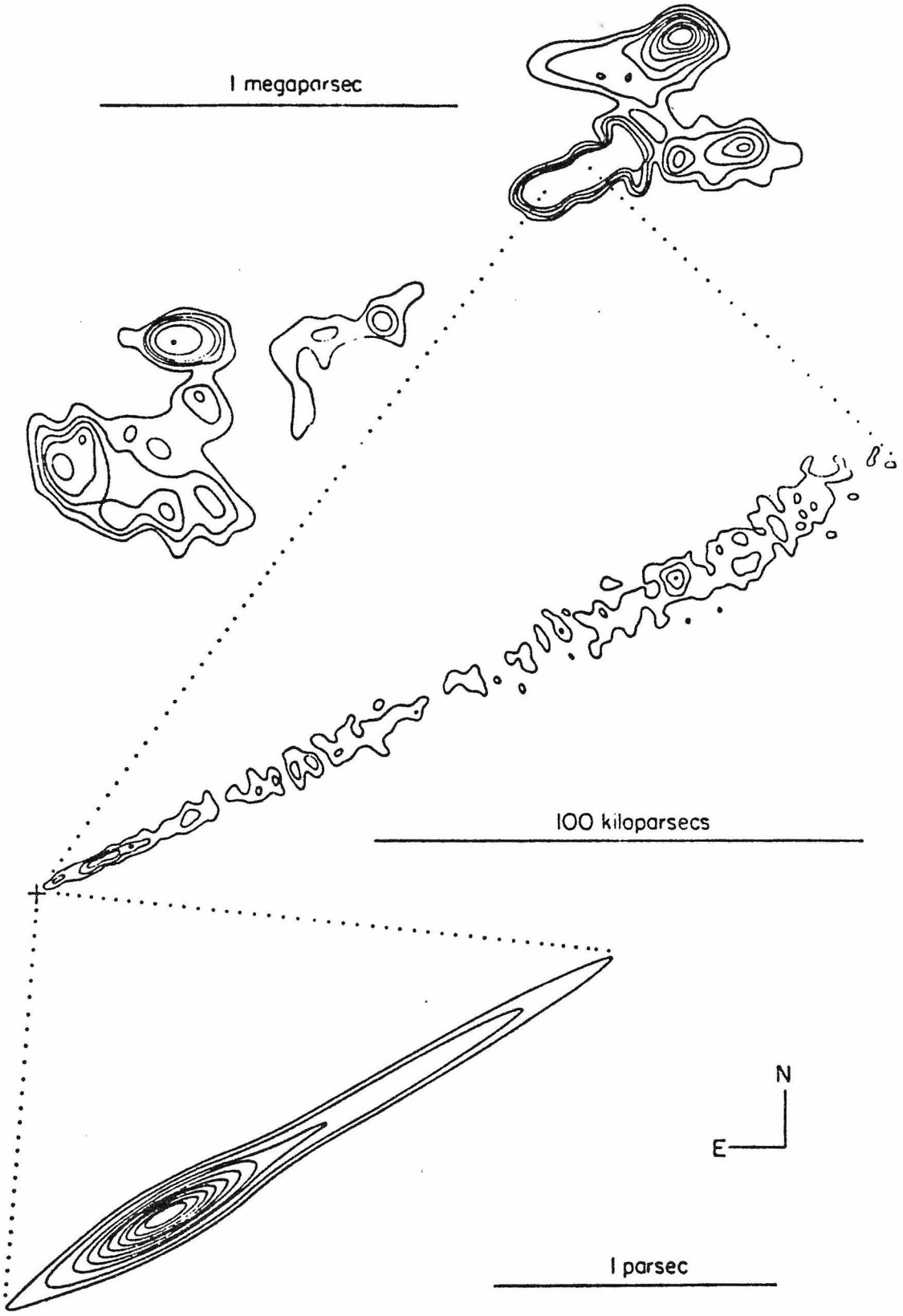

NGC 6251

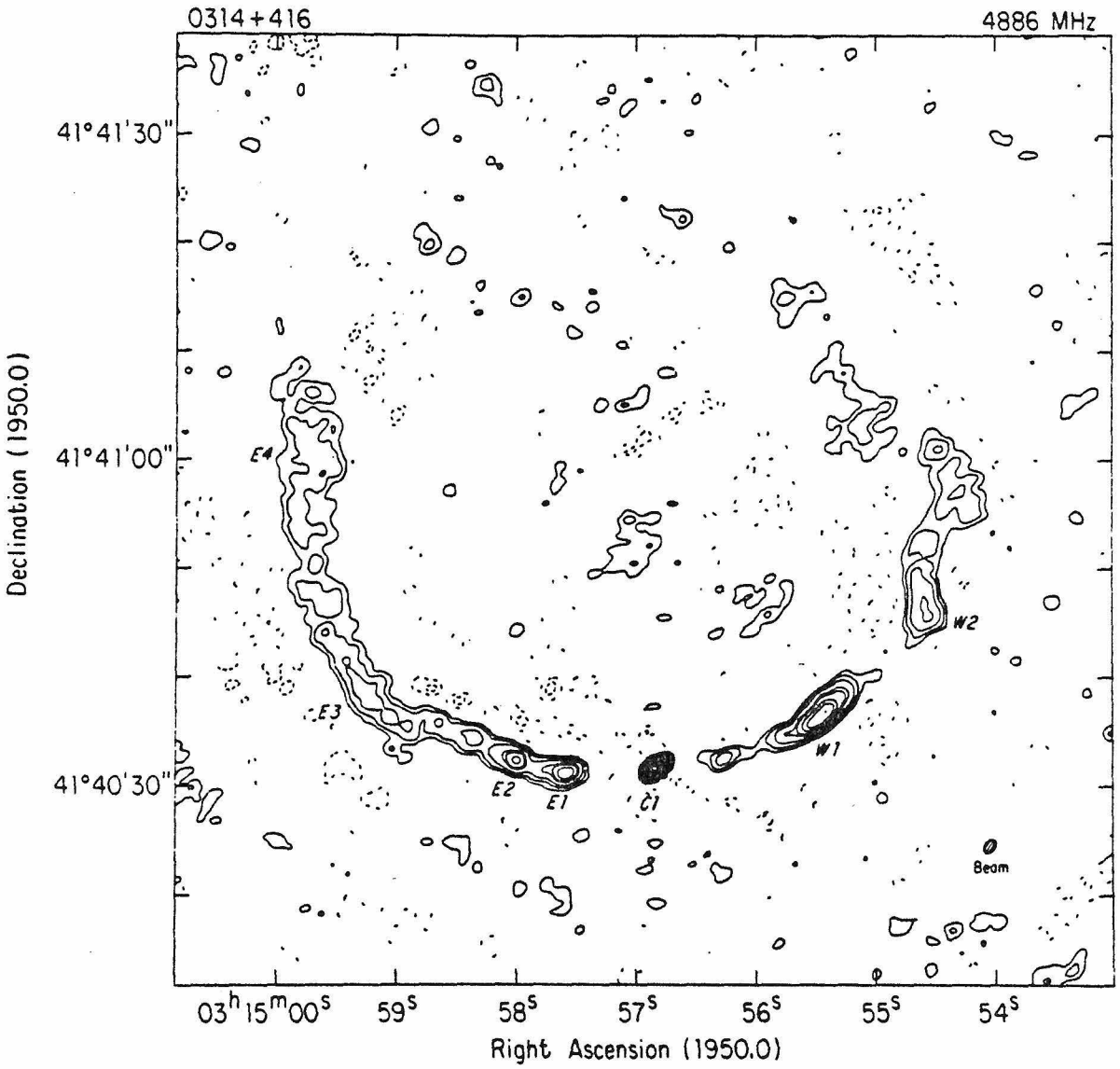
0314+416
4886 MHz
41°41'30"
41°41'00"
41°40'30"
Declination (1950.0)
E4
E3
E2
E1
C1
W1
W2
Beam
03h15m00s
59s
58s
57s
56s
55s
54s
Right Ascension (1950.0)

NGC 1265

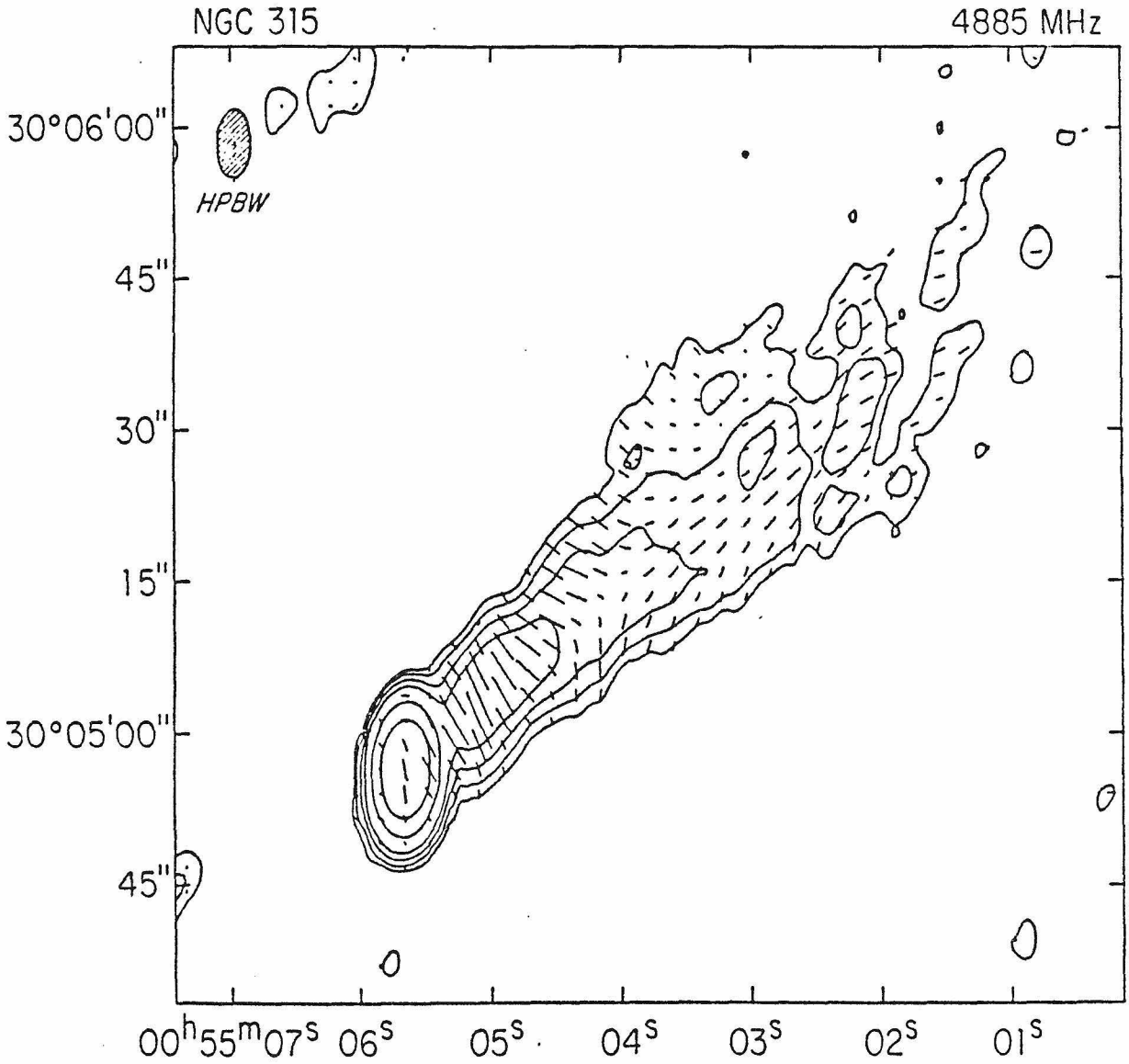
NGC 315
4885 MHz
30°06'00"
HPBW
45"
30"
15"
30°05'00"
45"
00h55m07s
06s
05s
04s
03s
02s
01s

NGC 315

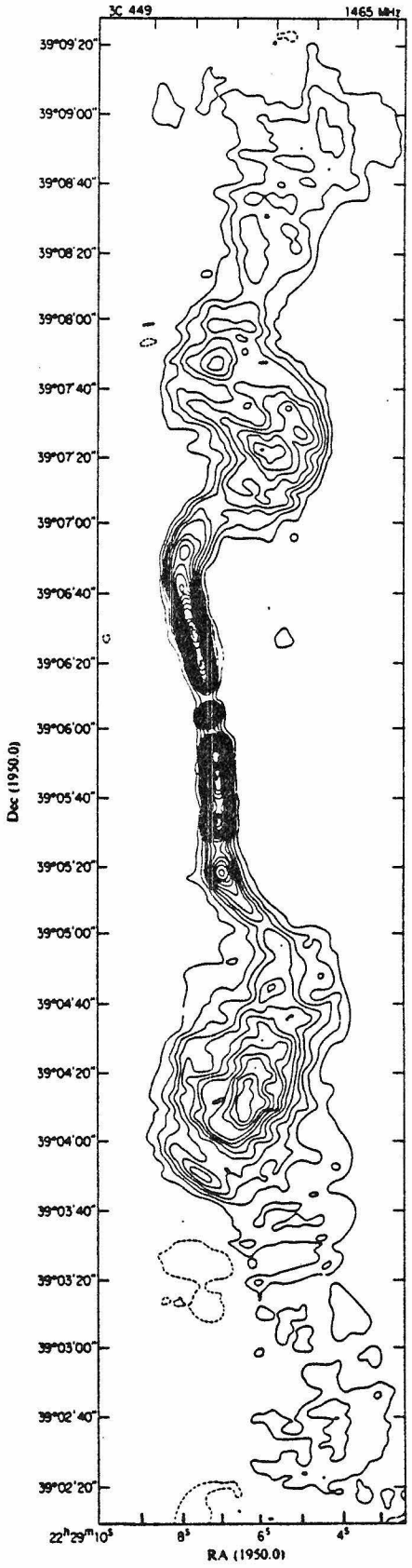
3C 449
1465 MHz
39°09'20"
39°09'00"
39°08'40"
39°08'20"
39°08'00"
39°07'40"
39°07'20"
39°07'00"
39°06'40"
39°06'20"
39°06'00"
39°05'40"
39°05'20"
39°05'00"
39°04'40"
39°04'20"
39°04'00"
39°03'40"
39°03'20"
39°03'00"
39°02'40"
39°02'20"
Dec (1950.0)
22h29m10s
8s
6s
4s
RA (1950.0)

3C449

PAPER 1

FLUX VARIATIONS IN RELATIVISTICALLY EXPANDING SPHERICAL RADIO SOURCES

I. INTRODUCTION

Relativistic expansion speeds have been proposed (Rees 1967) to account for superluminal flux variations in extragalactic radio sources, i.e., variations fast compared to the light travel across the apparent source. Subsequent VLBI observations of such sources could often be interpreted as two components separating with superluminal speeds (e.g., Cohen et al. 1977); this phenomenon probably also indicates very high expansion velocities (cf. Blandford, McKee, and Rees 1977), although it is not directly related to superluminal flux variations.

Incoherent synchrotron emission is considered the most plausible mechanism of radiation in these sources (Jones, O'Dell, and Stein 1974; henceforth JOS). In Rees' model the apparent effects are associated with emission from a relativistically expanding source which is initially opaque, but which becomes optically thin as it expands. It was argued that to a distant observer the flux would appear to change very rapidly, and that the actual source dimensions could far exceed the limit ct_v set by the variability timescale t_v. Further calculations (Jones and Tobin 1977, Vitello and Pacini 1977) have shown that models of adiabatically expanding spherical sources in which the entire volume is luminous would be inefficient in producing superluminal effects due to the fact that they are dominated by the optically thin emission from near the source center, where the expansion speeds are relatively low. This result led to the prediction (Jones and Tobin 1977) that shells should be the most effective structure in producing such effects, since they feature emission from larger radii.

However, it has now been claimed (Terrell 1977; henceforth Terrell) that even shell sources which expand relativistically, and in which the

optically thin emission is neglected, would not produce superluminal flux variations. This conclusion was based on a study of a steadily expanding luminous spherical surface which was assumed to become optically thin (and thereupon fade away) when it reached a certain distance from the center. It was shown that the length of a pulse received from this source would still be determined essentially by the actual size of the surface, despite the relativistic expansion.

The present paper considers the conditions under which a relativistically expanding shell could produce superluminal flux variations. It is shown that whether or not such variations are produced depends on the specific model under consideration and on the values of the relevant parameters, but that superluminal flux variations cannot be ruled out in general. As a specific example we consider a relativistically expanding thin spherical shell emitting synchrotron radiation. [Similar configurations arise in models based on relativistic blast waves (cf. Blandford and McKee 1977), in which the thickness of the shell is a fraction $1/\gamma^2$ of the radius, γ being the expansion Lorentz factor.] In this case one can define, for each frequency, an effective cutoff time (measured in the rest frame of the source) after which the shell is transparent to radiation at that frequency. In Terrell's model the cutoff time was assumed to be the same for all frequencies, but in general it may vary with the frequency.

The geometry of a steadily expanding shell is described in §II where, following Terrell, it is assumed that only the optically thick parts are observed. Expressions are obtained for the apparent time evolution of the source, generalizing those in Terrell by means of a suitably defined power-law exponent (f), which is associated with the assumed variation of the cutoff time with frequency. The flux variations produced by the shell are then

analyzed in §III, using the assumptions of the standard model. In particular, the exponent f is expressed as a function of one parameter of this model and it is demonstrated that, depending on the value of f, the flux variations could be either superluminal or subluminal. The effect of the optically thin flux is also considered. In §IV some effects associated with a change in the frequency of observation are discussed. It is suggested that certain apparent discrepancies between the standard model and observations may be reconciled if the source expands relativistically, which could be the case even when the observed flux variations are not superluminal. A summary of our results is given in the Conclusion.

II. KINEMATICS OF A RELATIVISTICALLY EXPANDING SPHERICAL SURFACE

Let an explosion occur at the origin O at time t = 0 as measured by an observer at P, a large distance R away and at rest relative to O. An observer at O subsequently sees an expanding spherical surface (an idealization of a very thin shell) moving with a constant speed v = βc. As seen at P, the equation of the surface at time t is given (Rees 1967) by

$$r(\theta) = \frac{\beta ct}{1 - \beta \cos \theta}, \tag{1}$$

where θ is the angle between the radius vector and the line OP. It can also be given in terms of the Doppler shift

$$D(\theta) = \frac{1}{\gamma(1 - \beta \cos \theta)}, \tag{2}$$

where $\gamma = (1 - \beta^2)^{-\frac{1}{2}}$, by $r = \gamma D \beta ct$.

The apparent shape would thus be an ellipsoid with focus at O, semi-major axis along the line OP, and eccentricity β (see Fig. 1). However, if at the frequency of observation (ν) the source is initially opaque, a

distant observer would see only the forward half (between $\theta = 0$ and $\theta_{max} = \cos^{-1}\beta$). Suppose now that, as seen in a frame comoving with the source (a frame labeled hereafter with a prime), the whole surface becomes optically thin to radiation at a certain proper frequency $\nu' = \nu'_c$ at a given proper time $t' = t'_c$ (the corresponding cutoff time), after which the emission at that frequency may be neglected. Because of the relativistic Doppler effect, the observer at P would see the source turn optically thin only gradually, starting at the time $t = T_1(\nu)$. The locus of the points where the surface becomes transparent at times $t \geq T_1$ is given by the angle $\theta_c(t)$ or, equivalently, by the corresponding Doppler shift $D_c(t)$. The variation of D_c with t and with ν can be determined from the function $t'_c(\nu'_c)$, or from the inverse function $\nu'_c(t'_c)$ (which gives the time dependence of the frequency of spectral turnover in a given model), by using

$$t'_c = D_c t \quad , \quad \nu'_c = \nu/D_c \ . \tag{3}$$

If t'_c varies as some power of ν'_c, as is the case in a variety of models (including the standard model which we consider in this paper), then D_c has a similar dependence on t and on ν, and we can define the exponent f by

$$D_c(t) = D_1(t/T_1)^{-f} \ . \tag{4}$$

Specifically, if $t'_c \propto \nu'^{-g}_c$, then $f = (1-g)^{-1}$ and $T_1(\nu) \propto \nu^{-g}$.

We shall henceforth assume that D_c is a decreasing function of time ($f > 0$); in this case $D_1 = \gamma(1+\beta)$, and the forward vertex of the ellipsoid becomes optically thin first. Provided that the extremities of the optically thick regions determine the shape of the source as seen at P, the apparent (transverse) radius $r_a(t)$ would be

$$r_a(t) = \gamma\beta ct \qquad \text{for } 0 \le t \le T_2 \tag{5a}$$

$$r_a(t) = r(\theta_c)\sin\theta_c = \left\{1 - 1/\beta^2\left[1 - (1-\beta)(t/T_1)^f\right]^2\right\}^{\frac{1}{2}}(t/T_1)^{1-f}\,\beta cT_1/(1-\beta) \tag{5b}$$
$$\text{for } T_2 \le t \le T_4 .$$

After the time $T_2 = (1+\beta)^{1/f}T_1$, when $D_c = \gamma$, $\theta_c = \theta_{max}$, only the back of the surface would be visible to the distant observer; however, because of the continuing expansion, the maximum apparent radius would be reached only later, at $t = T_3$. The source would eventually disappear from sight at the time $T_4 = [(1+\beta)/(1-\beta)]^{1/f}T_1$, when $D_c = \gamma(1-\beta)$, $\theta_c = \pi$. The definitions of $r_a(t)$ and of $T_1, \ldots, T_4$ given here generalize those in Terrell, which correspond to the case $f = 1$. In that case the emission is turned off simultaneously at all frequencies in the comoving frame, but the distant observer sees the radiation at higher proper frequencies disappear from sight earlier due to the Doppler effect; the reason why the surface appears to that observer to fade away faster when $f > 1$ is that the emission at higher proper frequencies is then also turned off earlier at the source.

In analyzing the flux variations produced by the expanding surface we shall assume that it is a synchrotron radiation source, whose evolution is prescribed by the standard model (e.g., van der Laan 1966). We shall also assume that, as seen at O, the thickness of the shell is a constant fraction, $1 - \eta$, of its outer radius. Our thin shell may then be regarded as a limiting case of the homologously expanding spherical configurations discussed in Rees (1967).

III. FLUX VARIABILITY IN THE STANDARD MODEL

We assume that the shell is composed of relativistic electrons which, in the comoving frame, have a power law energy spectrum $N(E)dE = KE^{-\Gamma}dE$ (cm^{-3}) in a bounded range, and which emit synchrotron radiation as they move in an isotropic magnetic field B. In the case of a steady, homologous expansion the dynamical assumptions of the standard model imply $K \propto t'^{-(\Gamma+2)}$ and $B \propto t'^{-2}$.

If the frequency ν is sufficiently low, the source would initially be optically thick due to self absorption by the relativistic electrons (cf. JOS). The absorption coefficient in the comoving frame is given by

$$\mu'_{\nu'} = C_1(\Gamma)\, K\, B^{\frac{1}{2}(\Gamma+2)}\, \nu'^{-\frac{1}{2}(\Gamma+4)}, \qquad (6)$$

where the constant C_1 [as well as C_2 in eq. (7)] depends on Γ (e.g., Pacholczyk 1970). In the standard model the optical depth $\tau_{\nu'}(t')$ is $\propto \mu'_{\nu'}(t')\, t'$ and decreases as the shell expands, so that the source eventually becomes optically thin.

In order to simulate the conditions assumed in Terrell, we neglect at first the emission from the shell at a frequency ν' after the optical depth $\tau_{\nu'}$ corresponding to that frequency has decreased to unity, and ignore the angular variation of $\tau_{\nu'}$ in the comoving frame. The distant observer would then see the source evolve in the manner described in §II, with D_c decreasing as a power of t. The exponent f is in this case a function of Γ [$f(\Gamma) = (4\Gamma+6)/(3\Gamma+2)$], obtained by setting $\tau_{\nu'_c}(t'_c) = 1$. The flux (at the frequency ν) received by the observer at P from an element of optically thick source ($\tau_\nu \gg 1$) with Doppler shift D is

$$(\Delta F_\nu)_{thick} = (I_\nu)_{thick}\, \Delta\Omega = [C_2(\Gamma)\, \nu^{2.5}\, D^{\frac{1}{2}}\, B^{-\frac{1}{2}}]\, \Delta\Omega, \qquad (7)$$

where $\Delta\Omega = \pi/R^2 \, d/d\theta \, [r(\theta) \sin\theta] \, d\theta$ is the solid angle subtended by the element (e.g., Rees 1967). Having chosen to neglect, for the time being, the optically thin contribution to the flux, we may approximate the total flux received at P at the time t by the integral of equation (7) over those regions of the source with $\tau_\nu > 1$ which are visible to the distant observer at that instant (cf. Rees 1967; these regions are represented in Fig. 1 by heavy lines). A more accurate approximation to the total flux from a thin shell, including the optically thin emission, is considered below.

The extent to which the flux variations appear superluminal can be measured by the index of variability

$$i_v = \Delta r_a/(ct_v) \qquad \text{(JOS)}. \tag{8}$$

Here t_v is a time scale for flux variations and Δr_a is the observed transverse radius of the source. The variations are superluminal if $i_v \gg 1$. In computing i_v for a given pulse we shall assume that only the upper half of the flux curve is detected as a signal, and take t_v to be the full width of the curve at half-maximum. For Δr_a we shall take the mean of the maximum and the minimum values of r_a in the interval t_v. With these definitions i_v will characterize the variability of the entire pulse.

We now show that the degree of flux variability attributed to the shell in the present approximation is influenced by the particular assumptions of our model through the Doppler shift and time dependence of the surface brightness $[(I_\nu)_{\text{thick}} \propto D^{3/2}t]$ and through the function f. In particular we show that, depending on the value of f, i_v may be either $\gg 1$, implying a greatly shortened pulse, or < 1, in which case the relativistic expansion leads in fact to a very long pulse, as described in Terrell.

Figure 2 displays the time evolution of $(F_\nu)_{thick}$ and of r_a in this model, with $\gamma = 5$, for two values of f. In Figure 2a f = 1.75 (corresponding to $\Gamma = 2$), whereas in Figure 2b f = 1 (corresponding to $\Gamma = -4$). Figure 2b is not sensitive to the prescribed time dependence of the magnetic field, and hence nearly reproduces the behavior of the synchrotron source (with B = constant) described in Terrell.

In Figure 2a the signal is received before $t = T_2$; hence equation (5a) is applicable, and with the relatively small value of t_v yields $i_v = 14.5$ (the apparent transverse speed $d/dt\ r_a = 4.9c$ in this case). In Figure 2b the variability timescale is rather large and the signal is received after $t = T_2$, when r_a no longer increases linearly with time [cf. eq. (5b)]; these effects combine to give $i_v = 0.5$.

The reason why the flux variations are superluminal for f = 1.75 but not for f = 1 can be understood by analyzing the evolution of the flux at times $t > T_1$. Two opposing trends are at work after the source starts turning optically thin: The substitution of flux from low Doppler-shift regions (in the back of the ellipsoid) for radiation from the brighter forward regions causes the initial slump in the flux curve. Meanwhile, the continuing increase in the apparent area (πr_a^2) tends to bring the curve up again, and the flux eventually attains a second maximum. The relative height of the two peaks, as well as the length of the signal, depends on how fast the source is turning optically thin, i.e., on the exponent f in $D_c(t)$. In Figure 2a the source becomes transparent so rapidly that the curve does not climb all the way back to half-maximum and the signal is very short. In Figure 2b, on the other hand, f is sufficiently small so that the flux essentially follows the increase in the apparent radius, rising well over the initial peak to a maximum at $t \approx T_3 \gg T_1$.

We now consider the effects of the optically thin flux. If the thickness of the shell is small enough ($\eta \gtrsim \beta$), we can approximate the flux from an optically thin element of the source ($\tau_\nu \ll 1$) by

$$(\Delta F_\nu)_{thin} = (I_\nu)_{thin}\,\Delta\Omega = \left[\text{const.}\; K\, B^{\frac{1}{2}(\Gamma+1)}\; \nu^{-\frac{1}{2}(\Gamma-1)}\; t\, D^{3+\frac{1}{2}(\Gamma-1)}\right]\Delta\Omega\ , \qquad (9)$$

where the constant is determined by requiring $(I_\nu)_{thin}\,(t) = (I_\nu)_{thick}\,(t)$ at $D = D_c(t)$. The total flux at time t is then the integral over $d\Theta$ (from 0 to Θ_{max}) of

$$\Delta F_\nu(\Theta) = (\Delta F_\nu)_{thick}(\Theta)[1 - \exp(-\tau_\nu(\Theta)] + (\Delta F_\nu)_{thick}(\Theta^*)[1 - \exp(-\tau_\nu(\Theta^*)]\ \exp[-\tau_\nu(\Theta)], \qquad (10)$$

where Θ^* is related to Θ by $r(\Theta^*)\sin\Theta^* = r(\Theta)\sin\Theta$, and where $\tau_\nu(\Theta) = (I_\nu)_{thin}(\Theta)/(I_\nu)_{thick}(\Theta)$ [footnote 1].

---

[1] For the sake of simplicity we continue to ignore the limb-brightening factor $1/|\cos\Theta'| = \gamma\beta/|D(\Theta) - \gamma|$ in $\tau_\nu(\Theta)$, as well as any variation with Θ' of the effective component of the magnetic field (the component which in the comoving frame is normal to the line OP). Both of these effects are emphasized in a thin shell, but an explicit calculation has verified that they do not affect any of the qualitative results presented in this paper.

We have integrated equation (10) numerically and calculated the flux variations in the standard model for different values of the power-law index Γ in the range (e.g., JOS) $1 \le \Gamma \le 3$ of typical variable radio sources. Figure 3 shows the time evolution of F_ν in this model (with $\gamma = 5$) for $\Gamma = 1$, 2, and 3. A comparison with Figure 2a reveals that the optically thin contri-

bution slows down the decay of the flux, thereby increasing t_v. This effect is most pronounced in the $\Gamma = 1$ curve. However, the sharp initial decline in the optically thick flux wins over as the value of Γ is increased, giving rise to a progressively growing narrow pulse (whose width decreases with γ). At high values of Γ the flux variations could therefore be interpreted as one superluminal outburst followed by another outburst of longer duration.

We conclude that superluminal flux variations cannot be excluded in the case of the standard model. Such variations do not occur in Terrell's model because of the assumption that, in the rest frame of the source, all the optically thick emission is turned off at once. As mentioned by Terrell, this assumption could apply to Type I supernovae (cf. Morrison and Sartori 1969), where the visible emission is stimulated by outflowing ultraviolet radiation from a central source and where a single cutoff time can be associated with the mean-free-path of the exciting photons (note that in this example the frequency is not Doppler shifted because the emitting atoms are stationary). On the other hand, this assumption is not realistic in the context of the standard model, as it implies $\Gamma = -4$, whereas actual synchrotron sources are characterized by positive values of Γ.

IV. SOME OBSERVATIONAL IMPLICATIONS OF THE MODEL

In this section we discuss briefly a few effects which are associated with a change in the frequency of observation ν.

Figure 3 shows that, following the initial rise, the flux eventually settles down to a continuous decline. When the decaying flux is compared at two different frequencies ν_1 and ν_2, it is found to decrease faster at the higher frequency. It follows that if the spectral index α were inferred

from the relation $\alpha = - \log (\dot{F}_{\nu_2}/\dot{F}_{\nu_1})/\log (\nu_2/\nu_1)$ (where a dot represents a time derivative),[2] then it would be negative during the decay of the outburst

---

[2]The time derivative enables one to separate the varying component of the flux from any underlying component which is not associated with the outburst (cf. Altschuler and Wardle 1977).

(and thus the inferred power-law index $\Gamma = 2\alpha + 1$ would have less than the actual value). Altschuler and Wardle (1977) have observed this effect in a number of variable compact sources and noted that it cannot be accounted for by the nonrelativistic standard model, in which the decaying flux is optically thin and $\propto \nu^{-\frac{1}{2}(\Gamma - 1)}$ (cf. van der Laan 1966). In the relativistic model, however, the flux received at this stage is approximately the sum of the optically thick flux [the integral of eq. (7)] from the back of the source and of the optically thin flux [the integral of eq. (9)] from the regions where $\tau_\nu < 1$ (cf. Rees 1967). Moreover, since the expressions for $(F_\nu)_{\text{thick}}$ and $(F_\nu)_{\text{thin}}$ contain various powers of $D_c \propto t^{-f}\ \nu^{-(f-1)}$, they have a different dependence on t and on ν than in the nonrelativistic model. In fact, in the relativistic case both $(\dot{F}_\nu)_{\text{thick}}$ and $(\dot{F}_\nu)_{\text{thin}}$ are decreasing functions of ν for all values of t at which the decaying outburst is likely to be observed. These conclusions apply also when the entire volume of the sphere is filled (cf. Jones and Burbidge 1973).

It is also found that the apparent radius, computed now more accurately as the traverse radius which encloses half of the total flux, attains higher values when the frequency of observation is decreased [cf. Jones and Tobin (1977), where an analogous result was obtained for a filled sphere]. The increase in the maximum apparent radius is a consequence of the fact that,

as the frequency is decreased, the outermost regions of the expanding source remain optically thick for a longer period of time. This effect, too, has been observed, but the observations have previously been interpreted in a nonrelativistic context [cf. Kellermann et al. (1971); see also Condon and Dressel (1973)].

As we have noted, these results do not depend on whether the source is a shell or a sphere, and it turns out that they are also not very sensitive to the dynamical assumptions of the synchrotron source model. In order for the above-mentioned phenomena to be observed it is necessary, however, that the expansion speed be at least moderately relativistic. In view of the results of §III this could be the case even if the source does not exhibit superluminal flux variations.

V. CONCLUSION

We have examined the flux variations produced by a synchrotron source in the form of a thin spherical shell which expands relativistically at a steady rate. Our conclusions are:

1) The claim, made in Terrell, that relativistic expansion does not lead to greatly shortened pulses, is a model- (and parameter-) dependent conclusion, which does not apply in general.

2) The variability timescale in a thin shell, which is initially opaque due to self absorption, is determined essentially by the rate at which the optically thick emission appears to be turned off. In a given model this in turn depends on the power-law index Γ and on the Lorentz factor γ. In the case of the standard model very short pulses are produced when the values of Γ and of γ are sufficiently large.

3) The shell configuration leads to a steepening of the initial decrease in the optically thick flux. This strengthens the argument, mentioned in the

Introduction, about the effectiveness of shells in producing superluminal flux variations. The optically thin flux tends to decrease the variability, in shells as well as in filled spheres.

4) Some observed spectral effects in compact radio sources could be produced by relativistic expansion of the source.

The simple model that we have considered, while easy to analyze, is by no means a complete, or even a realistic model of compact radio sources. In particular, the expansion speed is not likely to be constant; for example, relativistic blast waves under most circumstances are decelerating (cf. Blandford and McKee 1977), in which case the variability index may be reduced (cf. Jones and Tobin 1977). A self-consistent model which will account for all the phenomena observed in compact radio sources still remains to be constructed, but in this paper we have at least verified that superluminal flux variations are a possible feature of such a model.

ACKNOWLEDGMENTS

I thank Roger Blandford for many valuable suggestions and encouragement. I also thank Kip Thorne and Anthony Readhead for helpful comments on the manuscript.

REFERENCES

Altschuler, D. R., and Wardle, J. F. C. 1977, M.N.R.A.S., 179, 153.

Blandford, R. D., and McKee, C. F. 1977, M.N.R.A.S., 180, 343.

Blandford, R. D., McKee, C. F., and Rees, M. J. 1977, Nature, 267, 211.

Cohen, M. H., Lindfield, R. P., Moffet, A. T., Romney, J. D., Seielstad, G. A., Kellermann, K. I., Shaffer, D. B., Pauliny-Toth, I. I. K., Preuss, E., Witzel, A., Schilizzi, R. T., and Geldzahler, B. J. 1977, Nature, 268, 405.

Condon, J. J., and Dressel, L. L. 1973, Ap. Lett., 15, 203.

Jones, T. W., and Burbidge, G. R. 1973, Ap. J., 186, 791.

Jones, T. W., O'Dell, S. L., and Stein, W. A. 1974, Ap. J., 192, 261.

Jones, T. W., and Tobin, W. 1977, Ap. J., 215, 474.

Kellermann, K. I., Jauncey, D. L., Cohen, M. H., Shaffer, D. B., Clark, B. G., Broderick, J., Rönnäng, B., Rydbeck, O. E. H., Matveyenko, L., Moiseyev, I., Vitkevitch, V. V., Cooper, B. F. C., and Batchelor, R. 1971, Ap. J., 169, 1.

Morrison, P., and Sartori, L. 1969, Ap. J., 158, 541.

Pacholczyk, A. G. 1970, Radio Astrophysics (San Francisco: W. H. Freeman and Co.), p. 96 and Appendix 2.

Rees, M. J. 1967, M.N.R.A.S., 135, 345.

Terrell, J. 1977, Ap. J. (Letters), 213, L93.

van der Laan, H. 1966, Nature, 211, 1131.

Vitello, P., and Pacini, F. 1977: I. Ap. J., 215, 452; II. preprint.

FIGURE CAPTIONS

Fig. 1. Apparent shape of an expanding luminous spherical surface with $\gamma = 5$. The heavy lines represent those regions in the source which contribute to the optically thick flux at a given instant after the source has started turning optically thin.

Fig. 2a. Time evolution of the optically thick flux $(F_\nu)_{thick}$ in the standard model for the source of Fig. 1. Also shown is the time evolution of the apparent radius r_a of the optically thick regions in this source. Both curves are normalized to unity. As discussed in the text, the degree of flux variability depends on the exponent f, which determines the rate at which the source is turning optically thin; in this figure f = 1.75, and the pulse is superluminal.

Fig. 2b. The same as Fig. 2a, except that f = 1, resulting in a subluminal pulse.

Fig. 3. Time evolution of the total flux F_ν in the standard model for the source of Fig. 1. The three curves correspond to different values of the power-law index: $\Gamma = 3$, $\Gamma = 2$, and $\Gamma = 1$ (respectively, from left to right), and are normalized to unity.

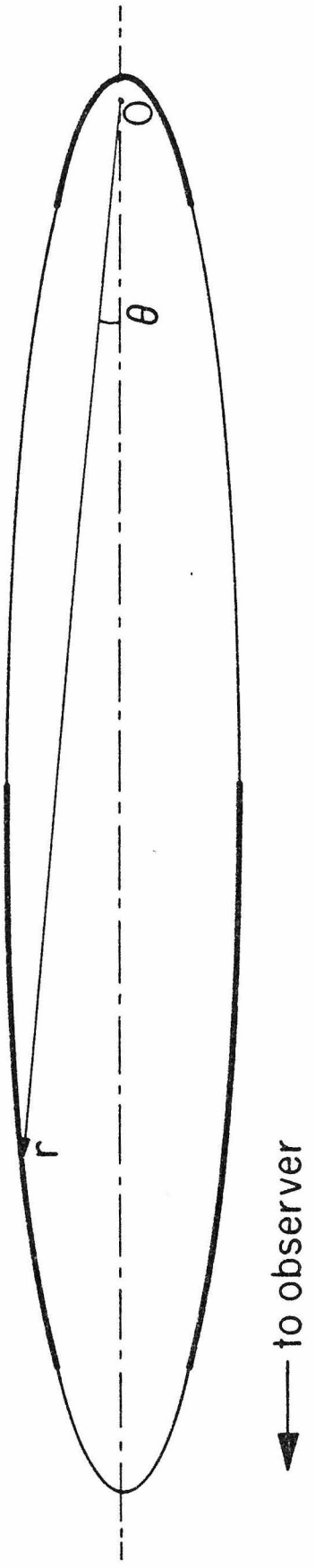

Fig. 1

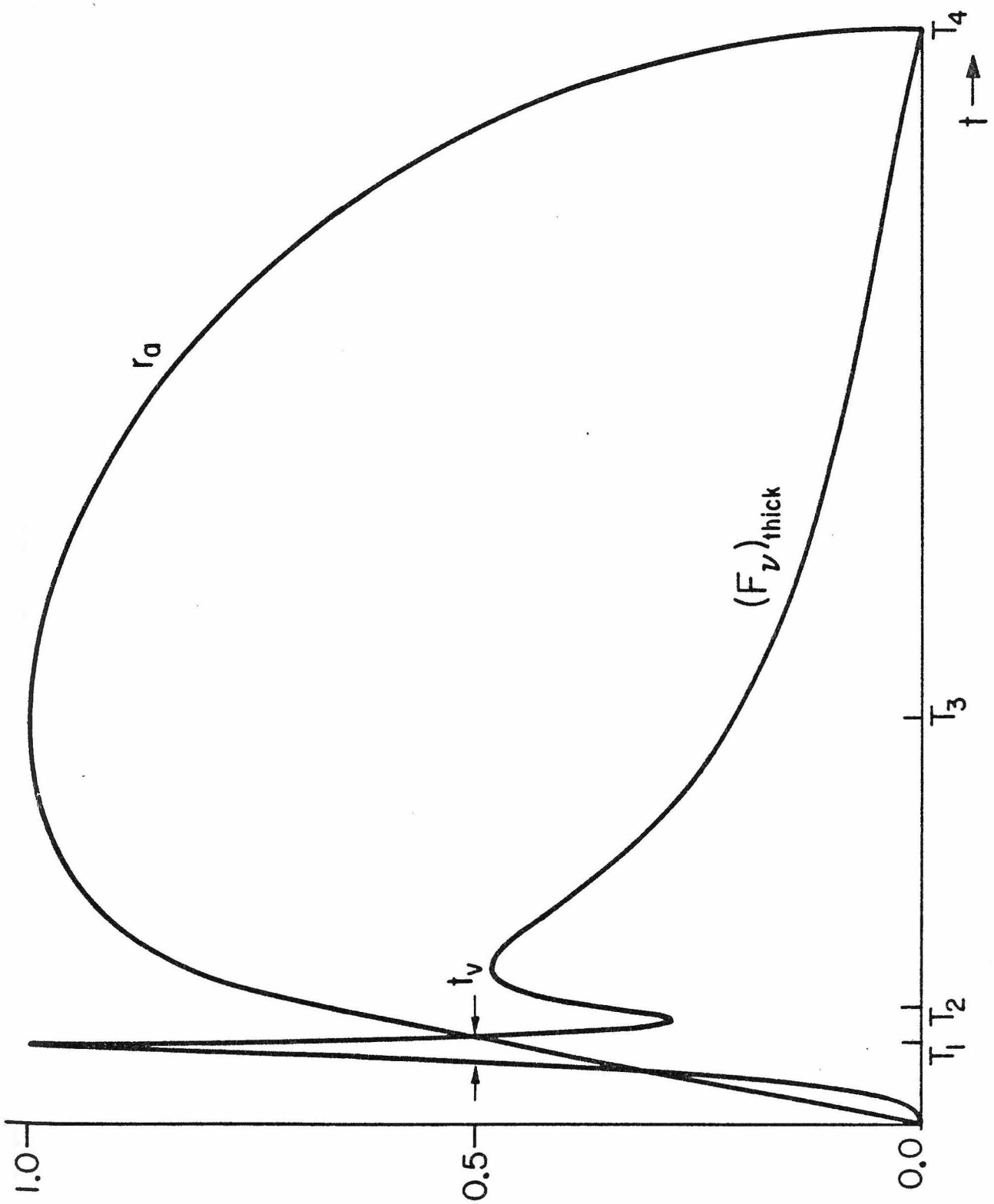

Fig. 2a

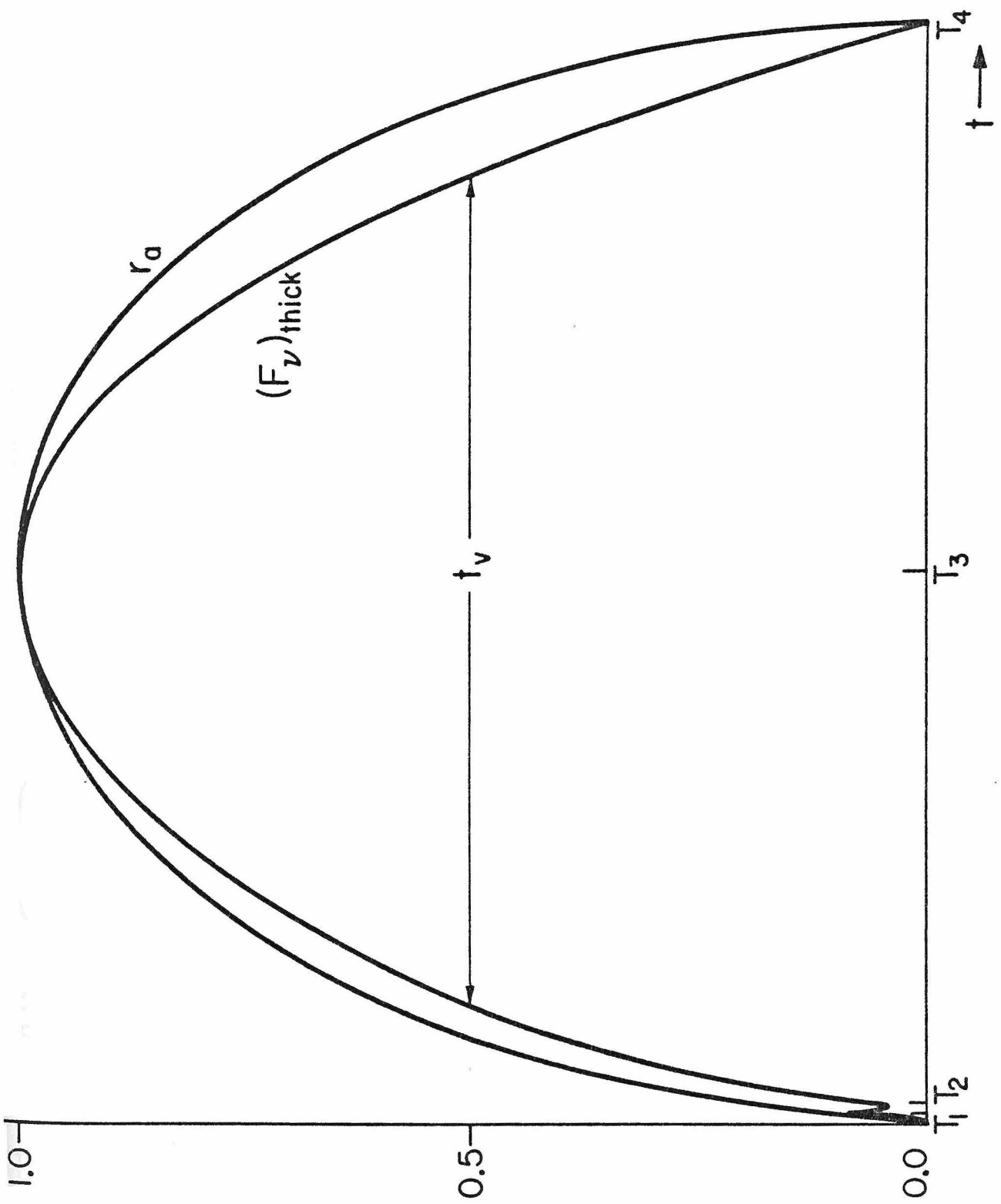

Fig. 2b

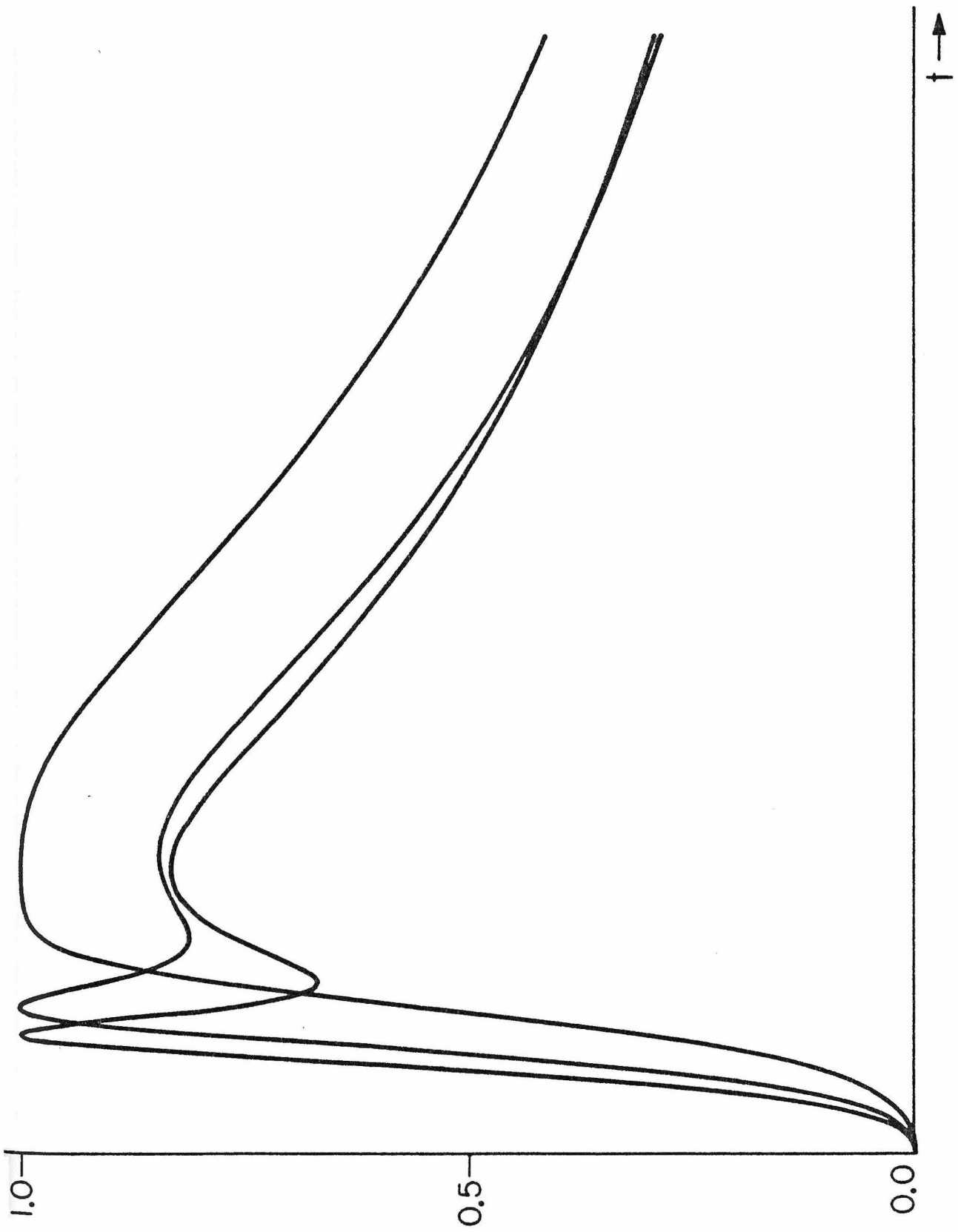

Fig. 3

PAPER 2

A MODEL FOR THE KNOTS IN THE M87 JET

(in collaboration with R. D. Blandford)

1. INTRODUCTION

The jet in M87 has long been known to contain several bright features (knots) displaying a featureless non-thermal continuum and high linear polarization [Baade and Minkowski (1954); Schmidt et al. (1978)]. These knots are also detectable at radio wavelengths [Wilkinson (1974); Turland (1975a)], as is an antiparallel counter-jet not seen optically.

At a distance of 15 Mpc, the knots appear to be unresolved optically, implying that their sizes are $\leq$ 25 pc [de Vaucouleurs et al. (1968); Arp and Lorre (1976)], and are located at distances from 0.2 kpc to 1.9 kpc from an unresolved ($\leq$ 0.1 pc, Kellermann et al. 1973) bright nucleus. The variation of the optical power radiated by the knots with distance from the nucleus is at first irregular, but after reaching a maximum value of $\sim 2.3 \times 10^{41}$ erg s^{-1} for knot A (at a distance ~ 1 kpc) it decreases monotonically, falling off by a factor of 45 between knot A and knot H. The degree of linear polarization in the knots is quite high ($\lesssim$ 20%), but the position angles do not seem to display any particular pattern.

There are now several other known examples of jets associated with extragalactic radio sources [e.g., Waggett et al. (1977); Readhead et al. (1978); Turland (1975b)], and at least one of them (3C147) also appears to contain knots (Wilkinson et al. 1977). The existence of these features had previously been hypothesized on the grounds that energy had to be supplied continuously to the components of extended double radio sources and that one attractive way of doing this is by means of a collimated supersonic beam of matter (e.g., De Young 1976). It is then natural to identify the jet with such a beam, possibly supplying power to the extended halo associated with M87 (e.g., Cameron 1971). In this paper we address the

problem of the interpretation of the knots in the context of the beam model.

Rees (1978) has recently suggested that the knots be attributed to the steepening of non-linear sound waves in the jet. When the waves "break," strong shocks are formed, behind which the relative energy of the flow can be dissipated in particle acceleration and synchrotron radiation. We explore here an alternative dynamical hypothesis — that the knots be identified with dense blobs of gas that are confined and swept outwards by the ram pressure of the jet. [A similar mechanism has recently been proposed (McKee et al. 1978) for the acceleration of high velocity clouds by spherical blast waves in supernova remnants.] For as long as the speed of the jet with respect to the blobs is supersonic, they will be followed by strong bow shocks (Fig. 1), behind which some of the beam momentum can be absorbed and kinetic energy can be dissipated.

In Section 2 we describe the dynamical behavior of such a cloud. In Section 3 we interpret the knots of M87 in terms of this model, and in Section 4 we speculate briefly on the possible implications of these ideas for discussions of extended double sources, quasar absorption lines and superluminal expansion.

2. DYNAMICS OF A CLOUD IN A JET

We suppose that a blob of gas of mass M and internal energy E_o is created at rest at a distance r_o from the nucleus, where the density is ρ_o. We further assume that the blob is immersed in a steady supersonic jet of speed w, which expands from the nucleus in a cone of solid angle Ω. The density in the jet at radius r is thus $\rho(r) = \rho_o(r/r_o)^{-2}$, and the total power of the jet is $L_j = 1/2\ \rho_o\ r_o^2\ \Omega\ w^3$. We ignore relativistic effects.

The cloud will be accelerated by the jet and move downstream, followed by a strong bow shock. Assuming its shape to be roughly spherical, the force on the cloud and its internal energy are given by

$$Mg = C_F \rho(w - v)^2 h^2 \tag{1}$$

$$E = C_E Mg h \quad . \tag{2}$$

Here v is the speed of the cloud, $g = dv/dt$ its acceleration, and h, the scale height, is defined by $h = p_a/\rho_a g$ [where p_a and ρ_a are, respectively, the pressure and the density at the apex of the blob (Fig. 1)], and is assumed to be $\ll \Omega^{1/2} r$. C_F and C_E are constants, which depend on the particular model adopted for the cloud. We assume that the blob is much denser than its surroundings ($\rho_a/\rho_o \gg 1$), which implies that the time ($\sim (h/g)^{1/2}$) taken for it to come into rough hydrostatic equilibrium is much less than the acceleration time ($\sim w/g$).

As the blob moves downstream, the pressure applied by the jet decreases but the scale height increases. The internal energy will then decrease adiabatically according to the relation

$$E = E_o(h/h_o)^{-2} \ , \tag{3}$$

where a value of $\gamma = 5/3$ for the ratio of specific heats is being assumed. Combining Eqs. (1)-(3) and setting $x = r/r_o$, $y = v/w$, we find:

$$g = C_F \rho_o w^2 h_o^2 M^{-1} x^{-6/5}(1 - y)^{6/5} \tag{4}$$

and

$$h = h_o x^{2/5}(1 - y)^{-2/5} \quad . \tag{5}$$

Although all the incident momentum flux is taken up by the cloud, only a small fraction of the incident energy flux is used in increasing the kinetic

energy of the blob. Roughly half of the bulk kinetic energy incident on the cloud is converted in the bow shock into internal energy, and so the power dissipated by the shock is $\sim 1/2\,(w - v)\,Mg \sim (w - v)^3/w^3\ (h^2/\Omega r^2)\,L_j$, only a small fraction of the total power in the jet. (Additional dissipation may occur as the shocked fluid mixes with the ambient flow further downstream.) If we assume that some fixed fraction $C_L \leq 1$ of this power is radiated, then we can write:

$$L_{rad} = 1/2\ C_L(w - v)\ Mg$$

$$= 1/2\ C_L\ C_F\ \rho_o\ h_o^2\ w^3\ x^{-6/5}(1 - y)^{11/5} \quad . \tag{6}$$

Substituting now $w^2/r_o\ y(dy/dx)$ for g, we can integrate Eq. (4) to obtain:

$$(1 - y/5)(1 - y)^{-1/5} - 1 = z(1 - x^{-1/5}) \ , \tag{7}$$

where $z = 4/5\ C_F\rho_o r_o h_o^2 M^{-1}$. According to this relation the cloud will never acquire the jet velocity, but will approach a certain maximum speed v_{max}, whose value increases with z (for example: $v_{max} \sim 0.9\ w$ for $z \sim 1$, $v_{max} \sim 0.6\ w$ for $z \sim 0.1$, and $v_{max} \sim 0.2\ w$ for $z \sim 0.01$). Thus, if z is large, the speed of the jet with respect to the blob may become subsonic, in which case the bow shock will disappear and L_{rad} will be sharply reduced. In general, most of the acceleration occurs near r_o, so that v is close to v_{max} for most of the time. Equation (4) can be integrated once more (numerically) to obtain x(t). The function $f(x) = x^{-6/5}(1 - y)^{11/5} \propto L_{rad}$ can then be studied, and is found to fall off rapidly near x = 1 (much faster than $x^{-6/5}$ for $z \gtrsim 1$).

We shall henceforth adopt for the cloud the isothermal model of De Young and Axford [(1967); cf. also Longair et al. (1973)]. For this model (and for $\gamma = 5/3$) the maximum transverse radius is πh, and the constants in Eqs. (1) and (2) are: $C_F = 8.11$ and $C_E = 1.50$. For future reference we now rewrite Eq. (6), setting $C_F = 8.11$ and expressing ρ_o in units of 10^{-26} g cm^{-3}, h_o in units of 1 pc and w in units of 10^{10} cm sec^{-1}:

$$L_{rad} \sim 3.9 \times 10^{41} C_L \rho_{o-26} h_o^2 w_{10}^3 X^{-4/5}(1-y)^{11/5} \text{ erg sec}^{-1} . \quad (8)$$

Similarly,

$$E_o = 3.6 \times 10^{50} \rho_{o-26} w_{10}^2 h_o^3 \text{ erg} , \quad (9)$$

and, expressing M in $M_\odot$ and r_o in kpc,

$$z = 0.96 \rho_{o-26} r_{o3} h_o^2 M^{-1} . \quad (10)$$

Since the blobs are assumed to be much denser than the surrounding medium, they will be subject to the Rayleigh-Taylor instability at the contact discontinuity with the shocked wind (it seems unlikely that the post-shock density exceeds that in the blob, despite the fact that the shock will be somewhat radiative). Kelvin-Helmholtz instability in the shear flow along the sides of the clouds is also possible. Blake (1972) has investigated the growth times and the non-linear development of these instabilities for the De Young and Axford (1967) model, and has discussed the possible stabilizing effect of a magnetic field. Although such an effect will be present in our case if the wind carries a frozen-in magnetic field, we still expect some fragmentation to occur especially during the initial acceleration. If the blob is broken up into a number of fragments with different initial scale heights h_o, then each of them will subsequently

evolve as an independent cloud, with $g \propto h_o^{-1}$ and $L_{rad} \propto h_o^2$ (cf. Blake 1972).

3. APPLICATION TO THE M87 JET

Interpretation of the Knots

The interpretation of the knots as accelerating blobs of gas has several attractive features. The knots appear to be smaller than the total transverse extent of the jet and are not exactly collinear [cf. de Vaucouleurs et al. (1968); Arp and Lorre (1976)]. This is what is expected if the scale height h of the clouds is smaller than the jet's width. [The short ($\leq$ 20 yr) reported variability time scale of some knots (Pronik and Scherbakov 1972) in fact suggests sizes $\leq$ 10 pc.] Furthermore, it is well known that the minimum energy density associated with the knots is extremely difficult to confine by any thermal pressure associated with the surrounding medium (e.g., Okoye 1973). If the cloud is totally immersed in the jet, then it can be confined by the jet's ram pressure, without necessarily requiring a large external pressure to confine the jet. (If the jet's Mach number exceeds $\sim \Omega^{-1/2}$, then no external pressure need be invoked.)

All eight knots could, of course, have been created in separate, unrelated events. However, it is possible to interpret the five outermost knots as fragments of one large blob which broke up following the onset of dynamical instability (a similar interpretation of the innermost knots would require at least one additional blob). As we have noted, the smaller fragments would have larger accelerations but smaller luminosities, and hence, at a given time, the luminosity would be a decreasing function of distance, which is the observed behavior. As an illustrative example, we plot in Fig. 2a L_{rad}

[Eq. (6)] as a function of x for four clouds, labeled A, B, C, and G, with $z_A = 0.1$, $h_{oB}/h_{oA} = 5/6$, $h_{oC}/h_{oA} = 2/3$, and $h_{oG}/h_{oA} = 10/21$. In this example the ratios of luminosities and distances of the clouds at the time when $x_A = 2$ correspond roughly to the present ratios in the optical knots A, B, C, and G in M87 [$L_B/L_A \sim 2/3$, $L_C/L_A \sim 1/3$, $L_G/L_A \sim 1/10$, $x_B/x_A \sim 1.2$, $x_C/x_A \sim 1.4$, $x_G/x_A \sim 1.7$; cf. de Vaucouleurs et al. (1968)]. As this example demonstrates, the luminosity of each blob decreases with time, but the more distant blobs become fainter more rapidly, as indeed has been reported (Pronik and Scherbakov 1972). The hypothesis of a simultaneous formation of the five outer knots implies that the size of the knots should decrease with distance, a prediction which could presumably be tested in observations with $\lesssim 0.1$" resolution using "speckle" techniques in the optical or long-baseline interferometry at high radio frequencies. Figure 2b displays the scale height h [Eq. (5)] as a function of x for the clouds of Fig. 2a; it shows that, while the size of each blob increases with time, the more distant blobs expand more rapidly.

Particle Acceleration and Polarization

If, as indicated by the high polarization, the optical emission is synchrotron radiation, then the emitting electrons must be accelerated within the knots. This conclusion is supported by the observed flattening of the spectrum near the knots (cf. Forster et al. 1978). The bow shock is the natural site of this acceleration; relativistic electrons accelerated in the shocked jet can radiate in a magnetic field compressed behind the shock. A prediction of our model is, then, that the brightness distribution across each knot be non-symmetrical, being concentrated at the upstream end of the knot. [The reverse prediction can presumably be made in the case of

Rees' (1978) model.]

The present model provides a simple interpretation of the complex polarization pattern of the knots. If the jet carries a magnetic field whose component parallel to the flow does not greatly exceed the transverse component, then in the emitting region behind the shock the field will be predominantly parallel to the shock and wrapped around the knot. The strong polarization in each knot and the variation of the position angle from knot to knot can then be accounted for if the field is coherent on length h but chaotic on the scale of the distances between the knots.

The shock should stand off a distance ~ h from the apex of the cloud (cf. Spreiter and Alksne 1968). We can thus equate h with the cooling length of the most energetic relativistic electrons. The spectrum of the knots extends with spectral index ~ 0.5 from ~ 10^8 Hz up to ~ 10^{15} Hz, where it appears to steepen [Turland (1975a); Redman (1978)]. Across the shock the velocity of the fluid relative to the blob is reduced by a factor ~ 4, while the magnetic field B in the jet is increased by a factor ~ 4. Taking v ~ 1/2 w, we find $B \sim 10^{-4}\ w_{10}^{2/3}\ h^{-2/3}$ G, which should exceed the inverse-Compton limit $\sim 2 \times 10^{-4}\ h^{-1}(L_{rad}/2.3 \times 10^{41})^{1/2}$ G. (An inverse-Compton X-ray flux $\gtrsim 10^{38}$ erg s^{-1} from the brightest knots should be detectable by HEAO B, and may constrain B and h.) For w_{10} and h(pc) of order unity the post-shock field is less than the equipartition field in knot A (cf. Schmidt et al. 1978) and is not expected to influence the shock jump conditions; in fact, the ratio of particle to magnetic energy density behind the shock is $\gtrsim 10^3\ h^{-2/3}\ w_{10}^{-7/3}$.

Unless the energy density in protons behind the shock greatly exceeds that in electrons, then the fact that the spectral index is ~ 0.5 implies that the electron energy density is distributed uniformly over each decade of

electron energy. Assuming that half of the internal energy behind the shock is associated with the electrons and may thus be radiated away, we can roughly estimate the constant C_L in Eq. (6) to be $\sim 1/2\,[\ln(\nu_{max}/\nu_{min})^{1/2}]^{-1} \sim 0.1$. For $w \sim 10^{10}$ cm sec^{-1} and $B \sim 10^{-4}$ G, the mean Lorentz factor of the electrons behind the shock is $\gamma \sim 300$ and they would radiate at a frequency ~ 0.1 GHz (cf. Blandford and McKee 1977). It is therefore necessary to accelerate the electrons and produce an energy distribution function $N_\gamma \propto \gamma^{-2}$ behind the shock which extends over more than three decades of energy, to $\gamma \sim 9 \times 10^5$. This may conceivably be achieved by the Fermi mechanism [Bell (1978); Blandford and Ostriker (1978)].

The Faraday rotation associated with the knots is probably $\lesssim 0.7$ rad beyond 800 pc (Schmidt et al. 1978). Rotation may arise from the thermal electrons both behind the shock and along the line of sight inside the jet. For uniform field and density this limit then implies $\rho_{-26}\, B(h + 60 r_3 \Omega^{1/2}) \lesssim 2.5 \times 10^{-3}$, where B is measured in Gauss, r in kpc, and h in pc.

Nature of the Clouds

The main requirements for an accelerated cloud to be an effective radiator are that it have sufficient inertia not to be swept away too rapidly, and a sufficiently large size (which in turn means sufficiently large internal energy) in order to obstruct a reasonable fraction of the jet. The main candidates among astronomical objects which satisfy the necessary requirements appear to be supernova remnants and interstellar clouds.

Adopting $z_A \sim 0.1$ and $r_{o3} \sim 0.5$ as characteristic parameters for knot A (cf. Fig. 2), and setting $\rho_{0-26} \sim 1$ [consistent with the Faraday rotation

constraint; cf. Mathews (1978)] and $C_L \sim 0.1$, we find $w_{10} \sim 2.8\ h_o^{-2/3}$ and $M_A \sim 4.8\ h_o^2$. As an example, for $h_o = 1.5$ we get $M_A \sim 10$ and $E_o \sim 5 \times 10^{51}$ erg, which could correspond to a powerful supernova. The actual transverse radius of such a blob at $r_3 \sim 1$ would be $\sim \pi h \sim 7$ pc. In this case $\rho_a/\rho_o \sim 10^3$ and, since $y(x = 2) \sim 0.3$, the kinematics can still be treated nonrelativistically. A supernova remnant of mass M and kinetic energy U exploding at r_o will expand virtually undecelerated with a speed $v_s = \sqrt{2U/M}$ until the momentum per steradian equals the impulse delivered by the shocked jet, i.e., until it reaches a radius $R \simeq 2.6\ U_{51}^{1/3}\ \rho_{o-26}^{-1/3}\ w_{10}^{-2/3}$ pc, where U is expressed in units of 10^{51} erg. A strong shock will then be driven through the remnant in the downstream direction at a speed $\sim v_s$, traversing it in a time $\tau \simeq 250\ U_{51}^{-1/6}\ M^{1/2}\ \rho_{o-26}^{-1/3}\ w_{10}^{-2/3}$ yr, and raising the internal energy to $E_o \sim 3U$, the temperature to $T_o \sim 2 \times 10^9\ U_{51}\ M^{-1}$ K, and the density to $\sim 10^{-23}$ g cm^{-3}. After the passage of the shock the remnant may fragment (cf. Chevalier 1977) but, in any case, we expect an approximate hydrostatic equilibrium to be established in a time $\sim 3\tau \sim 10^3$ yr after the explosion, at which stage the ram pressure of the jet will start accelerating the blob downstream. At these densities and temperatures the cooling time of the remnant is $\sim 2 \times 10^7$ yr, greatly exceeding the travel time $\sim (r - r_o)/v_{max} \sim 10^4$ yr, and so the radiated X-ray power from inside the blob is negligible.

What is the likelihood of $\gtrsim 2$ supernovae occurring within the last 10^4 yr in the jet? Estimating the solid angle of the jet as $\Omega \sim 0.1$, the required rate is $\sim 3/(100\ \text{yr})$ within the central ~ 1 kpc of the galaxy. A typical rate for elliptical galaxies is $0.25\ (10^{10}\ L_\odot)^{-1}\ (100\ \text{yr})^{-1}$ (Tammann 1974). From the results of Sargent et al. (1978) the luminosity within ~ 1 kpc from the nucleus of M87 is $\sim 0.3 \times 10^{10}\ L_\odot$ (the corresponding mass is $\sim 3 \times 10^{10}\ M_\odot$), implying a rate which is too small by a factor ~ 40. It

follows that the knots are unlikely to be supernova remnants unless the supernova rate in M87 greatly exceeds the rate in standard elliptical galaxies, perhaps as a result of continuous star formation near the center of the galaxy. [In fact, some tentative evidence for early-type stars in the nucleus of M87 has been reported (Young et al. 1978).]

Interstellar clouds may be more abundant than supernova remnants (even in elliptical galaxies), and may also have larger masses and sizes. However, their initial internal energies are small and must therefore be increased substantially by the initial shock before they reach pressure equilibrium with the impinging jet. Assuming that in the vicinity of the jet there are $\lesssim 1$ interstellar clouds along the line of sight, each with a density of $\sim 10^{-23}$ g cm^{-3} and size ~ 10 pc, then the expected flux of optical emission lines (in particular H_α) need not exceed the present observational limit of ~ 10^{-15} erg cm^{-2} s^{-1} [obtained from the data in Redman (1978)]. Even if the clouds were not present along the original trajectory of the jet, they could have penetrated the beam if the jet has been swinging from side to side.

Origin of the Jet Asymmetry

One of the most puzzling features of the M87 jet is the absence of an observed optical counter-jet. This may be explained by invoking relativistic motion of the knots [cf. Shklovskii (1977); Rees (1978)] — a velocity $\gtrsim 0.9$ c and a jet orientation with respect to the line of sight $\lesssim 30^\circ$ is certainly adequate to account for the asymmetry. Relativistic motion can also be invoked to interpret the initial rise and subsequent fall of the knot luminosities with radius r if all the knots have similar intrinsic luminosities.

In this case the apparent variation may reflect the dependence of the Doppler factor $(1 - v^2/c^2)^{1/2} (1 - v/c \cos \Theta)^{-1}$ on v: it is maximized when $v = c \cos \Theta$, which could occur around the position of knot A. If we do not appeal to relativistic effects, we can still argue that, since all the observed knots could be produced in only two events, it is just as likely that they occur in the same jet as in opposite jets.

4. DISCUSSION

We have interpreted the knots in M87 as supernova remnants or interstellar clouds, and mentioned a few immediate predictions of this simple model (they include: knot sizes small compared with the jet width, non-collinearity, asymmetry in the brightness distribution, X-ray emission, and possibly also variability). It is of interest to speculate upon the subsequent evolution of similar objects in more extended sources.

In the first two phases of its evolution, the cloud is successively heated and accelerated, and as it approaches its asymptotic velocity it gradually expands and cools. If sufficient mass is injected into the jet, then it may be possible to transform most of the momentum flux produced by the nucleus into the momenta of cold, dense clouds that can propagate ballistically into the surrounding medium, and perhaps form eventually a double radio-source componenent [cf. De Young and Burbidge (1973); Christiansen (1973)]. These cold clouds may have a much less severe dynamical interaction with the surrounding intergalactic medium than a homogeneous fluid jet. In addition, in those cases when the observer is looking along a mildly relativistic jet, he may detect intrinsic absorption lines that are blue-shifted with respect to the emission lines associated with the nucleus. Conventional explanations of such absorption lines (if indeed they are intrinsic) usually rely on

accelerating the clouds by radiation pressure (e.g., Kippenhahn et al. 1975); however, acceleration by subrelativistic winds would be more efficient than acceleration by photons simply because of the larger ratio of momentum to energy in the winds (e.g., Goldreich and Sargent 1976).

Finally, we remark that a small-scale version of this model, generalized to include relativistic jet speeds, may form the basis for a model of apparent super-luminal expansion in compact ratio sources. This will be discussed elsewhere [Blandford and Königl (1978), in preparation].

ACKNOWLEDGMENTS

We thank J. Pringle, A. Readhead, R. Redman, M. Rees, and W. Sargent for helpful and stimulating discussions.

REFERENCES

Arp, H. C. and Lorre, J., 1976, Ap. J., 210, 58.

Baade, W. and Minkowski, R., 1954, Ap. J., 119, 215.

Bell, A. R., 1978, Monthly Notices Roy. Astron. Soc., 182, I.147, II.443.

Blake, G. M., 1972, Monthly Notices Roy. Astron. Soc., 156, 67.

Blandford, R. D. and McKee, C. F., 1977, Monthly Notices Roy. Astron. Soc., 180, 343.

Blandford, R. D. and Ostriker, J. P., 1978, Ap. J. (Letters), 221, L29.

Cameron, M. J., 1971, Monthly Notices Roy. Astron. Soc., 152, 439.

Chevalier, R. A., 1977, Ann. Rev. Astr. Ap., 15, 175.

Christiansen, W. A., 1973, Monthly Notices Roy. Astron. Soc., 164, 211.

de Vaucouleurs, G., Angione, R., and Fraser, C. W., 1968, Astrophys. Letters, 2, 141.

De Young, D. S., 1976, Ann. Rev. Astr. Ap., 14, 447.

De Young, D. S. and Axford, W. I., 1967, Nature, 216, 129.

De Young, D. S. and Burbidge, G., 1973, Comm. Astrophys., 5, 29.

Forster, J. R., Dreher, J., Wright, M. C. H., and Welch, W. J., 1978, Ap. J. (Letters), 221, L3.

Goldreich, P., and Sargent, W., 1976, Comm. Astrophys., 6, 133.

Kellermann, K. I., Clark, B. G., Cohen, M. H., Shaffer, D. B., Broderick, J. J., and Jauncey, D. L., 1973, Ap. J. (Letters), 179, L141.

Kippenhahn, R., Mestel, L., and Perry, J. J., 1975, Astron. Astrophys., 44, 123.

Longair, M. S., Ryle, M., and Scheuer, P. A. G., 1973, Monthly Notices Roy. Astron. Soc., 164, 243.

Mathews, W. G., 1978, Ap. J., 219, 408.

McKee, C. F., Cowie, L. L., and Ostriker, J. P., 1978, Ap. J. (Letters), 219, L23.

Okoye, S. E., 1973, Monthly Notices Roy. Astron. Soc., 165, 393.

Pronik, V. I. and Scherbakov, A. G., 1972, Astrofiz., 8, 337 (English translation in Astrophys., 8, 201).

Readhead, A. C. S., Cohen, M. H., and Blandford, R. D., 1978, Nature, 272, 131.

Redman, R. O., 1978 (preprint).

Rees, M. J., 1978 (preprint).

Sargent, W. L. W., Young, P. J., Bokensberg, A., Shortridge, K., Lynds, C. R., and Hartwick, F. D. A., 1978, Ap. J., 221, 731.

Schmidt, G. D., Peterson, B. M., and Beaver, E. A., 1978, Ap. J. (Letters), 220, L31.

Shklovskii, I. S., 1977, Astron. Zh. Akad. Nauk SSSR, 54, 713.

Spreiter, J. R. and Alksne, A. Y., 1968, Planet. Space Sci., 16, 971.

Tammann, G. A., 1974, in Supernovae and Supernova Remnants (C. B. Cosmovici, ed.), Dordrecht: D. Reidel Pub. Co., p. 155.

Turland, B. D., 1975a, Monthly Notices Roy. Astron. Soc., 170, 281.

_____ 1975b, Monthly Notices Roy. Astron. Soc., 172, 181.

Waggett, P. C., Warner, P. J., and Baldwin, J. E., 1977, Monthly Notices Roy. Astron. Soc., 181, 465.

Wilkinson, P. N., 1974, Nature, 252, 661.

Wilkinson, P. N., Readhead, A. C. S., Purcell, G. H., and Anderson, B., 1977, Nature, 269, 764.

Young, P. J., Westphal, J. A., Kristian, J., Wilson, C. P., and Landauer, F. P., 1978, Ap. J., 221, 721.

FIGURE CAPTIONS

Fig. 1. Schematic configuration of a cloud. The jet (density ρ, velocity w) is shocked upstream from a dense blob of gas, whose density decreases from a maximum ρ_a at the apex with scale height h, and which moves in the direction of the jet with velocity v.

Fig. 2. The radiated power L_{rad} (Fig. 2a) and the scale height h (Fig. 2b) as a function of the dimensionless distance x for four clouds, labeled A, B, C, and G, under the assumption that they are formed simultaneously from the breakup of a single large blob. In this example $z_A = 0.1$, $h_{oB}/h_{oA} = 5/6$, $h_{oC}/h_{oA} = 2/3$, and $h_{oG}/h_{oA} = 10/21$. The positions of the clouds at three different times: $t = 0$ (the breakup time), $t = t_1$ and $t = 1.5\ t_1$ are marked with ▲, ●, and ■, respectively. The time t_1 corresponds to the present configuration of the respective knots in M87. L_{rad} and h are normalized by the corresponding values for A at the time t_1. The parameters of the clouds scale according to $L_{rad} \propto h_o^{2}$, $z \propto h_o^{-1}$, and $M \propto h_o^{3}$.

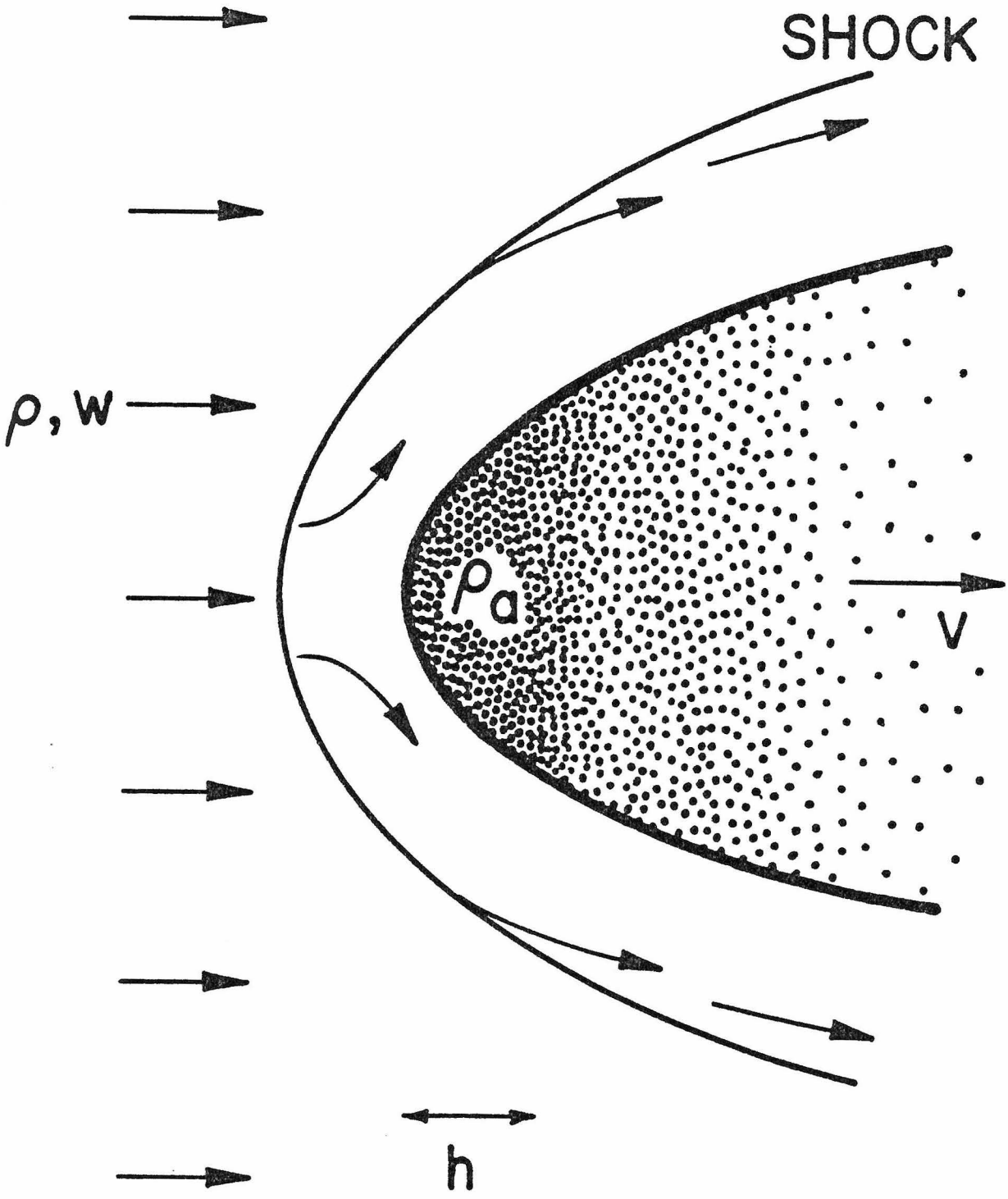

Fig. 1

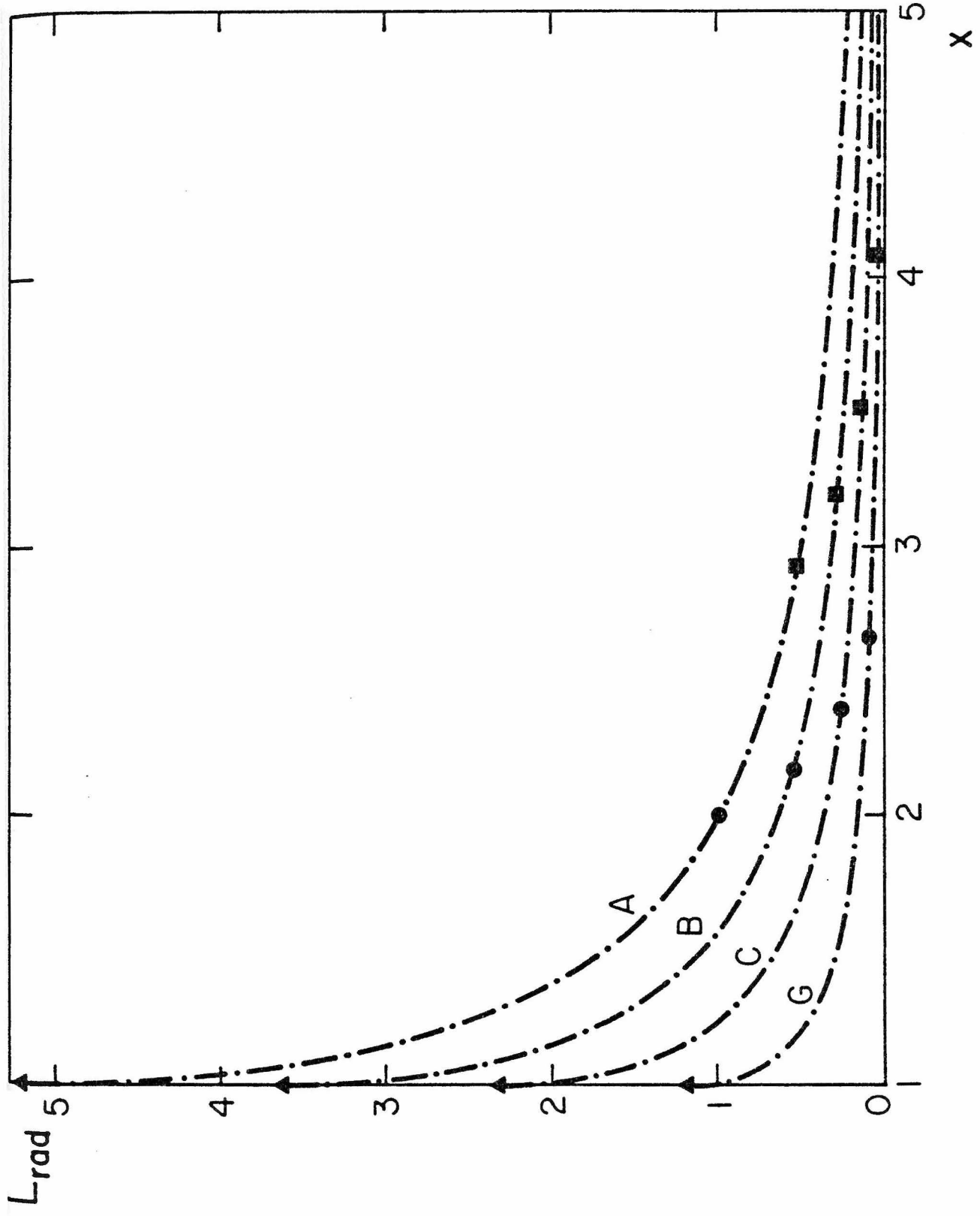

Fig. 2a

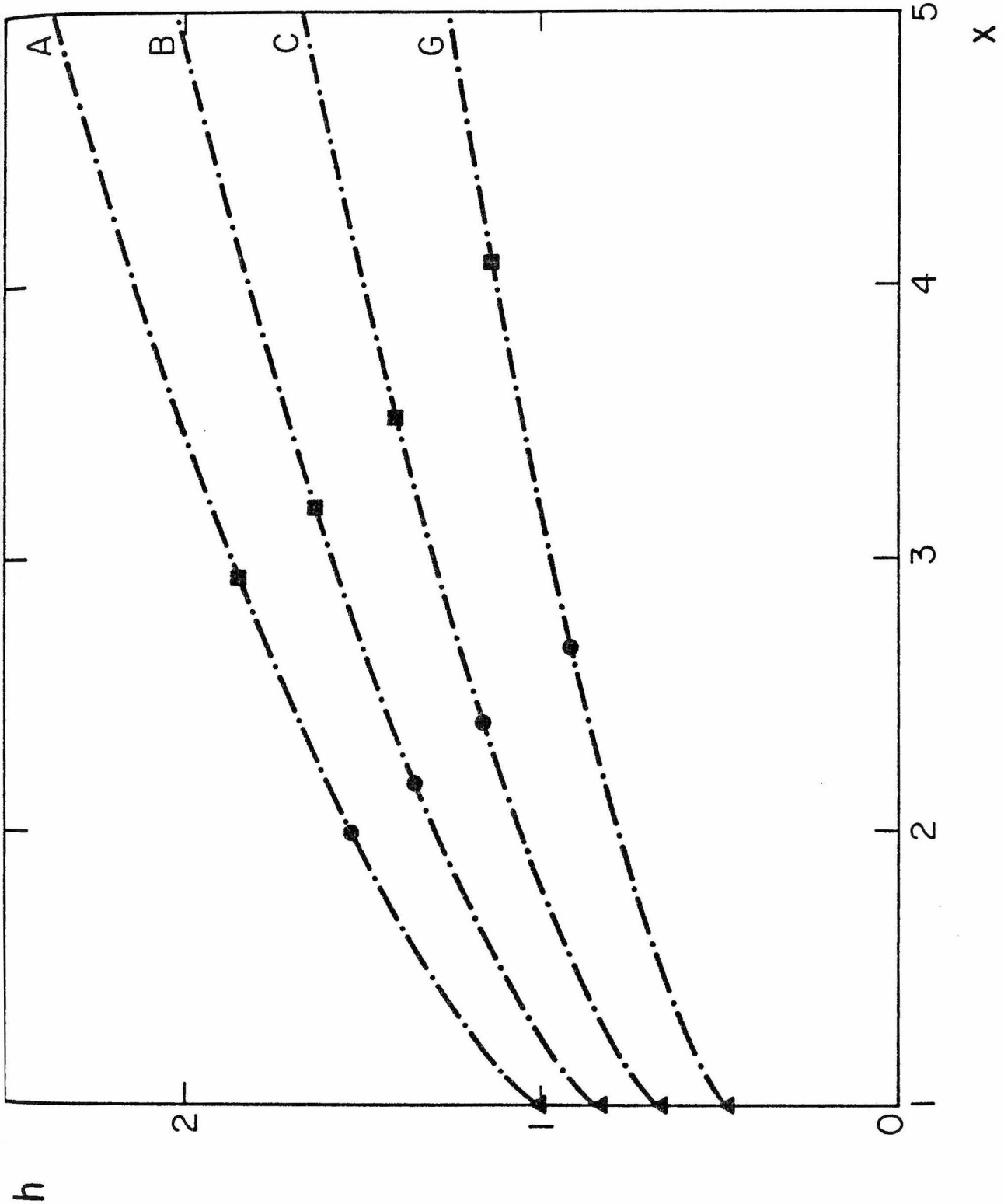

Fig. 2b

PAPER 3

RELATIVISTIC JETS AS COMPACT RADIO SOURCES

(in collaboration with R. D. Blandford)

I. INTRODUCTION

Variable radio emission from active galactic nuclei and quasars is conventionally interpreted as incoherent synchrotron radiation from a non-thermal distribution of relativistic electrons (e.g., Jones, O'Dell, and Stein 1974). For many sources there is no need to question this explanation, but for a sizeable fraction of the brighter sources there is ample evidence that simple physical models are inadequate and either must be replaced by more complex models or the synchrotron hypothesis abandoned. The difficulties originate from several types of observation. For some sources, the variability time scales t_{var} are so short that the radio brightness temperatures, based on an estimated source size of $c\ t_{var}$, exceed the "inverse Compton" limit of $\sim 10^{12}$ K (e.g., Kellermann and Pauliny-Toth 1969). For some low-frequency variables, temperatures as high as 10^{15} K are derived in this fashion (e.g., Hunstead 1972) and current indications are that this phenomenon is not rare (Condon et al. 1978).

VLBI observations of compact sources usually show an elongated radio structure, the position angle of which is roughly fixed and in some cases is related to larger scale radio structure. Apparent superluminal motion of individual components has been measured convincingly in a few cases, and appears to be fairly common amongst strong sources (Cohen et al. 1979). Finally, radio polarization observations in several sources indicate the absence of dynamically significant amounts of thermal plasma (e.g., Wardle 1977, Jones and O'Dell 1977).

These observations strongly suggest the presence of relativistic motion within the emitting region (cf. O'Dell 1978 and references cited therein), and several models (reviewed in Blandford, McKee, and Rees 1977) which incorporate

such motion have been investigated. In this paper we describe another general model that we believe has some kinematical, dynamical and radiative advantages in explaining the data. We suggest that the radio emission originates within a supersonic jet of the type that has been inferred to supply extended radio sources with mass, momentum and energy (e.g., De Young 1976), and indeed in several cases is directly observed (e.g., Waggett, Warner, and Baldwin 1977; Burch 1977).

The relativistic electrons responsible for the observed synchrotron emission must be accelerated locally within the jet, otherwise expansion losses would lead to very high total power requirements. One way of achieving this, which is discussed in Blandford and McKee (1977); Jones and Tobin (1977); Marscher (1978), utilizes strong shock waves. The mean electron energy behind a mildly relativistic shock propagating into an electron-proton plasma is likely to be $\gtrsim$ 100 MeV, which is adequate to account for the observed radio emission. For this reason, the non-thermal radiative efficiency of the shock can be quite high. The above papers dealt with spherical blast waves and concentrated on the radiative properties of the shocks. In this paper we turn our attention more to the geometrical consequences of assuming that these shocks are confined to a jet. Such shocks could be associated either with dense clouds accelerated by the flow or with an unsteady velocity field in the jet.

In §II we describe some general kinematical consequences of relativistic motion which are relevant to our model. In §III we present an idealized description of the steady radio emission from a relativistic jet, based on a set of simple assumptions. The variable component of the emission, which we associate with shock waves traveling in the jet, is discussed in §IV.

Specifically, we examine the dynamical and radiative properties of accelerated clouds and of velocity disturbances which steepen to form propagating shocks. In §V we show that several observed features of compact radio sources can be interpreted on the assumption that these sources are relativistic jets which are viewed at small angles to their axes. In addition, we examine several other consequences of this hypothesis. Our results are summarized in §VI.

II. OBSERVABLE CONSEQUENCES OF RELATIVISTIC MOTION

a) Kinematics

The kinematical consequences of relativistic motion have been described by several authors and are reviewed in Blandford, McKee, and Rees (1977). For a source moving at time t with a space velocity (in units of c) $\underline{\beta}(t)$ in a direction making an angle Θ with the direction of the observer $\underline{n}$, the observed velocity $\underline{\beta}_{ob}$ is given by

$$\underline{\beta}_{ob} = \frac{\underline{n} \times (\underline{\beta} \times \underline{n})}{1 - \underline{\beta} \cdot \underline{n}} \quad . \tag{1}$$

The acceleration of the source is

$$\underline{g} = d(\gamma\underline{\beta})/dt = \gamma d\underline{\beta}/dt + \gamma^3(\underline{\beta} \cdot d\underline{\beta}/dt)\ \underline{\beta} \quad , \tag{2}$$

where $\gamma = (1 - \beta^2)^{-1/2}$. The observed rate of change of $\underline{\beta}_{ob}$ is

$$\frac{d\underline{\beta}_{ob}}{dt_{ob}} = (1 - \underline{\beta} \cdot \underline{n})^{-3} [(1 - \underline{\beta} \cdot \underline{n})\ d\underline{\beta}/dt + (d\underline{\beta}/dt \cdot \underline{n})\ (\underline{\beta} - \underline{n})] \quad , \tag{3}$$

where t_{ob} is the observer's time. In the case of linear acceleration ($\underline{g} \times \underline{\beta} = 0$), the vector $d\underline{\beta}_{ob}/dt_{ob}$ is collinear with $\underline{\beta}_{ob}$ and of magnitude

$$\frac{d\beta_{ob}}{dt_{ob}} = \mathcal{D}^3 \sin\Theta\ g \quad , \tag{4}$$

where $\mathcal{D}$, the Doppler factor, is given by $\mathcal{D} = \gamma^{-1}(1 - \underline{\beta} \cdot \underline{n})^{-1}$. The maximum value of $d\beta_{ob}/dt_{ob}$ is $g\ \mathrm{cosec}^2\Theta$. For a uniform circular motion ($\underline{g} \cdot \underline{\beta} = 0$), $\mathcal{D}$ will be maximized when $\underline{g} \cdot \underline{n} = 0$, and then

$$d\underline{\beta}_{ob}/dt_{ob} = \gamma\mathcal{D}^2\underline{g} \quad . \tag{5}$$

The Doppler factor can also be written in terms of β_{ob} as

$$\mathcal{D} = (1 - \beta_{ob}^2 + 2\beta_{ob} \cot \theta)^{1/2} \quad . \tag{6}$$

For a given value of θ (less than $\pi/2$), $\mathcal{D}$ rises with increasing β_{ob} as $1 + \beta_{ob} \cot \theta$ for $\beta_{ob} \ll 1$, reaches a maximum value of cosec θ at $\beta_{ob} = \cot \theta$, declines to 1 when $\beta_{ob} = 2 \cot \theta$, and finally declines to zero as β_{ob} approaches its asymptotic value of $\cot(\theta/2)$.

b) Observed Flux

For a moving source we can relate S_{ob}, the observed flux density, to S, the flux density that would be observed at the same frequency ν in the co-moving frame, by

$$S_{ob}(\nu) = S(\nu)\, \mathcal{D}^{3+\alpha} \quad , \tag{7}$$

where α is the spectral index ($- d\ell nS/d\ell n\nu$). [Equation (7) is true for optically-thin sources and spherical optically-thick sources. For non-spherical optically-thick sources, changes in aspect must be taken into account.] In Figure 1 we plot $S_{ob}(\beta_{ob})$ for different viewing angles θ, assuming that $\alpha = 0.5$ and that S is constant. For an accelerating source, the flux will at first rise until $\beta = \cos \theta$, and then decline as the emitted radiation is beamed away from the observer direction.

For a narrow stationary cylindrical jet, however, it is the observed surface brightness Σ_{ob} that is important. For an optically thin source, this is related to the surface brightness $\Sigma_{\perp}$ that would be measured by a co-moving observer whose line of sight was perpendicular to the jet velocity

by

$$\Sigma_{ob}(\nu) = \Sigma_{\perp}(\nu)\, \mathcal{D}^{(2+\alpha)} \text{ cosec } \Theta \quad . \tag{8}$$

If a source combines parts moving with different speeds, then according to both equations (7) and (8) a distant observer will see predominantly those parts that are moving with $\beta \sim \cos\Theta$, for which the Doppler factor $\mathcal{D}$ is maximized.

c) Flux Variation

The observed flux from a relativistically moving source can vary either kinematically or as a consequence of intrinsic variability in the co-moving flux S. Differentiating equation (7), we obtain

$$\delta \ell n S_{ob} = \delta \ell n S + (3 + \alpha)\left\{\left(\frac{\mathcal{D} - \gamma}{\gamma\beta^2}\right) \delta \ell n \gamma + \gamma\beta\mathcal{D}\delta \cos\Theta\right\} \quad . \tag{9}$$

In the small angle, ultra-relativistic approximation, this becomes

$$\delta \ell n S_{ob} = S \ell n S + \frac{(3 + \alpha)}{(1 + \gamma^2\Theta^2)} \left\{(1 - \gamma^2\Theta^2)\, \delta \ell n \gamma - 2\gamma^2\Theta\delta\Theta\right\} \quad . \tag{10}$$

In this limit, it is the third term associated with curvature in the trajectory that is most likely to dominate the variation.

d) Observer-Averaged Mean Flux

If an observed compact radio source comprises several rapidly moving components, then we must use the observer time-average for the mean flux. If similar radio sources are formed at a rate R with a constant intrinsic flux S and move with a fixed velocity $\underline{\beta}$ out to some fixed radius r_d

(roughly the length scale for decay of the flux), then the mean observed flux will be given by

$$\overline{S}_{ob} = \mathcal{D}^{(3+\alpha)} \, (1 - \beta \cos \Theta) \, R(r_d/\beta c) \, S \quad . \tag{11}$$

Alternatively, if each source has an acceleration $\underline{g}(\gamma\beta)$, then the observed flux will peak when β is closest to cos Θ. For linear acceleration, the mean observed flux will be given by

$$\overline{S}_{ob} = \int d\beta \, R \, S \, g^{-1} \gamma^2 \mathcal{D}^{2+\alpha} \quad . \tag{12}$$

For uniform circular motion,

$$\overline{S}_{ob} = \int d\chi \, R \, S \, \beta \, g^{-1} \mathcal{D}^{2+\alpha} \quad , \tag{13}$$

where χ, the orbital phase, is related to Θ and Θ_o, the inclination of the orbital plane, through cos Θ = cos Θ_o cos χ.

The integrals in equations (12) and (13) are elementary if S and g are constant (a fair approximation for small Θ) and $\alpha = 0$. Assuming that the linearly-accelerating source radiates for $0 \leq \beta \leq \beta_1$, we obtain

$$\overline{S}_{ob} = RSg^{-1}\beta_1(1 - \beta_1 \cos \Theta)^{-1} \quad . \tag{14}$$

Likewise, for a circularly-accelerating source radiating for a single revolution,

$$\overline{S}_{ob} = 2\pi RSg^{-1}\gamma^{-2}\beta(1 - \beta^2 \cos^2 \Theta_o)^{-3/2} \quad . \tag{15}$$

More generally, for $\Theta, \Theta_o \gtrsim \gamma^{-1}$, equations (12) and (13) can be approximated by $\overline{S}_{ob} \sim RSg^{-1}(\Theta) \, \Theta^{-(2+\alpha)}$ and $\overline{S}_{ob} \sim RSg^{-1}(\Theta_o) \, \Theta_o^{-(1+\alpha)}$, respectively. One

important corollary follows from these expressions. Suppose that the sources have roughly the same constant acceleration and intrinsic fluxes, and that their velocities are contained within a finite range of solid angles that includes the observer direction $\underline{n}$. Then if $\alpha > 0$, the mean observed power will be dominated, for both linear and circular accelerations, by those sources moving with $\Theta \lesssim \gamma^{-1}$. The background flux arising from sources that have $\Theta \gg \gamma^{-1}$ can generally be ignored. This argument is relevant to our interpretation of sources which are confined to two antiparallel jets (see § V).

e) Polarization

A further important feature of the radiation observed from an accelerating source is the characteristic swing in the polarization position angle.

We consider first the case of collinear acceleration. Suppose that the magnetic field $\underline{B}$ in the source is uniform and its observed direction is specified by the angles (η, ψ), as defined in Figure 2a. If the radiation is produced by the synchrotron process, then the electric vector $\underline{e}$ in the comoving frame will be normal to the magnetic field direction (as well as to the emission direction $\underline{k}$). We can thus use the fact that the Lorentz invariant $\underline{e} \cdot \underline{B} = 0$ to solve for the observed position angle ξ. A straightforward calculation yields

$$\tan \xi = \frac{\cos \psi[\beta - \cos \Theta(1 - \tan \psi \tan \Theta)]}{\tan \eta(\beta \cos \Theta - 1)} , \qquad (16)$$

where $\underline{\beta}c$ is the velocity of the source and Θ is the angle between $\underline{\beta}$ and the observer direction $\underline{n}$. The dependence of ξ on β is due to the fact that, as β changes, so does the aberration angle (the angle between $\underline{k}$ and $\underline{n}$),

and that $\underline{e}$ must remain normal to $\underline{k}$.

We shall be most interested in the limit $\psi, \Theta \ll 1$, $\beta \to 1$ appropriate for a relativistic source with magnetic field roughly perpendicular to its velocity (see §V). According to equation (16), ξ will then swing very rapidly from a constant value $\xi \sim (\pi/2 - \eta)$ to a constant value $\xi \sim (\eta - \pi/2)$ when $\beta \sim (\cos\Theta - \sin\Theta \tan\Psi)$. For a given value of the viewing angle Θ, the velocity at which the swing occurs depends rather sensitively on ψ, whereas the amplitude of the swing is determined primarily by η. The maximum observable amplitude of the swing is 180^{o}. A specific example of this phenomenon in an accelerating source is shown in Figure 2b and discussed in § V. (Sources decelerating from relativistic speeds would exhibit similar polarization swings.)

For a uniform circular motion (described by the angles Θ_o, χ as before), we can assume either that the magnetic field direction is fixed in space or that it is convected with a constant orientation with respect to $\underline{\beta}$. In the former case,

$$\tan\xi = \frac{\cos\psi[\beta\cos\chi - \cos\Theta_o(1 - \tan\Theta_o\tan\psi)]}{\tan\eta[\beta\cos\chi\cos\Theta_o - 1] + \beta\sin\chi\sin(\Theta_o + \psi)}\ , \qquad (17)$$

and the swing in position angle is similar to that given by equation (16). For a convected field,

$$\tan\xi = \frac{\cos\psi_o[\beta\cos\chi - \cos\Theta_o(1 - \tan\Theta_o\tan\psi_o\cos\chi)] + \sin\Theta_o\tan\eta_o\sin\chi}{\tan\eta_o(\beta\cos\Theta_o - \cos\chi) + \sin\chi(\sin\psi_o + \beta\cos\psi_o\sin\Theta_o)} \qquad (18)$$

(where η_o and ψ_o are the respective values of η and ψ at $\chi = 0$), and the observed polarization position angle behaves rather differently. In the limit $\gamma^{-1} \ll \Theta_o, \psi_o \ll 1$ the effects of convection and aberration will

cancel each other, and ξ will have an approximately constant value of $\sim (\eta - \pi/2)$ when the source is bright. Both types of magnetic field behavior could occur in realistic source geometries. Related formulae for the polarization swing in circular motion have been given by Ferguson (1971).

III. RADIO EMISSION FROM A STEADY JET

a) Jet Properties

In this section we present an idealized model of a steady radio jet. This allows us to quantify our discussion and derive expressions for observable quantities. We consider a narrow conical jet of small semi-angle φ whose axis makes an angle Θ with the direction of the observer (the observed opening angle is $\phi_{ob} = \phi$ cosec Θ). We assume that the jet is supersonic and free, and that it has a constant velocity β_j. The jet convects a tangled magnetic field B (measured in the frame of the fluid) which will vary as r^{-1}, where r is the distance from the apex (cf. the model of NGC 6251 in Readhead, Cohen, and Blandford 1978). We assume that relativistic electrons can be accelerated continuously within the jet, and that their distribution function is $N(\gamma_e) = K\gamma_e^{-2}$, with $\gamma_{e\ min} < \gamma_e < \gamma_{e\ max}$ and $\gamma_{e\ max} \gg \gamma_{e\ min}$. These electrons will radiate synchrotron radiation with a spectral index $\alpha = 1/2$. The electron energy density $u_e = K\Lambda m_e c^2$ [with $\Lambda = \ell n(\gamma_{e\ max}/\gamma_{e\ min})$] is insensitive to the exact values of $\gamma_{e\ min}$ and $\gamma_{e\ max}$, and we assume approximate equipartition with the magnetic energy density,

$$u_e = k_e \Lambda B^2/8\pi \quad , \tag{19}$$

where k_e is a constant $\lesssim 1$. This implies that the effective Mach number $\mathcal{M}$

of the jet (the ratio of its proper velocity to the proper speed of sound) is constant. If the electrons (mass m_e) are neutralized by protons (mass m_p) exerting a negligible pressure, then

$$\mathcal{M} \sim [\gamma_{e\ min}(m_e/m_p)(\Lambda/3 + 1/k_e)]^{-1/2}\ \gamma_j\beta_j \quad , \tag{20}$$

$$1 \ll \gamma_{e\ min} \ll (m_p/m_e) \quad .$$

A free jet would have $\phi \gtrsim \mathcal{M}^{-1}$, but if $\gamma_{e\ min} \sim$ 10-100, as indicated by Faraday rotation measurements (e.g., Wardle 1977), then we expect that $\phi \lesssim \gamma_j^{-1}$. This relation should also hold in the case of a relativistic electron-positron plasma (for which $\mathcal{M} \sim \gamma_j\beta_j$) if γ_j is large.

b) Radiative Properties

An important consequence of the equipartition assumption is that the relativistic electrons must remain roughly isothermal as the particle density and internal energy density both decay as r^{-2}. There must then be ongoing particle acceleration to compensate for the cooling associated with adiabatic decompression in the expanding jet. An estimate of the upper cutoff in the electron distribution function $\gamma_{e\ max}$ can be obtained by equating the synchrotron cooling time $t_s' \sim 3 \times 10^7\ \gamma_j \mathcal{D}_j^{1/2} \nu_9^{-1/2} B^{-3/2} s$ to the expansion time $\sim 1 \times 10^8\ r_{ob}$ cosec $\Theta\ \beta_j^{-1} s$, which should be comparable to the re-acceleration time scale of the relativistic electrons. Here $\mathcal{D}_j$ is the Doppler factor of the jet, ν is measured in GHz, B is measured in Gauss and $\mathcal{D}_j / r_{ob} = r \sin \Theta$, the observed radius, is measured in pc. The observed optically thin spectrum from r_{ob} should thus have a slope of $\alpha = 0.5$ up to the frequency

$$\nu_{u9}(r_{ob}) = 0.07\ (1 + z)^{-1}\ \gamma_j^2 \beta_j^2 \mathcal{D}_j\ \text{cosec}\ \Theta\ B_1^{-3} r_{ob} \quad , \tag{21}$$

which is the characteristic emission frequency of an electron with Lorentz factor $\gamma_{e\ max}$. (z is the redshift of the source and the subscript 1 indicates a quantity measured at r = 1 pc.) Provided that the injected electron distribution function has the same slope for $\gamma_e \gtrsim \gamma_{e\,max}$, then the local radiation spectrum would steepen at frequencies $\nu > \nu_u$ to $\alpha \sim 1$, as a result of synchrotron losses (cf. Kellermann 1966). If the emission region extends from r_{min} to r_{max} then, apart from some model-dependent geometrical and spectral factors of order unity, the total synchrotron power radiated by the jet is

$$L_s \approx 1/2\ k_e(1 + 2/3\ k_e\Lambda)^{-1}\ L \quad , \tag{22}$$

where $L = 10^{44}L_{44}$ erg s^{-1} is the total power carried by the jet in the form of relativistic electrons and magnetic field, and is given by

$$L \approx 1/4\ \Delta(1 + 2/3\ k_e\Lambda)\ \gamma_j^{\,2}\beta_j c B_1^{\,2}\phi^2 \quad , \tag{23}$$

where $\Delta = \ell n(r_{max}/r_{min})$. (We assume that other contributions to the internal power in the jet can be ignored.) The jet is therefore a fairly efficient radiator, in which the radiated energy is constantly replenished by dissipation of the bulk kinetic energy. Indeed, we expect that γ_j would decline slowly with r. In addition, the ratio of the co-moving synchrotron-radiation energy density to the magnetic energy density is constant and given by

$$u_s/(B^2/8\pi) \sim k_e\beta_j\gamma_j\phi \quad . \tag{24}$$

If, as we expect, $\gamma_j \leq \phi^{-1}$ in the strongest observed sources,

then equation (24) implies that the Compton power will not exceed the synchrotron power. In fact, if γ_j were $\gg \phi^{-1}$, then the Compton losses would probably be so severe as to decelerate the jet until $\gamma_j \sim \phi^{-1}$.

The brightness temperature in the co-moving frame will not greatly differ from the critical value of $T' \sim 10^{12}$ K (e.g., Kellermann and Pauliny-Toth 1969). The observed brightness temperature can be calculated using equation (8). In our model,

$$T(\nu, r) \approx 3 \times 10^{10}(1+z)^{-1/2}\nu_9^{1/2}B_1^{-1/2}\mathcal{D}_j^{1/2}r_{ob}^{1/2}(\sin\theta)^{-1/2}\,(1 - e^{-\tau})\ \mathrm{K}\ , \quad (25)$$

where τ is the optical depth to synchrotron self-absorption which, for a line of sight through the jet that passes at a distance d from the jet axis, is given by

$$\tau(\nu, r) \approx 500(1+z)^{-3}K_1B_1^{2}\nu_9^{-3}\mathcal{D}_j^{2}\sin^2\theta(\phi^2 - \delta^2)^{1/2}\, r_{ob}^{-3}\ , \quad (26)$$

$$0 \le \delta = \tan^{-1}(d/r) \le \phi\ .$$

Differentiating equation (25) with respect to r and substituting equations (19), (21), and (23), we find that the brightness temperature has a maximum value, <u>independent of frequency</u>, of

$$T_{max} = \mathcal{D}_j(1+z)^{-1}T'_{max} \approx 3 \times 10^{11}(1+z)^{-1}k_e^{1/6}(1 + 2/3\ k_e\Lambda)^{-1/12}$$
$$\Delta^{-1/12}\gamma_j^{-1/6}\beta_j^{-1/12}\,\mathcal{D}_j^{5/6}(\sin\theta)^{-1/3}\phi_{ob}^{-1/6}L_{44}^{1/12}K \quad (27)$$

on the jet axis ($\delta = 0$), at a projected radius of

$$r_{max\ ob} \approx 3(1+z)^{-1}\ k_e^{1/3}\Delta^{-2/3}(1 + 2/3\ k_e\Lambda)^{-2/3}\gamma_j^{-4/3}\beta_j^{-2/3}$$
$$\mathcal{D}_j^{2/3}(\sin\theta)^{-1/3}\ \phi_{ob}^{-1}L_{44}^{2/3}\nu_9^{-1}\ . \quad (28)$$

Note that, apart from the Doppler factor, equation (27) is very insensitive to the jet parameters. Since, for a given baseline, the angular resolution of a VLBI measurement is proportional to the observed wavelength, the fact that $r_{ob\ max} \propto \nu^{-1}$ indicates that if the "core" of the jet appears to be unresolved at a given frequency, it will remain so at other frequencies.

The observed flux $S_{ob} \propto \nu^2 r_{ob\ max}^2 T_{max}$ is also independent of frequency, and so the jet will appear to have a flat spectrum of flux density

$$S_{ob} \approx 0.5(1+z) k_e^{5/6} \Delta^{-17/12} (1 + 2/3\ k_e \Lambda)^{-17/12} \gamma_j^{-17/6} \beta_j^{-17/12} \mathcal{D}_j^{13/6} (\sin\Theta)^{-5/6} \phi_{ob}^{-1} L_{44}^{17/12} D_{\ell 9}^{-2} J_y \quad , \tag{29}$$

where $D_{\ell 9}$ Gpc is the <u>luminosity</u> distance to the source.

The spectrum will be flat up to the frequency ν_b, the upper cutoff frequency ν_u of the electron energy distribution evaluated at the radius r_b, where the maximum brightness temperature is achieved. Combining equations (21) and (28), we obtain (for $\delta = 0$)

$$\nu_{b9} \approx 60(1+z)^{-1} k_e^{1/6} \Delta^{5/12} (1 + 2/3\ k_e \Lambda)^{5/12} \gamma_j^{11/6} \beta_j^{17/12} \mathcal{D}_j^{5/6} (\sin\Theta)^{5/6} \phi_{ob} L_{44}^{-5/12} \tag{30}$$

and

$$r_{b\ ob} \approx 0.04\ k_e^{1/6} \Delta^{-13/12} (1 + 2/3\ k_e \Lambda)^{-13/12} \gamma_j^{-19/6} \beta_j^{-25/12} \mathcal{D}_j^{-1/6} (\sin\Theta)^{-7/6}\ \phi_{ob}^{-2} L_{44}^{13/12} \quad . \tag{31}$$

For $\nu > \nu_b$ the spectrum will be dominated by the contribution from $r \lesssim r_b$ and will steepen to $\alpha \sim 1$ (again, as a consequence of synchrotron losses). The detailed high frequency spectrum depends on the efficiency of the particle acceleration in the innermost parts of the jet.

c) Polarization

The degree of polarization of the synchrotron radiation from the jet reflects the degree of order in the magnetic field. The magnetic field law $B \propto r^{-1}$ refers in fact only to the transverse component, whereas the parallel component scales as $B_{\|} \propto r^{-2}$. However, only a small degree of shear in the flow is necessary to isotropize the field. The degree of polarization should be higher at optical wavelengths than at radio wavelengths, because for $\nu > \nu_b$ the jet is optically-thin, and also because the magnetic field will presumably maintain a higher degree of order over the smaller emission region ($r \lesssim r_b$) of the optical radiation. The observed position angle is more difficult to interpret, especially if the angle Θ is small, as we suggest below, and projection effects become important. Furthermore, as the emission at different frequencies originates from different radii, both the degree and the direction of intrinsic polarization may vary with radio frequency.

We can, however, estimate the Faraday rotation across the jet. This is probably dominated by the lowest energy relativistic electrons (Wardle 1977, Jones and O'Dell 1977). As long as the electron distribution function remains unchanged, the rotation $\Delta\Phi \propto KB\nu^{-2}r$, evaluated at $r_{max}(\nu)$ is also independent of frequency, and is given (for $\delta = 0$) by

$$\Delta\Phi(r_{max}(\nu)) \approx 4 \times 10^{4}\ k_e^{1/3}\Delta^{-1/6}(1 + 2/3\ \ k_e\Lambda)^{-1/6}\gamma_j^{-1/3}\beta_j^{-1/6}\mathcal{D}_j^{-1/3}(\sin\Theta)^{-1/3}$$
$$L_{44}^{1/6}F \text{ rad} \quad , \qquad (32)$$

where F is a factor determined by the shape of the distribution function near $\gamma_{e\ min}$. For a finite power law,

$$F \sim \gamma_{e\ min}^{-3} \ell n(\gamma_{e\ min}) \qquad (33)$$

(Wardle 1977). Equation (32) represents an upper bound for $\Delta\Phi$ in the optically-thin regions of the jet, which can be reduced if there is small-scale disorder in the field. For a relativistic electron-positron plasma, the Faraday rotation will be zero, although the effects of repolarization may be observable.

Equations (27)-(32) are the principal results of our study of this model and allow the parameters of the jet to be estimated using observed quantities. (However, they may also apply to other models which do not involve jets.) In deriving these expressions we have combined some fairly common assumptions, such as flux freezing and equipartition, with a few rather specific postulates (constant γ_j and φ, emission spectrum with $\alpha = 0.5$) in order to make the model as simple as possible. In §V we apply these estimates to the source 3C345.

IV. RADIO VARIABILITY

In the previous section we showed how steady radio emission may originate from a relativistic jet. Compact radio sources, however, are characterized by variability in both their total flux and radio structure. In this section we describe two mechanisms whereby time-dependent phenomena can arise — the acceleration of clouds and the propagation of shocks within the jet.

a) Dynamics of a Cloud

If we immerse a small, dense blob of gas in a rapidly moving jet, it will quickly come into rough pressure equilibrium with its surroundings,

and form a cloud of mass M and internal energy E_o. (The subscript o will be used to denote the initial parameters of the cloud.) The cloud will then be accelerated by the jet and expand as it moves downstream. We shall assume that the expansion is adiabatic with a specific heat ratio $\Gamma = 5/3$ [the generalization to a relativistic equation of state is straightforward; cf. Christiansen, Scott, and Vestrand (1978)]. The equations governing the acceleration and expansion of the cloud are

$$Mg = Mcd(\gamma\beta)/dt = k_a p_a h^2 \tag{34}$$

$$p_a = k_b \gamma^2 (\beta_j - \beta)^2 \omega_j \tag{35}$$

$$E = k_c Mgh = E_o (h/h_o)^{-2} \tag{36}$$

(cf. Blandford and Königl 1978). Here γ and βc are the Lorentz factor and velocity of the cloud, respectively, and h, the scale height of the cloud, is defined by $h = p_a/\rho_a g$ (where p_a and ρ_a are the pressure and rest mass density of the cloud at its upstream end). ω_j is the enthalpy density in the jet. In the model of §III, $\omega_j \sim K m_p c^2/\gamma_{e\ min}$ for a plasma dominated by the inertia of cold protons, whereas $\omega_j \sim (4/3\ K\Lambda m_e c^2 + B^2/4\pi)$ for a relativistic electron-positron plasma. In this section we allow the cross-sectional area A of the jet to increase as an arbitrary power of the radius, $A \propto r^n$. (n = 2 gives a conical jet which may be free. n = 1 corresponds to a paraboloidal jet which requires transverse pressure support.) We assume that the speed of the jet is highly supersonic with respect to the cloud, in which case a strong standing bow shock will form upstream from the cloud (cf. Blandford and Königl 1978). k_a, k_b, and k_c are constants fixed by detailed assumptions about the nature of the shock and of the cloud. k_b

may be estimated by imposing the continuity conditions for the energy and momentum fluxes across the shock in the frame of the cloud, and assuming that behind the shock the fluid flows adiabatically with a specific heat ratio $\Gamma = 4/3$. With these assumptions $k_b = 0.84$. (For comparison, $k_b = 0.88$ in the Newtonian limit.) In addition, we adopt for the cloud the isothermal model of De Young and Axford (1967), for which $k_a = (\pi/2)(\pi^2 - 4) = 9.2$ and $k_c = 1.5$.

We now specialize to an ultra-relativistic jet with constant velocity $\beta_j \sim 1$. For a cloud starting from rest at r_o, the equation of motion is

$$\left(\frac{1+\beta}{1-\beta}\right)^{3/5} \beta \frac{d(\gamma\beta)}{dx} = a x^{-3n/5} \quad , \tag{37}$$

where $x = r/r_o$ and

$$a = \frac{k_a k_b r_o h_o^2 \gamma_j^2 \omega_j}{Mc^2} = 4.4 \times 10^{-2} k_d r_o L_{44} M^{-1} (h_o^2/A_o) \quad , \tag{38}$$

measuring r_o in pc and M in $M_\odot$. k_d is a constant which, in the model of §III, equals $(k_e/\gamma_{e\,min})(m_p/m_e)[\Delta(2 + 4/3\, k_e \Lambda)]^{-1}$ for an electron-proton plasma, and Δ^{-1} for an electron-positron plasma. Equation (37) has the approximate solution

$$\begin{aligned} \gamma\beta &\simeq \left[\frac{10a}{5-3n}\left(x^{(5-3n)/5} - 1\right)\right]^{1/2} && \text{for } \gamma\beta \ll 1 \\ &\simeq \left[2^{-6/5}\frac{11a}{5-3n}\left(x^{(5-3n)/5} - 1\right)\right]^{5/11} && \text{for } \gamma\beta \gg 1 \quad . \end{aligned} \tag{39}$$

Thus, if the channel area increases more rapidly with radius than $r^{5/3}$, as it does when the jet expands freely, then the cloud will not attain the jet velocity, but will instead approach a smaller maximum speed determined by the acceleration parameter a. If $n < 5/3$, the momentum flux falls

sufficiently slowly with r that the cloud will eventually be accelerated to $\beta \sim \beta_j$ for any value of a. g is always largest close to r_o, which is probably much smaller than the radius at which the source is observed. In this case no significant acceleration would be observed for $n > 5/3$, and for $n < 5/3$ we can apply equation (4) when the source is brightest (i.e., when $\beta_{ob} = \text{cosec}\,\theta = \gamma = \mathcal{D}$) to obtain

$$\frac{d\ell n(\beta_{ob})}{d\ell n(r_{ob})} \simeq \left(\frac{5 - 3n}{11}\right) , \qquad n < 5/3 \quad . \tag{40}$$

The scale height h evolves according to

$$h = h_o x^{n/5} \gamma^{-2/5} (1 - \beta/\beta_j)^{-2/5} \quad , \tag{41}$$

and increases with x. In the ultra-relativistic case considered here, $h \propto x^{(2+n)/11}$ for $n < 5/3$ and $x \gg 1$; the requirement that h increase slower than the jet width then implies $n > 4/9$. The solution of equation (37) can be integrated once more (numerically) to obtain x(t). The general features of the motion do not seem to be particularly sensitive to our assumptions, unless inhomogeneity in the jet causes the cloud to be deflected through an angle $\delta\theta \gtrsim \gamma^{-1}$ (cf. Christiansen and Scott 1977).

b) Radiative Properties

A large fraction of the bulk kinetic energy flux in the jet which is incident upon the cloud will be dissipated in the strong bow shock, and some of this energy may appear in relativistic electrons behind the shock. In addition, if the jet carries a frozen-in magnetic field, it will be amplified behind the shock. This is therefore a likely site for synchrotron

and inverse-Compton radiation (cf. Blandford and McKee 1977, Jones and Tobin 1977). The nature of the flux variations that would be observed from a cloud accelerating according to equations (34)-(36) is illustrated in Figure 3 for a paraboloidal jet (n = 1). The observed time evolution of the flux is plotted for two different radiative assumptions:

(i) The power radiated in the frame of the cloud is proportional to the rate of dissipation of jet kinetic energy in the frame of the shock, and the spectrum extends up to a fixed maximum frequency with $\alpha = 0.5$, i.e.,

$$S_{ob}(\nu) \propto \mathcal{D}^{3.5}\, g\left(\frac{\beta_j - \beta}{1 - \beta\beta_j}\right) \quad . \tag{42}$$

(We are assuming that the radiation is emitted in a frame which moves with the velocity of the cloud, although in practice the relevant velocity will be somewhat greater than β.)

(ii) As in §III, we assume that the electrons behind the shock have a power-law energy distribution $N(\gamma_e) = K\gamma_e^{-2}$, and emit synchrotron radiation in an equipartition magnetic field, i.e., $K \propto B^2 \propto p_a$. The cloud may initially be optically thick due to synchrotron self-absorption, but the optical depth τ decreases as the cloud expands.

Also plotted in Figure 3 is the observed velocity β_{ob} [eq. (1)] as a function of t_{ob}. In order for superluminal motion to be observed, it is necessary that the flux remain appreciable when high values of β_{ob} are attained. This condition is not fulfilled in case (i), where the flux peaks at relatively small values of β_{ob}, and then declines rapidly with decreasing acceleration. In case (ii), however, the peak in the flux occurs when $\tau \sim 1$, and may be reached at large values of β_{ob} if the source is

initially opaque with $\tau_o \gg 1$.

c) Origin of the Clouds

The clouds that we envision are much denser than the jet and much smaller than the jet's width ($h \ll A^{1/2}$). Their sizes are also limited by the requirement that, as measured in the cloud frame, the time scale for pressure equilibration [$\sim (h/g)^{1/2}$] be much smaller than either the acceleration time scale ($\sim \beta c/g$) or the travel time [$\sim (r - r_o)/\gamma\beta c$]. However, the clouds should be large enough to form effective obstacles in the jet. The type of astronomical object which satisfies these requirements depends on the physical conditions in the jet at a distance $\lesssim 1$ pc from its origin, where we expect the clouds to be formed.

One plausible class of objects may be associated with emission-line filaments. Most quasars and Seyfert 1 galaxies exhibit broad emission lines in their spectra. These are generally interpreted as originating in dense ($\sim 10^{-15}$ g cm^{-3}), photo-ionized clouds. General arguments (e.g., Osterbrock 1978) indicate that these clouds are located at a distance $r_o \sim 0.3$ pc from the central continuum source and move coherently with a velocity $v \sim 10^4$ km s^{-1}. (However, if the optical continuum is itself beamed, r_o may be smaller.)

If a cloud of size h_o enters the jet with a transverse speed $v_\perp$, it will fragment whilst entering the flow unless $v_\perp$ is large enough, but will leave the opposite side of the jet before being accelerated by the flow if $v_\perp$ is too large. This implies that

$$(g_o h_o)^{1/2} \lesssim v_\perp \lesssim (g_o r_o)^{1/2}\, \varphi \quad . \tag{43}$$

Adopting the standard cloud parameters quoted above, and estimating g_o with equation (38) using $k_d = 1$, these inequalities become

$$(h_o/10^{13}\ \mathrm{cm}) \lesssim L_{44} \lesssim 10^5\, \varphi^2 \quad . \tag{44}$$

Conditions (44) will generally be satisfied by clouds of size $h_o \sim 10^{13} - 10^{15}$ cm, which is consistent with the range that is indicated by independent arguments (e.g., Shields 1978).

As discussed in Blandford and Königl (1978), supernova explosions provide an alternative source of clouds. It is difficult to assess the likelihood of this happening within a jet, but if the explosion involves an energy $U = 10^{51} U_{51}$ erg, then the ejecta will expand to a radius $\sim 10^{17}\, U_{51}^{1/3} L_{44}^{-1/3} A_{o34}^{1/3}$ cm before being stopped by the impact with the

jet. Large nova explosions with energies ~ 10^{48} erg may likewise give rise to clouds which, if formed sufficiently close to the origin of the jet, will block a significant fraction of its width.

d) Propagation of Shocks in a Relativistic Jet

An alternative source of radio variability is non-steady motion within the jet itself. Dissipative behavior close to the origin, resulting perhaps from surface instabilities, may lead to fluctuations in the radial velocity. Even if the amplitude of these disturbances is initially small, they may steepen and form shocks further out in the jet (Rees 1978). A sufficiently strong shock could appear to a distant observer like a separate radio component moving with a Lorentz factor $\gamma \gtrsim \gamma_j$. The Lorentz factor γ_1 of the emitting material behind the shock remains close to γ; in fact, $\gamma_1 = \gamma/\sqrt{2}$ for $\gamma \gg \gamma_j$, and becomes comparable to γ when γ approaches γ_j. The kinematical and radiative properties of the shock will thus be similar to those of a cloud moving with a Lorentz factor γ. For an electron-proton plasma, the mean Lorentz factor $\bar{\gamma}_e$ associated with the random electron motion behind the shock can be estimated in the limit $\gamma_j \gg 1$ as

$$\bar{\gamma}_e \sim \frac{500(\gamma^2 - \gamma_j^2)^2}{(\gamma^2 + \gamma_j^2)\,\gamma\gamma_j} \tag{45}$$

(Blandford and McKee 1977). Thus, as the shock weakens and γ approaches γ_j, the accelerated electrons will have the sub-GeV energies implied from radio observations. However, if the bulk motion is relativistic, the emission will still be beamed with a high Doppler factor, which will then in fact be comparable with the Doppler factor of the steady emission from

the jet.

It may be possible to discriminate observationally (with VLBI) between the accelerating cloud and propagating shock models, by searching for an asymmetry in the brightness distribution of moving radio components. Accelerating clouds should have the steepest radio contours facing the nuclear core, whereas the reverse should hold for propagating shocks, as well as for decelerating clouds (cf. Christiansen et al. 1978). Furthermore, it may even be possible for the acceleration or the deceleration to be directly observable [cf. eqs. (3)-(5) and (40)].

In §III we postulated that the relativistic electrons are able to remain effectively isothermal in the expanding jet. This may conceivably be achieved by weak shocks and fluid turbulence associated with noise in the jet. The details of these processes will be discussed elsewhere.

V. COMPACT RADIO SOURCES

a) Radio Flux

Compact radio sources (i.e., those whose flux at an intermediate radio frequency, e.g., ~ 1 GHz, is dominated by the contribution of a single bright component smaller than ~ 1 kpc in size) usually exhibit flat radio spectra and radio variability (e.g., Brandie et al. 1974). In addition, the ratio of optical to radio power tends to be higher in these objects than in steep-spectrum sources (e.g., Usher 1975), making identification easier (e.g., Condon et al. 1975). Flat-spectrum radio sources are nearly always associated with quasars (Wall 1975), although only ~ 5 percent of quasars are radio-loud (e.g., Sramek and Weedman 1978).

The fluxes at high (i.e., $\gtrsim$ 1 GHz) radio frequencies seem to vary on time scales roughly proportional to the wavelength, indicating the presence of a constant ($\sim 10^{12}$ K) brightness temperature (e.g., O'Dell 1978). This temperature, which is confirmed by VLBI measurements, is generally slightly greater than the inverse Compton limit for a non-relativistic source. In §III, we have described the radio properties of a simple model of a steady jet. We have found that if we make simple but natural assumptions about the magnetic field and relativistic electron distribution function, then the source inhomogeneity leads to a flat spectrum and constant temperature (cf. also Condon and Dressel 1973, de Bruyn 1976). Variability can be induced by either clouds or shocks, which will be observed moving at approximately a constant speed, as discussed in §IV. The variability time scale should be comparable to the dynamical time scale and will thus be roughly proportional to r, and hence to λ [cf. eq. (28)].

b) Angular Structure

The analysis of VLBI observations, whilst still somewhat subjective, has improved over recent years as a result of more complete baseline coverage and the use of more sophisticated Fourier-inversion techniques (e.g., Readhead and Wilkinson 1978). It now appears that most sources are of the core-jet type and exhibit an unresolved bright spot at one end of an elongated structure (e.g., Wilkinson et al. 1977; Readhead, Cohen, and Blandford 1978; Readhead et al. 1978). Observed with inferior baseline coverage, these source structures are compatible with the simple symmetric double and triple models reported in earlier investigations (Cohen et al. 1977).

Nearly half of the strong compact radio sources appear to exhibit

superluminal expansion (Cohen et al. 1977). The best example is 3C345 (Seielstad et al. 1979) for which an expansion velocity of (6.7 ± 0.8) c (H_o = 55 km $s^{-1}Mpc^{-1}$, q_o = 0.05, z = 0.595) over a six-year period is reported. During this time, the total angular size of the source more than doubled. Evidence has recently been presented that in some of the compact sources there is a significant rotation of the source position angle on going from the smallest to the largest angular scales (Readhead et al. 1978). This effect is not as yet apparent in the nuclear components of extended radio sources like Cygnus A and 3C111 (e.g., Kellermann 1978). As pointed out by Readhead et al. (1978), a natural interpretation of both the rapid expansion and the bending (as well as of the absence of an observed counter-jet) is possible if the brightest compact sources comprise relativistic jets whose axes make a small angle (~ 5^o-10^o) with the line of sight. The radio emission from the approaching component of the jet is then Doppler-brightened, and small deviations from collinearity will be exaggerated by the large projection effect. The brightest sources that we see will be those that are beamed towards us.

Nevertheless, there is a problem with this interpretation which must be overcome in any viable physical model. In order to see a systematic superluminal expansion, there must be a high relative velocity between two source components which should always be positive. However, the "emission" velocities of the two components should not be too different, for otherwise it would require an implausible coincidence to explain why the component in which the emitting material is moving faster was not considerably brighter than the slower one. In addition, if one component were not subject to relativistic beaming, then it would be difficult to explain why there were not many more bright compact sources viewed at large angles that do not exhibit large expansion velocities.

An attractive resolution of this paradox is possible in the context of the present model. Specifically, we propose that the unresolved core be identified with the innermost, optically-thick region of the approaching jet, and comprise largely time-independent emission. The location of the observed core should coincide with the peak in the surface brightness of the jet, which occurs roughly where the jet becomes optically thin at the observing frequency, i.e., at a radius $r_{\max\ ob}(\nu) \propto \nu^{-1}$ [eq. (28)], if we adopt the assumptions of §III. The moving radio component can be identified with perhaps an accelerating cloud or a propagating shock, as described in §IV. If the component is formed inside the optically thick region of the jet, then it will not be visible at radii $r_{ob} \lesssim r_{\max\ ob}(\nu)$, but at larger radii it will appear to separate from the stationary component. The observed separation velocity would thus correspond to the kinematical velocity of the moving component, which may be highly relativistic ($\gamma \gg 1$), and yet the "emission" velocities of the two source components could remain comparable and also highly relativistic. In fact, as we have argued in §IV, if the variable radio emission comes from behind a moving shock, then the shock velocity must be comparable to the velocity of the jet, and this conclusion can also be deduced on dynamical grounds if the cloud or the propagating shock are observed at sufficiently large distances from their initial locations. Moreover, if $\gamma \sim \gamma_j$, then the observed acceleration $c d\underline{\beta}_{ob}/dt_{ob}$ will be fairly small, as is indeed observed to be the case [cf. eqs. (3)-(5) and (40)].

The fact that the two separating components have usually been observed to have comparable fluxes and surface brightnesses could be due to a selection effect resulting from the limited dynamical range and resolution of the VLBI observations. However, in our model we expect the volume emissivities as well as the sizes of the two components to be similar, and so the observed

emission from the core and from a shock moving with $\gamma \sim \gamma_j$ should be roughly comparable.

c) Application to 3C345

It is clearly still premature to construct a detailed model of any particular source. However, in order to illustrate the application of the results of §III and §IV, we consider a source like 3C345, for which VLBI observations indicate that $\beta_{ob} \sim 7$ and $\Phi_{ob} \sim 15^{\circ}$ (cf. Seielstad et al. 1979, Readhead et al. 1979). Since 3C345 is one of the most rapidly expanding, as well as one of the brightest, compact extragalactic sources, we expect that both β_{ob} and Λ are nearly maximized for this source, and so we estimate that $\gamma_j \sim 7$ and $\Theta \sim 8^{\circ}$ [cf. eqs. (1) and (6)]. If we set $S_{ob} \sim 5$ Jy, $D_\ell \sim 4$ Gpc, $z = 0.6$, and adopt $\Lambda = 3$, $\Delta = 5$, and $k_e = 0.5$, then we deduce from equation (29) that $L \sim 1 \times 10^{46}$ erg s^{-1}. Substituting this into equations (27), (28), and (30), we obtain successively $T_{max} \sim 2 \times 10^{12}$ K, $(1 + z)^2 \, r_{max\ ob}/D_\ell \sim 1.8 \, \nu_9^{-1}$ milliarcsec, and $\nu_b \sim 1.2 \times 10^{11}$ Hz. These values seem to be quite consistent with existing observations. In addition, in order to reduce the Faraday rotation estimate [eq. (32)] to $\lesssim 1$ radian, we need $F \lesssim 4 \times 10^{-5}$ or $\gamma_{e\ min} \gtrsim 50$.

Consider next the fate of a "standard" emission-line cloud injected at $r_o \sim 0.3$ pc. From equation (38) with $k_d \sim 1$ we estimate $a \sim 1.2 \, h_{o15}^{-1}$, and hence from equation (39) we confirm that with $n = 2$ it is possible for the cloud to be accelerated to $\gamma \sim \gamma_j \sim 7$ as long as $h_o \lesssim 10^{14}$ cm. (This limit increases if the jet is confined.) The cloud will expand according to equation (41) to a diameter $\sim 2\pi h$, and will obstruct a reasonable fraction of the jet's area provided that $h_o \gtrsim 10^{14}$ cm. In addition, if the cloud penetrates the jet, a further constraint is imposed by the inequalities (44).

These four conditions are satisfied by h_o in the range 10^{14}-10^{15} cm.

Regarding the spectrum of the two major separating components in this source, our model predicts that the stationary component, which is associated with the nuclear core, should have a roughly flat spectrum and show comparatively little variability, whereas the moving component would have a variable flux which should eventually decline with a positive spectral index α. Recent VLBI measurements (Readhead et al. 1979 , Cohen et al. 1979) suggest that the separating components in 3C345, as well as in other, similar sources, are indeed evolving in this manner. It therefore seems possible to account for a source like 3C345 in terms of this general model.

d) Low-Frequency Variability

The problem of low-frequency variability has quite a long and controversial history. Recently Condon et al. (1978) have presented evidence to show that it is quite common in compact, flat-spectrum sources at the 20-30 percent level over periods of several years. The significance of these observations is that if the variability time is treated as a measure of the light crossing time of the source, then the derived brightness temperature $T_{var} = (1 + z)^{-4} D_\ell^{\,2} S_{ob}(\nu)/(2\nu^2 t_{var}^{\,2} k)$ is typically 10^{14}-10^{15} K, much greater than the Compton limit

$$T_c' \sim 10^{12}(\mathcal{D}/(1 + z)\ \nu_{10})^{1/5}\ \text{K} \quad . \tag{46}$$

Independent evidence that the true brightness temperatures do not greatly exceed this value is provided by the apparent absence of interstellar scintillation (e.g., Condon and Dennison 1978), although intergalactic scattering might obviate this argument.

It is well known that the co-moving brightness temperatures can be reduced below the Compton limit if there is relativistic expansion. Specifically, for a constant velocity source, the proper size and hence the observed transverse size of the emitting region is restricted by causality to $\sim (1 + z)^{-1}\, \mathcal{D} c t_{var}$. The true co-moving brightness temperature at the corresponding proper frequency $\nu' = \nu(1 + z)/\mathcal{D}$ then satisfies

$$T_{var}(\nu) \lesssim (1 + z)^{-3} \mathcal{D}^3 T'((1 + z)\nu/\mathcal{D}) \lesssim (1 + z)^{-3} \mathcal{D}^3 T'_c \quad . \tag{47}$$

Hence, for $\Theta \lesssim \gamma^{-1}$, a thousand-fold increase in apparent brightness temperature can be effected by Lorentz factors γ in the range 5-10.

However, as we showed in §II, it is possible to observe even faster variability if $\mathcal{D}$ itself can change. For example, for a constant source with $\alpha = 0.5$, moving along a non-linear path which is observed at an angle $\Theta_o \lesssim \gamma^{-1} \ll 1$, we can use equation (10) to show that there will be a change of $|\delta S_{ob}| = \varepsilon S_{ob}$ in S_{ob} in an observed time interval $t_{var} \sim (\varepsilon/3.5)(1 + z)^3 R/c\gamma^3 \sim 3.3\ (1 + z)^3\ \varepsilon(R/1\ pc)/\gamma^3$ yr, where R is the radius of curvature of the trajectory. The size of a coherently accelerating source is probably limited to R/γ^2, and so

$$T'((1 + z)\nu/\mathcal{D}) \gtrsim (\varepsilon/3.5)^2\ (1 + z)^3\ \gamma^{-3} T_{var}(\nu) \quad , \tag{48}$$

which implies that the values of γ which are needed to explain the apparent brightness temperature may in fact be smaller by a factor $(\varepsilon/3.5)^{2/3}$. A similar formula holds for linear acceleration. It is apparent that with the values $\Theta \sim 8^o$, $\gamma \sim 7$ suggested in (c), low-frequency variability can occur quite naturally in the strongest sources.

Unfortunately, many models that account for low-frequency variability in terms of relativistic expansion are energetically inefficient (e.g., Jones, O'Dell, and Stein 1974; Blandford and McKee 1977). This difficulty is alleviated in the case of radio emission from a relativistic jet because the radiation is beamed. To be quantitative, we can estimate the total proper internal energy of a moving source, for which the stronger inequality in (47) is satisfied, as

$$E' \gtrsim \left\{4\pi k t' \nu^3 t_{var}^3\right\} \left\{(1 + z)\ t'_s/\mathcal{D} t_{var}\right\} \quad , \tag{49}$$

where the braces contain, respectively, an estimate of the energy radiated and the ratio of the synchrotron cooling time t'_s (evaluated in the co-moving frame) to the dynamical time. For a synchrotron source we can estimate

$$t'_s \sim 10^{11} T'^3_{12} (1 + z)^{-2} \mathcal{D}^2 \nu_9^{-2} s \quad , \tag{50}$$

and thence calculate the total power dissipated <u>in the source</u> during the outburst to be

$$L \gtrsim E'(1 + z)\ \mathcal{D}^{-1} t_{var}^{-1} \gtrsim 3 \times 10^{42} T'^3_{12} \nu_9 t_{var} \text{ erg s}^{-1} \quad , \tag{51}$$

where we measure t_{var} in yr. Note that for a fixed co-moving brightness temperature $T' \sim T'_c$ this expression is independent of $\mathcal{D}$ and in fact <u>decreases</u> as the variability becomes more rapid and the observed frequency is lowered. Expression (51) is somewhat misleading, however, because it obscures the fact that $\mathcal{D}$ must be large enough to satisfy condition (47). Nevertheless, it does demonstrate that in a source model with relativistic beaming the power requirements need not be prohibitive.

e) Polarization

In §II we discussed how the plane of polarization of an accelerating radio source can rotate rapidly without there being necessarily an accompanying large change in the total flux. This behavior appears fairly frequently in the most variable optical and radio sources, and does not seem to be attributable to changes in rotation measure (e.g., Rudnick et al. 1978). The best example is contained in the 1975 observations of the Lacertid AO 0235 + 164, reported by Ledden and Aller (1978). In this case the swing occurred shortly after the peak of a large flux outburst and had an amplitude of ~ 130° and a fairly constant angular velocity. In Figure 2b we have used equation (16) to generate a fit to the data in the accelerating-cloud model of §IV. We have adopted $\gamma_j = 10$, $a = 100$ and $\Theta = 5^{\circ}$, and have chosen $\Psi = 15^{\circ}$, so that the swing occurs near the peak in the flux, computed under radiative assumption (i) (cf. Fig. 3); the fit was then obtained with $\eta = 5^{\circ}$. Of course, our choice of parameter values was quite arbitrary, and other values would yield a similar fit.

Various arguments (e.g., Ledden, Aller, and Dent 1976) suggest that this source moves relativistically and is viewed at a small angle to its velocity. According to equation (16), the large observed swing in the position angle is then consistent with the magnetic field being predominantly transverse to the velocity ($\Psi \ll 1$), as expected if the magnetic field originates in the jet (cf. §III). Furthermore, in this limit ($\Theta, \Psi \ll 1$, $\beta \to 1$) the position angle of the jet should coincide with the polarization position angle roughly at mid-swing, and so, on the basis of Figure 2b, we predict that the position angle of the putative jet in AO 0235 + 164 lies near $\xi = 0^{\circ}$.

f) Optical Observations

A small fraction of quasars (~ 1 percent of optically selected and 15 percent of radio selected quasars) can change their optical flux by more than a magnitude in a week, and are known as optically-violent variables (OVV's) (Penston and Cannon 1970, McGimsey et al. 1975). These objects are generally also highly active radio sources and display strong, variable, linear polarization, in contrast to the majority of quasars whose polarization appears to be very low and probably produced by scattering (Stockman and Angel 1978, Stockman 1978). OVV's are similar in many respects (apart from the prominence of emission lines) to Lacertids (reviewed in Stein, O'Dell, and Strittmatter 1976, and in Wolfe 1978).

In the light of the foregoing discussion, it seems natural to hypothesize that the sequence (radio-quiet quasars, radio-loud quasars, OVV quasars, Lacertids) corresponds to similar strong sources associated with relativistic jets, which are viewed at progressively decreasing angles θ to their axes (cf. Blandford and Rees 1978). The fact that several Lacertids appear to be surrounded by large elliptical galaxies (e.g., Miller 1978) suggests that these sources be identified with active nuclei of elliptical galaxies. In this picture, then, each nucleus comprises an isotropic, fairly steady and unpolarized optical continuum responsible for photo-ionizing the emission-line gas, and in addition a variable and strongly polarized synchrotron source associated with the jet and beamed in a cone of solid angle $\sim \gamma_j^{-2}$, which in general would be larger than the solid angle subtended by the jet. Only when the observer is located within this cone does the non-thermal contribution dominate the isotropic component. Lacertids would be sources in which the Doppler boost is so large that the lines can barely be seen

against the bright continuum.

If we adopt equation (11) as giving the mean observed flux and assume the constancy of R, β, r_d and S, then $\bar{S}_{ob} \propto (1 - \beta \cos\theta)^{-(2+\alpha)}$, and the number of sources with $\bar{S}_{ob}$ in the range $d\bar{S}_{ob}$ satisfies

$$\frac{dN}{d\bar{S}_{ob}} \propto \bar{S}_{ob}^{-(3+\alpha)/(2+\alpha)} \quad . \tag{52}$$

That is to say, for a given population of relativistically moving sources, there will be a larger fraction of steep-spectrum sources amongst the beamed sources of a given $\bar{S}_{ob}$ than amongst the unbeamed sources. [A similar conclusion would be reached if $\bar{S}_{ob}$ were given instead by equations (14), (15), or (29)]. It is perhaps for this reason that Lacertids typically have steeper spectra than quasars. However, with a knowledge of neither the relevant luminosity function nor of the distribution of Lorentz factors amongst sources, it is difficult to give a quantitative estimate of the ratio of beamed to unbeamed sources at a given flux.

There is some evidence that all the non-thermal emission at frequencies $\gtrsim$100 GHz from OVV's and Lacertids arises in the same region (e.g., Rudnick et al. 1978). This too is consistent with the simple model outlined in §III, if the frequency ν_b lies below ~ 100 GHz.

g) Relationship to Double Radio Sources

In the spirit of the above discussion it is possible to present a unified interpretation of extended double radio sources and compact, variable radio sources. We postulate that the brightest doubles (like Cygnus A) are intrinsically the brightest sources in the sky and are viewed at a large angle θ, so that their compact cores are not Doppler-boosted. The brightest compact sources (like 3C345) then comprise the small fraction

of beamed sources in the larger population of intrinsically-fainter doubles. We therefore expect these compact sources to be surrounded by a low-surface-brightness, steep-spectrum radio halo, corresponding to an intermediate-power double-source component of transverse size ~ 10-100 kpc which is viewed along its symmetry axis. (In fact, the morphology of these halo sources need not be simply circular, because many lower-power doubles show quite complex radio structure.) There are already indications of radio halos around several compact sources, including 3C345 (Davis, Stannard, and Conway 1977) and many Lacertids (Wardle 1978). Further observational support for this viewpoint may be provided by the report (Miley and Miller, 1979) that H_β profiles in compact radio sources are in general simpler and narrower than in the nuclei of double radio sources. This can be understood if the line-emitting clouds in galactic nuclei and quasars are Doppler-broadened by rotation in a disk whose normal is parallel to the radio-source axis.

It will be difficult to test the hypothesis that the comparatively low-power central components of extended double sources are the unboosted counterparts of the powerful compact sources. This is because the radio-emitting electrons are unable to cool in the jet (except in its innermost parts), and so the bulk of the radio flux might come from a stationary cocoon surrounding the jet, which for a similar intrinsic surface brightness would be a factor ~ $\mathcal{D}_j^{-2}(\theta \sim \pi/2) \sim \gamma^2$ brighter than the jet [cf. eq. (8)].

h) Evolutionary Considerations

The hypothesis that the brightest observed compact sources are a small subset of a larger population, highlighted by relativistic beaming towards us, has important cosmological consequences. This matter has been addressed

independently by Scheuer and Readhead (1979). We defer to this paper for a discussion of the potential and difficulties associated with the beaming hypothesis, restricting ourselves to some remarks specific to the model outlined in the present paper.

In a particular set of sources, characterized by fixed L, γ, ϕ, etc. and comprising a sufficiently large population, we expect that the viewing angle θ would be sampled well enough to test the hypothesis that relativistic beaming occurs. The variation of S_{ob} with θ for a given set of parameters depends on the model. For instance, equations (11), (14), (15) and (29) give, for flat-spectrum sources, $S_{ob} \propto (1 - \beta \cos\theta)^{-2}$, $(1 - \beta_1 \cos\theta)^{-1}$, $(1 - \beta^2\cos^2\theta_o)^{-3/2}$ and $(\sin\theta)^{1/6}(1 - \beta\cos\theta)^{-13/6}$, respectively, and the ranges of fluxes predicted by these models are quite different. However, it will in general be true that for every superluminal source exhibiting an expansion speed of $\beta_{ob}c$, there will be $\sim \beta_{ob}^{\ 2}$ sources of lower flux, viewed from a larger angle θ. It is encouraging that there are roughly fifty times as many radio-quiet quasars as "superluminal" quasars brighter than a given optical flux, which is consistent with the value of ~ 7 for β_{ob} suggested by the VLBI observations. This hypothesis may also be tested by more sensitive searches for radio emission from the brightest radio-quiet quasars and by VLBI studies of the nuclei of the strongest extended doubles which should not exhibit expansion speeds much in excess of 2c.

Similarly, there are at present seven low-redshift ($z \lesssim 0.1$) Lacertids known (Miller 1978), and this yields an estimate of ~ 100 Gpc^{-3} for their local space density, which is believed to be somewhat less than the local density of flat-spectrum radio sources of comparable brightness (e.g., Schmidt 1978). This estimated density is a fraction $\lesssim 10^{-3}$ of the density of bright elliptical galaxies, with which some Lacertids at least have been identified. The number of both Lacertids and flat-spectrum radio sources

does not appear to increase as dramatically with increasing redshift as the steep-spectrum radio sources (e.g., Schmidt 1976). This cannot be explained solely in terms of geometrical beaming unless the degree of relativistic beaming itself evolves, in the sense that younger sources move with smaller Lorentz factors.

VI. CONCLUSIONS

We have presented a general model for compact radio sources in which the radio emission (together with non-thermal radiation at high frequencies) is presumed to originate from a collimated relativistic jet. Temporal and spatial variability may be attributed to the motion of individual density inhomogeneities within the outer parts of the jet.

The following observed features find an explanation in this model:

(i) the flat radio spectra and steep optical spectra associated with quasars;

(ii) superluminal expansion and flux variability;

(iii) rapid swings in polarization angle;

(iv) the relationship between radio-quiet quasars, radio-loud quasars, OVV's, and Lacertids;

(v) the relative weakness of the central components of the powerful extended double sources.

If our classification of these objects is largely determined by our orientation with respect to the jet direction, then the following general observational tests are suggested:

(i) weak, steep-spectrum radio halos should be found surrounding the most powerful variable radio sources;

(ii) powerful compact radio sources should be strongly asymmetrical and may frequently display rotation of the source position angle and superluminal expansion;

(iii) the relatively weak central components of the powerful doubles like Cygnus A should be more symmetrical and better aligned with the outer components, and not show observed expansion velocities larger than ~ 2c.

Predictions relevant to specific objects like 3C345 and A0 0235 + 164 can also be made.

ACKNOWLEDGMENTS

The authors thank A. Readhead and M. Rees for discussions and encouragement/ and T. Jones for helpful comments on the manuscript. Hospitality at the Santa Cruz Summer Workshop on Quasars and Active Galactic Nuclei (R.B. and A.K) and the Institute of Astronomy, Cambridge (facilitated by a grant from the NATO Scientific Affairs Division) (R.B) is gratefully acknowledged.

REFERENCES

Blandford, R. D., and Königl, A. 1978, Ap. Letters (in press).

Blandford, R. D., and McKee, C. F. 1977, M.N.R.A.S., 180, 343.

Blandford, R. D., McKee, C. F., and Rees, M. J. 1977, Nature, 267, 211.

Blandford, R. D., and Rees, M. J. 1978, to appear in Proceedings of Pittsburgh Conference on BL Lac Objects (ed. A. M. Wolfe).

Brandie, G. W., Bridle, A. H., and Kesteven, M. J. L. 1974, Nature, 252, 212.

de Bruyn, A. G. 1976, Astr. and Ap., 52, 439.

Burch, S. F. 1977, M.N.R.A.S., 181, 599.

Christiansen, W. A., and Scott, J. S. 1977, Ap. J. (Letters), 216, L1.

Christiansen, W. A., Scott, J. S., and Vestrand, W. T. 1978, Ap. J. 223, 13.

Cohen, M. H., et al., 1977, Nature, 268, 405.

Cohen, M. H., Pearson, T. J., Readhead, A. C. S., Seielstad, G. A., Simon, R. S., and Walker, R. C. 1979, Ap. J. (submitted).

Condon, J. J., Balonek, T. J., and Jauncey, D. L. 1975, Ap. J., 80, 887.

Condon, J. J., and Dennison, B. 1978, Ap. J., 224, 835.

Condon, J. J., and Dressel, L. L. 1973, Ap. Letters, 15, 203.

Condon, J. J., Ledden, J. E., O'Dell, S. L., and Dennison, B. 1978, Aston.J. (in press).

Davis, R. J., Stannard, D., and Conway, R. G. 1977, Nature, 267, 596.

De Young, D. S. 1976, Ann. Rev. Astr. Ap., 14, 447.

De Young, D. S., and Axford, W. I. 1967, Nature, 216, 129.

Ferguson, D. C. 1971, Nature Phys. Sci., 234, 86.

Hunstead, R. W. 1972, Ap. Letters, 12, 193.

Jones, T. W., and O'Dell, S. L. 1977, Astr. and Ap., 61, 291.

Jones, T. W., O'Dell, S. L., and Stein, W. A. 1974, Ap. J., 192, 261.

Jones, T. W., and Tobin, W. 1977, Ap. J., 215, 474.

Kellermann, K. I. 1966, Ap. J., 146, 621.

Kellermann, K. I. 1978, Physica Scripta, 17, 257.

Kellermann, K. I., and Pauliny-Toth, I. I. K. 1969, Ap. J. (Letters), 155, L71.

Ledden, J. E., and Aller, H. D. 1978, Ap. J. (Letters) (submitted).

Ledden, J. E., Aller, H. D., and Dent, W. A. 1976, Nature, 260, 752.

Marscher, A. P. 1978, Ap. J., 219, 392.

McGimsey, B. Q., et al., 1975, Astr. J., 80, 895.

Miley, G. K., and Miller, J.S. 1979, Ap. J. (Letters) (in press).

Miller, J. S. 1978, to appear in Proceedings of Pittsburgh Conference on BL Lac Objects (ed. A. M. Wolfe).

O'Dell, S. L. 1978, to appear in Proceedings of Pittsburgh Conference on BL Lac Objects (ed. A. M. Wolfe).

Osterbrock, D. E. 1978, Physica Scripta, 17, 285.

Penston, M. V., and Cannon, R. D. 1970, R. Obs. Bull., 159, 85.

Readhead, A. C. S., Cohen, M. H., and Blandford, R. D. 1978, Nature, 272, 131.

Readhead, A. C. S., Cohen, M. H. Pearson, T. J., and Wilkinson, P. N. 1978 , Nature, 276,768.

Readhead, A. C. S., Pearson, T. J., Cohen, M. H., Ewing, M. S., and Moffett, A. T. 1979 , Ap. J. (submitted).

Readhead, A. C. S., and Wilkinson, P. N. 1978, Ap. J., 223, 25.

Rees, M. J. 1978, M.N.R.A.S., 184, 61.

Rudnick, L., Owen, F. N., Jones, T. W., Puschell, J. J., and Stein, W. A. 1978, Ap. J. (Letters), 225, L5.

Scheuer, P. A. G., and Readhead, A. C. S. 1979, Nature (submitted).

Schmidt, M. 1976, Ap. J. (Letters), 209, L55.

Schmidt, M. 1978, Physica Scripta, 17, 135.

Seielstad, G. A., Cohen, M. H., Linfield, R. P., Moffett, A. T., Romney, J. D., Schilizzi, R. T., and Shaffer, D. B. 1979, Ap. J. (in press).

Shields, G. A. 1978, to appear in Proceedings of Pittsburgh Conference on BL Lac Objects (ed. A. M. Wolfe).

Sramek, R. A., and Weedman, D. W. 1978, Ap. J., 221, 468.

Stein, W. A., O'Dell, S. L., and Strittmatter, P. A. 1976, Ann. Rev. Astr. Ap., 14, 173.

Stockman, H. S. 1978, to appear in Proceedings of Pittsburgh Conference on BL Lac Objects (ed. A. M. Wolfe).

Stockman, H. S., and Angel, J. R. P. 1978, Ap. J. (Letters), 220, L67.

Usher, P. D. 1975, Ap. J. (Letters), 198, L57.

Waggett, P. C., Warner, P. J., and Baldwin, J. E. 1977, M.N.R.A.S., 181, 465.

Wall, J. V. 1975, Observatory, 95, 196.

Wardle, J. F. C. 1977, Nature, 269, 563.

Wardle, J. F. C. 1978, to appear in Proceedings of Pittsburgh Conference on BL Lac Objects (ed. A. M. Wolfe).

Wilkinson, P. N., Readhead, A. C. S., Purcell, G. H., and Anderson, B. 1977, Nature, 269, 764.

Wolfe, A. M. 1978, to appear in Proceedings of Pittsburgh Conference on BL Lac Objects (ed. A. M. Wolfe).

FIGURE CAPTIONS

Fig. 1. The observed flux density S_{ob} from a moving source as a function of the observed velocity β_{ob}, under the assumption that in the frame of the source the flux is constant and has spectral index $\alpha = 0.5$. The curves are distinguished by different values of Θ, the angle in the observer's frame between the direction of motion and the line of sight. The tick marks on each curve indicate values of the proper velocity $\gamma\beta$.

Fig. 2. (a) Geometry of the emission region, which moves with a velocity $\underline{\beta}$, as seen in a stationary frame. Synchrotron radiation (electric field $\underline{e}_{ob}$) is emitted by relativistic electrons which move in a static magnetic field $\underline{B}_{ob}$. The vector $\underline{e}_{ob}$ ($\underline{B}_{ob}$) makes an angle $\xi(\eta)$ with the plane containing $\underline{\beta}$ and the observer direction $\underline{n}$, and its projection on this plane makes an angle $\Theta(\Psi)$ with the z axis.

(b) The observed polarization position-angle ξ in the 1975 outburst of AO 0235 + 164 (reproduced from Ledden and Aller 1978). The measurements were made at 8.0(0) and at 14.5(x) GHz, with standard errors as shown. The solid line represents a fit to the data in the accelerating-cloud model of §IV, for a cloud with acceleration parameter a = 100 which starts from rest at a distance r_o = 10 pc from the origin of a paraboloidal jet with a constant Lorentz factor γ_j = 10. The values of Θ, Ψ, and η which give rise to this curve are not unique. One possible choice is $\Theta = 5^o$, $\Psi = 15^o$, and $\eta = 5^o$.

Fig. 3. The observed flux density (normalized by $S_{ob\ max}$) from an accelerating cloud as a function of the observer's time t_{ob}, measured in units of r_o/c. [For a cloud which has been accelerated from r_o to r in time t, $t_{ob} = t - (r - r_o) \cos \Theta/c$.] The curves labelled (i) and (ii) correspond to the two radiative assumptions discussed in the text; in case (ii) the cloud is initially optically thick, with optical depth $\tau_o = 10^7$. Also shown is the time evolution of the observed velocity β_{ob}. In this example the jet is paraboloidal with $\gamma_j = 7$, the acceleration parameter a = 90, and the jet is viewed at an angle $\Theta = 8^o$ to its axis.

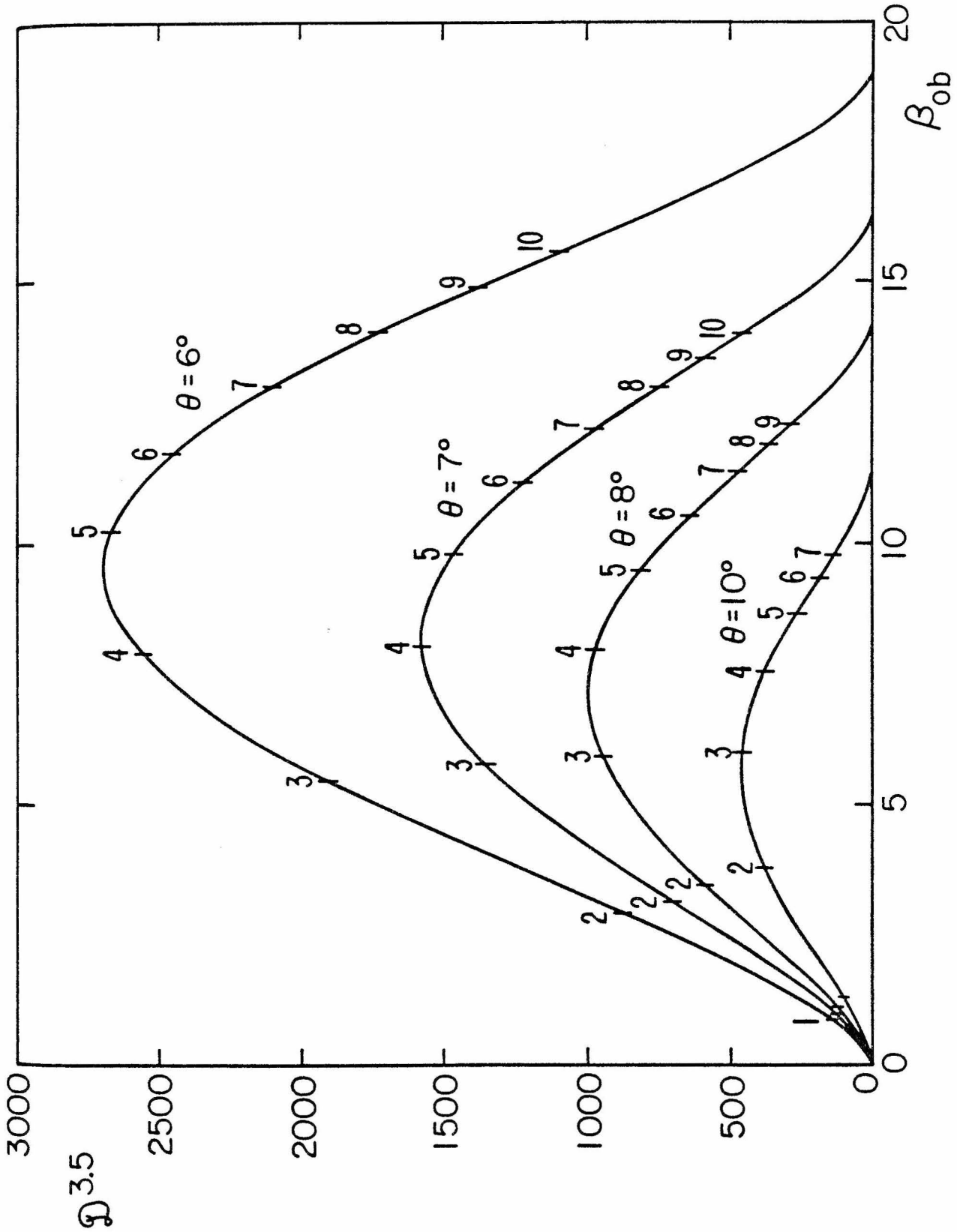
3000
2500
2000
1500
1000
500
0
$\mathfrak{D}^{3.5}$
0
5
10
15
20
β_{ob}
θ=6°
θ=7°
θ=8°
θ=10°

Fig. 1

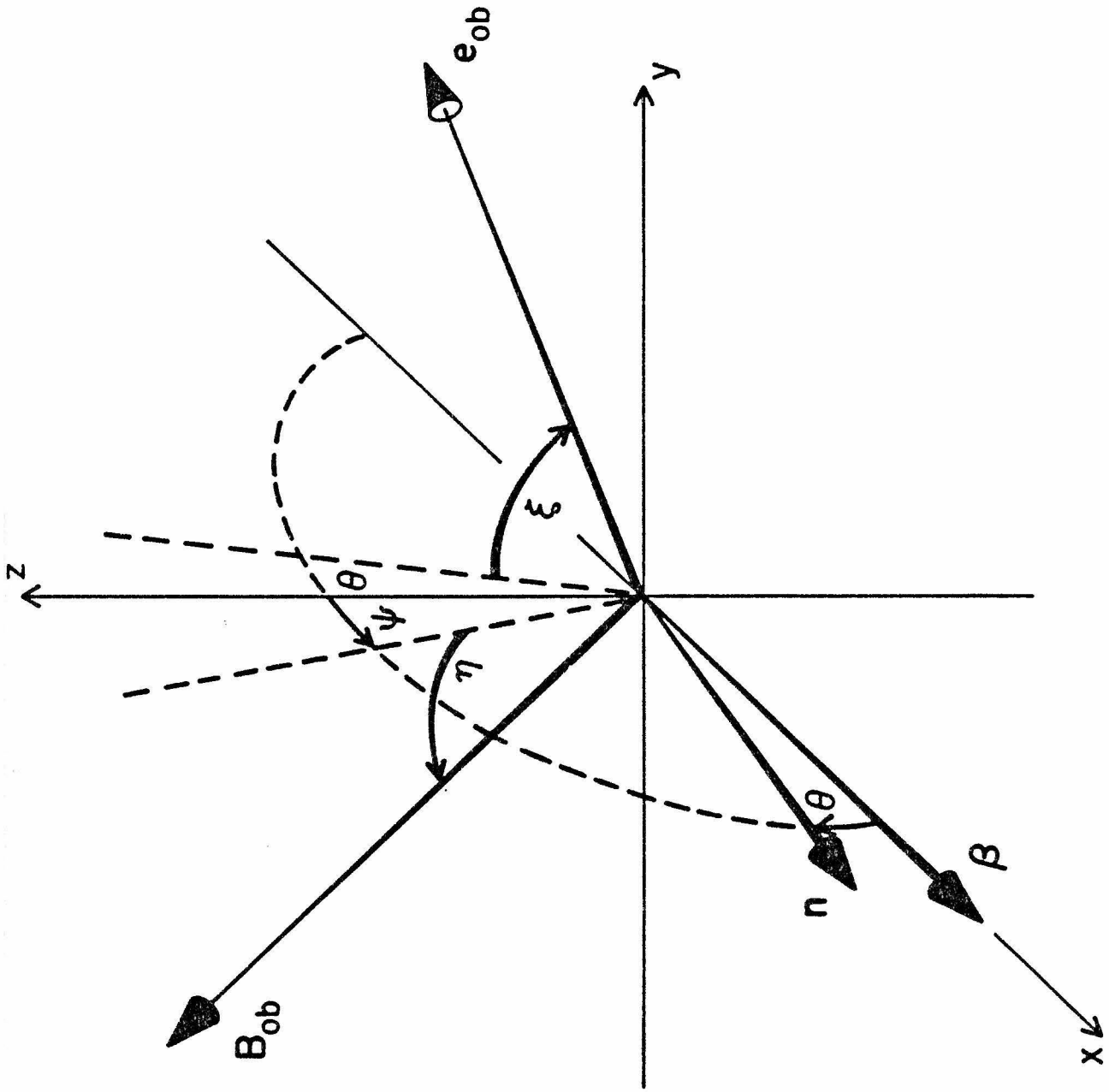

Fig. 2a

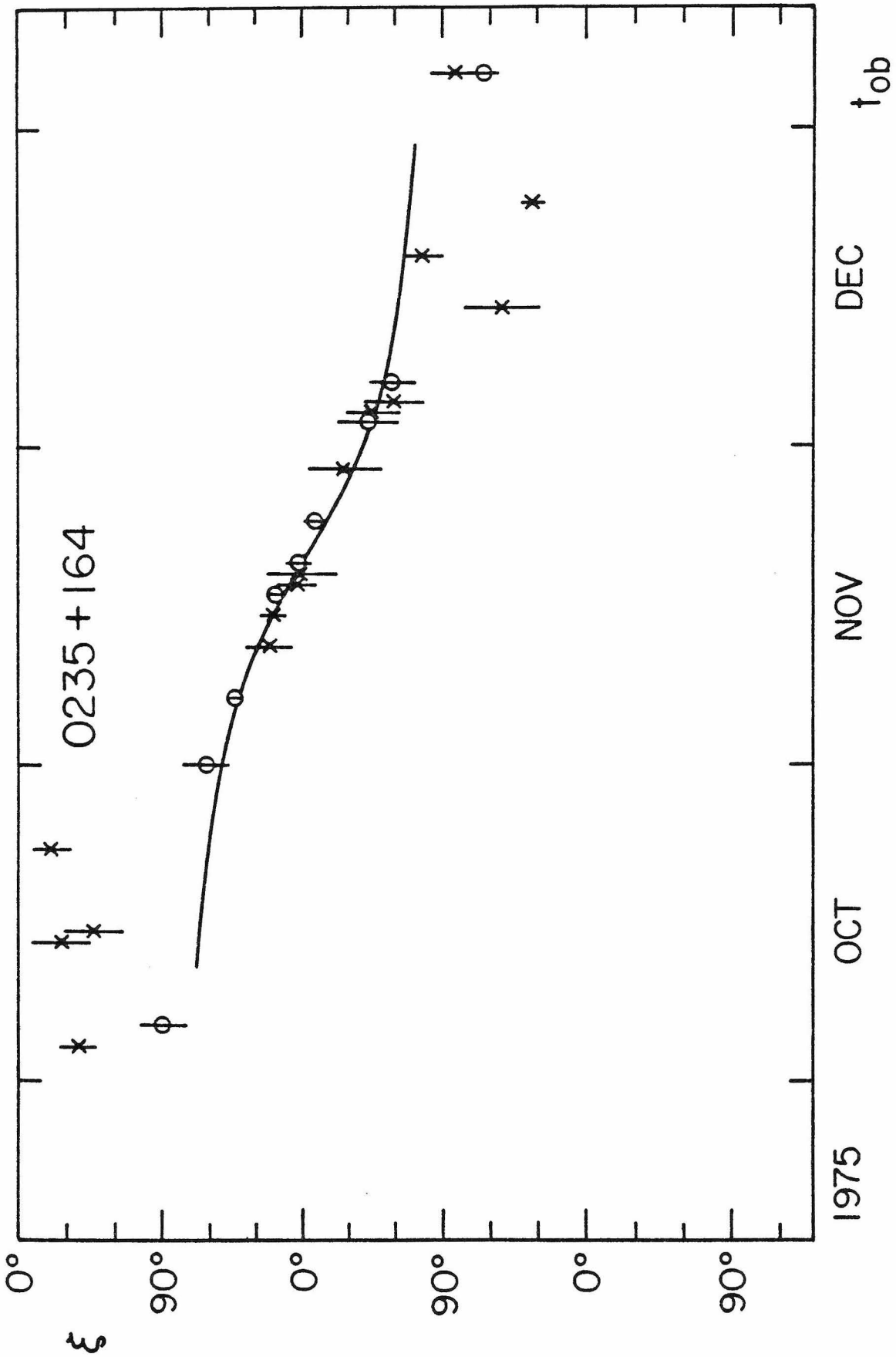

Fig. 2b

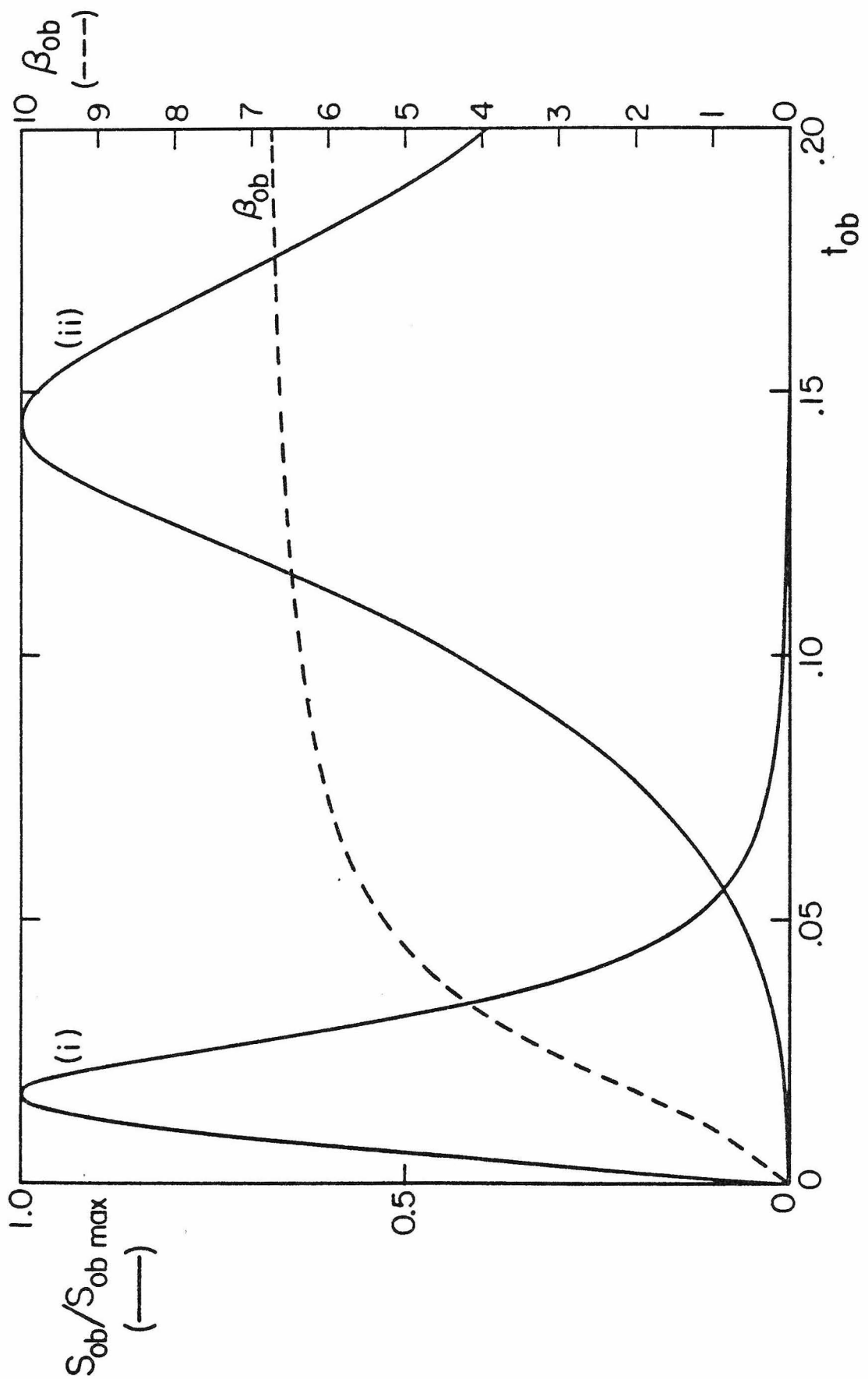
$S_{ob}/S_{ob\ max}$ (——)
β_{ob} (– – –)
t_{ob}
(i)
(ii)
β_{ob}
1.0
0.5
0
0
.05
.10
.15
.20
10
9
8
7
6
5
4
3
2
1
0

Fig. 3

PAPER 4

RELATIVISTIC JETS AS X-RAY AND γ-RAY SOURCES

I. INTRODUCTION

A growing number of extragalactic radio sources are being found to possess narrow, elongated features (jets) which connect the extended radio components with a central compact core. It is currently believed that these jets supply the extended components with matter and energy from a central "power-house," which is usually identified with a quasar or an active galactic nucleus (e.g., Blandford and Rees 1978a). The radio emission is generally interpreted as incoherent synchrotron radiation from a non-thermal distribution of relativistic electrons. Many strong compact sources also show evidence for relativistic bulk motion, most notably in apparent superluminal separation velocities of individual components (e.g., Cohen et al. 1979). In fact, it has been argued (Scheuer and Readhead 1979; Blandford and Königl 1979b, hereafter Paper I) that the majority of bright compact radio sources could be identified with relativistic supersonic jets which are observed at small angles to their axes. In this picture, the sequence: radio-quiet quasars, radio-loud quasars, and blazars (i.e., optically-violent variable quasars and BL Lac objects), corresponds to similar strong sources, associated with relativistic jets, which are viewed at progressively smaller angles to their axes. As the angle of observation decreases, the contribution of the highly variable and strongly polarized beamed emission component increases relative to the steady and unpolarized isotropic component which is responsible for photoionizing the emission-line gas near the nucleus. Blazars are interpreted as sources in which the beamed component dominates the observed emission (cf. Angel and Stockman 1980).

Relativistic jets associated with compact radio sources are also expected to be x-ray and γ-ray sources, with synchrotron and inverse-Compton being the most likely emission mechanisms. Recent x-ray observations (e.g., Tananbaum et al. 1979, Ku 1980) have indicated that a

substantial fraction of radio-selected quasars, and most blazars, are indeed x-ray sources, and that blazars can be highly variable also in the x-ray regime (e.g., Ricketts, Cooke, and Pounds 1976, Mushotzky et al. 1979). Furthermore, the only quasar identified so far as a high-energy ($\gtrsim$ 100 MeV) γ-ray source is 3C273 (Swanenburg et al. 1978), which is also a bright compact radio source that displays apparent superluminal velocities (e.g., Cohen et al. 1979). When interpreted in the context of the relativistic-jet model, these observations appear to suggest that the beamed component also contributes significantly to the observed x-ray and γ-ray radiation in sources which are viewed at small angles to their jet axes. In this paper, the relativistic-jet model for compact radio sources is extended and applied to the interpretation of extragalactic x-ray and γ-ray sources. The synchrotron and inverse-Compton spectra of an inhomogeneous relativistic jet are calculated in §II on the basis of a simple emission model. This calculation generalizes the results of Paper I. The model is then applied in §III to the interpretation of the spectra of BL Lac objects and of 3C273. In addition, the postulated local synchrotron spectrum is applied to the resolved x-ray jet in Cen A. Some general properties of extragalactic x-ray sources, and the contribution of relativistic jets to the diffuse x-ray and γ-ray background, are discussed in §IV. A summary of the results is given in §V.

II. SYNCHROTRON AND INVERSE-COMPTON EMISSION FROM A RELATIVISTIC JET

In this section, the synchrotron and inverse-Compton spectra are calculated for a resolved jet and for an unresolved inhomogeneous jet. The local synchrotron spectrum is described in §IIa. It is assumed to be

produced by a power-law distribution of continuously reaccelerated relativistic electrons, and to break as a result of synchrotron radiation losses. The local synchrotron self-Compton spectrum is then calculated in the δ-function approximation. The corresponding spectra for an unresolved jet are obtained in §IIb by adding up the contributions of the local emission spectra from the entire jet. In this calculation it is assumed that the relativistic-electron distribution has the same power-law throughout the source, but the coefficient of the distribution and the magnitude of the magnetic field in which the electrons radiate are allowed to vary along the jet.

a) Local Emission Spectrum

Consider a narrow conical jet of semiangle φ which has a constant velocity β_j (in units of the speed of light c) and which is seen at an angle θ to the axis. Assume that a portion of the jet at a distance r from the apex, subtending a solid angle $\Delta\Omega_{ob}$ at the observer, emits optically-thin radiation at frequency ν' with spectral emissivity $\varepsilon(\nu')$, as measured in the rest frame of the jet. The observed frequency is $\nu = \mathcal{D}_j \nu'/(1+z)$, where z is the redshift of the source and $\mathcal{D}_j = \gamma_j^{-1}(1 - \beta_j \cos\theta)^{-1}$, with $\gamma_j = (1 - \beta_j^2)^{-\frac{1}{2}}$, is the relativistic Doppler factor. The observed flux density is then

$$S_{ob}(\nu) \approx (1+z)^{-3}\, \mathcal{D}_j^2 (2r\varphi \csc\theta)(\Delta\Omega_{ob}/4\pi)\, \varepsilon[1+z)\nu/\mathcal{D}_j]. \qquad (1)$$

(Note that the observed radius and cone angle are given by $r_{ob} = r \sin\theta$ and $\varphi_{ob} = \varphi \csc\theta$, respectively.)

The synchrotron emissivity ε_s due to relativistic electrons with a power-law distribution $n_e(\gamma_e) = K_e \gamma_e^{-(2\alpha_e+1)}$, $\gamma_{e\,min} \le \gamma_e \le \gamma_{e\,max}$, radiating isotopically in a magnetic field B, is given by

$$\varepsilon_s[(1+z)\nu_s/\mathcal{D}_j] = (1+z)^{-\alpha_e}\mathcal{D}_j^{\alpha_e}\nu_s^{-\alpha_e}C_1(\alpha_e)K_e B^{1+\alpha_e}, \quad \nu_{s\,min} \leq \nu_s \leq \nu_{s\,max}, \quad (2)$$

where $C_1(\alpha_e)$ is a constant (e.g., Blumenthal and Gould 1970; $C_1(0.5) = 3.6 \times 10^{-19}$ cgs). The spectral energy density of the optically-thin radiation can be approximated by $[\varepsilon_s(\nu'_s)t'_{es}]$, where $t'_{es} \approx r\varphi/c$ is the mean photon lifetime before escape. In what follows, it will be assumed that the relativistic electrons are injected continuously with $K_e = K$, $\alpha_e = \alpha_o$, and with Lorentz factors in the range $\gamma_{e\ell} \leq \gamma_e \leq \gamma_{eu}$, but that α_e increases to $(\alpha_o + 0.5)$ for $\gamma_e > \gamma_{eb}$ ($\gamma_{e\ell} \ll \gamma_{eb} \ll \gamma_{eu}$) due to synchrotron-radiation losses (cf. Kellermann 1966). The model synchrotron spectrum is illustrated in Figure 1. Below the frequency ν_{sm} the source is optically-thick to synchrotron self-absorption and the flux density rises as $\nu_s^{2.5}$. The optically-thin spectrum has a spectral index $\alpha_s = \alpha_o$ between ν_{sm} and ν_{sb}, and $\alpha_s = \alpha_o + 0.5$ between ν_{sb} and ν_{su}, where ν_{sb} and ν_{su} are the characteristic emission frequencies of electrons with Lorentz factors γ_{eb} and γ_{eu}, respectively. Above ν_{su} the flux density falls off exponentially with frequency. The frequency $\nu_{sm}(r)$ is approximated by setting the optical depth to synchrotron self-absorption equal to unity. Assuming that $B = B_1 r^{-m}$ and $K = K_1 r^{-n}$ (where cgs units apply to every quantity except for r, which is expressed in parsecs), one obtains

$$\nu_{sm}(r) \approx (1+z)^{-1}\left[6.2 \times 10^{18}\, C_2(\alpha_o)\, \mathcal{D}_j^{1.5+\alpha_o} K_1 B_1^{1.5+\alpha_o}\, \varphi \csc\theta\right]^{1/(2.5+\alpha_o)} r^{-k_m} \quad \text{Hz}, \quad (3)$$

where $k_m = [(3 + 2\alpha_o)m + 2n - 2]/(5 + 2\alpha_o)$, and where $C_2(\alpha_o)$ is a constant (e.g., Blumenthal and Gould 1970; $C_2(0.5) = 8.4 \times 10^{10}$ cgs). The observed size of the optically-thick "core" of the jet thus varies with frequency

as ν_s^{-1/k_m}. The frequency $\nu_{sb}(r)$ is estimated by equating the jet travel time to a distance r with the synchrotron cooling time (cf. Paper I). This gives

$$\nu_{sb}(r) \approx 6.9 \times 10^7 \ (1+z)^{-1} \ \mathcal{D}_j \gamma_j^{\ 2} \beta_j^{\ 2} B_1^{-3} r^{k_b} \qquad \text{Hz}, \qquad (4)$$

where $k_b = (3m - 2)$. It will be assumed, for simplicity, that the values of $\gamma_{e\ell}$ and γ_{eu} are independent of r. (Note, however, that the discharge of relativistic electrons will be conserved along the jet only if the number density $n_e \propto K\gamma_{e\ell}^{-2\alpha_o/2\alpha_o}$ scales as r^{-2}.) This assumption will be consistent with the requirements $\nu_{sm}(r)/\nu_{sb}(r) > \gamma_{e\ell}^{\ 2}/\gamma_{eb}^{\ 2}$ and $\nu_{su}(r) = 10^6 \ (1+z)^{-1} \ \mathcal{D}_j B_1 \gamma_{eu}^{\ 2} \ r^{-m} > \nu_{sb}(r)$ as long as r is not too large. The smallest radius from which optically-thin emission with $\alpha = \alpha_o$ is observed can be determined by setting $\nu_{sb}(r) = \nu_{sm}(r)$, and is given, for $\alpha_o = 0.5$, by

$$r_M \approx [1.6 \times 10^6 \ \mathcal{D}_j^{-1} (\gamma_j \beta_j)^{-6} K_1 B_1^{\ 11} \varphi \csc \theta]^{1/(11m+n-7)} \quad \text{pc.} \quad (5)$$

The frequency $\nu_{sm}(r_M) \equiv \nu_{sM}$ is given, for $\alpha_o = 0.5$, by

$$\nu_{sM} \approx 6.9 \times 10^7 \ (1+z)^{-1} \left[(1.6 \times 10^6 \ K_1 \varphi \csc \theta)^{3m-2} \right.$$
$$\left. \mathcal{D}_j^{\ 8m+n-5} (\gamma_j \beta_j)^{4m+2n-2} \ B_1^{-(3n+1)} \right]^{1/(11m+n-7)} \qquad \text{Hz.} \quad (6)$$

The emissivity ε_c due to a single inverse-Compton scattering of synchrotron photons (with spectral index α_s) by relativistic electrons (with emission spectral index α_e) can be estimated using the δ-function approximation (e.g., Rieke and Weekes 1969). According to this approximation, the final frequency of a scattered photon is given by $\nu_c' \approx \gamma_e^{\ 2} \nu_s'$ and $\nu_c' \approx \gamma_e m_e c^2$ for $\gamma_e h\nu_s' \leq m_e c^2$ (the Thomson regime) and $\gamma_e h\nu_s' > m_e c^2$

(the Klein-Nishina regime) respectively, where ν_s' is the initial frequency of the photon, γ_e is the Lorentz factor of the scattering electron, m_e is the electron's rest-mass, and h is Planck's constant. The emissivity ε_c^T due to scattering with the Thomson cross section σ_T is then given by

$$\left.\begin{aligned} &\varepsilon_c^T[(1+z)\nu_c/\mathcal{D}_j] \approx K_e\,\sigma_T\, r\,\varphi\,\varepsilon_s[(1+z)\nu_c/\mathcal{D}_j]\int_{\gamma_{min}}^{\gamma_{max}} \gamma^{2(\alpha_s-\alpha_e)-1}\,d\gamma, \\ &\gamma_{e\ min}^2\,\nu_{s\ min} \le \nu_c \le \min\left\{\gamma_{e\ max}^2\,\nu_{s\ max};\ \gamma_{e\ max}\,\mathcal{D}_j m_e c^2/(1+z)h;\right. \\ &\left.\left(\mathcal{D}_j m_e c^2/(1+z)h\right)^2/\nu_{s\ min}\right\}, \end{aligned}\right\} \quad (7)$$

where

$$\left.\begin{aligned} \gamma_{min} &= \max\left\{\gamma_{e\ min};\ (\nu_c/\nu_{s\ max})^{\frac{1}{2}};\ (1+z)h\nu_c/\mathcal{D}_j m_e c^2\right\}, \\ \gamma_{max} &= \min\left\{\gamma_{e\ max};\ (\nu_c/\nu_{s\ min})^{\frac{1}{2}}\right\}, \end{aligned}\right\} \quad (8)$$

and where the appropriate values of α_s, α_e, K_e, $\gamma_{e\ min}$, $\gamma_{e\ max}$, $\nu_{s\ min}$, and $\nu_{s\ max}$ are summarized in Table 1. The emissivity ε_c^{KN} due to scattering with the Klein-Nishina cross section is given in this approximation by

$$\left.\begin{aligned} &\varepsilon_c^{KN}\,[(1+z)\nu_c/\mathcal{D}_j] \approx \tfrac{3}{8}\,K_e\sigma_T r\,\varphi\,\varepsilon_s[(1+z)\nu_c/\mathcal{D}_j]\left(\mathcal{D}_j m_e c^2/(1+z)h\right)^{2(\alpha_e+1)} \\ &\nu_c^{\alpha_s-2\alpha_e-1}\left(\frac{\nu^{-(\alpha_s+1)}}{\alpha_s+1}\left\{\frac{\alpha_s+3}{2(\alpha_s+1)}+\ln\left[\left(\frac{(1+z)h}{\mathcal{D}_j m_e c^2}\right)^2 2\nu\nu_c\right]\right\}\right)_{\nu_{max}}^{\nu_{min}}, \\ &\max\left\{\mathcal{D}_j\gamma_{e\ min} m_e c^2/(1+z)h;\left(\mathcal{D}_j m_e c^2/(1+z)h\right)^2/\nu_{s\ max}\right\} \le \nu_c \le \\ &\le \mathcal{D}_j\gamma_{e\ max} m_e c^2/(1+z)h, \end{aligned}\right\} \quad (9)$$

where $\nu_{min} = \max\{\nu_{s\,min}, (\mathcal{D}_j m_e c^2/(1+z)h)^2/\nu_c\}$ and $\nu_{max} = \nu_{s\,max}$ (cf. Rieke and Weekes 1969). The total inverse-Compton emissivity, $\varepsilon_c = \varepsilon_c^T + \varepsilon_c^{KN}$, is generally dominated by ε_c^T in the scattered-photon frequency range where the Thomson regime and the Klein-Nishina regime overlap. (Note that the Klein-Nishina frequency range, given in equation (9), is contained entirely in the Thomson frequency range, given in equation (7), when $\gamma_{e\,max}\, h\nu'_{s\,min} < m_e c^2$.) The δ-function approximation yields an overestimate of the true emissivity, since the scattered photons are given roughly the maximum possible energy. For example, in the limit $\gamma_{e\,min}^2\, \nu_{s\,max} \leq \nu_c \leq \gamma_{e\,max}^2\, \nu_{s\,min}$, equation (7) overestimates the correct emissivity (e.g., Blumenthal and Gould 1970) by a factor $\lesssim 2$ (for $0 \leq \alpha_e \leq 1$). This approximation, however, is sufficiently accurate for the applications discussed in this paper.

The once-scattered synchrotron self-Compton spectrum corresponding to the optically-thin portion of the model synchrotron spectrum is illustrated in Figure 1. (The inverse-Compton emission associated with the optically-thick portion of the synchrotron spectrum is relatively small and can be neglected.) The spectrum extends between the frequencies $\nu_{cm} \equiv \gamma_{e\ell}^2 \nu_{sm}$ and $\min\{\nu_{cu}, \nu_{KN}\}$, where $\nu_{cu} \equiv \gamma_{eu}^2 \nu_{su}$ and $\nu_{KN} \equiv \gamma_{eu} \mathcal{D}_j m_e c^2/(1+z)h$. It essentially reproduces the shape of the optically-thin synchrotron spectrum, with a break occurring near $\nu_{cb} \equiv \gamma_{eb}^2 \nu_{sb}$ ($\gamma_{eb}^2 \approx 10^{-6}\ (1+z)\ \mathcal{D}_j^{-1} B^{-1} \nu_{sb}$), where the spectral index changes from $\alpha_c \approx \alpha_o$ to $\alpha_c \approx \alpha_o + 0.5$. The spectra corresponding to higher-order inverse-Compton scatterings of the synchrotron photons can be calculated in an analogous way, and have similar shapes.

The observed timescale for flux variability cannot be shorter than the cooling time of the relativistic electrons which emit the observed radiation. The radiative cooling time is given by

$$t_{cool} \approx 3 \times 10^7 \ (1+z) \ \mathcal{D}_j^{-1} \gamma_e^{-1} [(1+\eta_c) B^2/8\pi]^{-1} \quad s, \tag{10}$$

where $\eta_c \approx (K_e \sigma_T r\varphi) \int_{\gamma_{e\,min}}^{\gamma_{e\,max}} \gamma_e^{1-2\alpha_e} \, d\gamma_e$ is the ratio of the Compton-scattered photon energy density to the synchrotron energy density. Since the source is assumed to be synchrotron-loss dominated ($\eta_c \ll 1$), t_{cool} is essentially the synchrotron cooling time. For synchrotron radiation observed at a frequency ν_s, $\gamma_e^{-1} \approx 10^3 \ (1+z)^{-\frac{1}{2}} \mathcal{D}_j^{\frac{1}{2}} B^{\frac{1}{2}} \nu_s^{-\frac{1}{2}}$. For Thomson-scattered synchrotron radiation observed at a frequency ν_c, a lower limit on t_{cool} is obtained by substituting $\nu_s^{-\frac{1}{2}} \approx \nu_c^{-\frac{1}{2}} \gamma_{min}$ [cf. eq. (8)] in the expression for γ_e^{-1}. The cooling timescale generally increases with radius.

The above expressions are used in §IIb to derive a model spectrum for an unresolved nonuniform jet. However, they are also useful for an analysis of the observed spectrum from a homogeneous emission region, as is illustrated in §IIIc.

b) Spectrum of an Unresolved Jet

The observed optically-thin flux density $S_{ob}(\nu)$ emitted between r_{min} and r_{max} from an unresolved conical jet is given by

$$S_{ob}(\nu) = \left[(1+z) \mathcal{D}_j^2 / 4\pi D_\ell^2\right] \int_{r_{min}}^{r_{max}} \varepsilon[(1+z)\nu/\mathcal{D}_j] \, \pi \, (r\varphi)^2 \, dr \, , \tag{11}$$

where $D_\ell = 10^9 \, D_{\ell 9}$ pc is the luminosity distance to the source. Equation (11) is now used to calculate the synchrotron and inverse-Compton spectra for an inhomogeneous jet extending between r_ℓ and r_u ($r_\ell \ll r_u$), with ε, r_{min}, and r_{max} determined on the basis of the model presented in §IIa.

Consider first the synchrotron spectrum, for which the emissivity is given by equation (2). In the frequency range $\nu_{sm}(r_u) \lesssim \nu_s \leq \nu_{sM}$, where ν_{sM} is given by equation (6), the observed flux density at ν_s is dominated by emission from $r_{min}(\nu_s) = (\nu_s/\nu_{sM})^{-1/k_m} r_M$, obtained from equation (3) by setting $\nu_{sm}(r) = \nu_s$ and substituting for r_M from equation (5). Note that $r_{min}(\nu_s)$ decreases to r_M as ν_s increases to ν_{sM}. For frequencies in the range $\nu_{sM} \leq \nu_s \lesssim \nu_{sb}(r_u)$, the flux density is dominated by emission from $r_{min}(\nu_s) = (\nu_s/\nu_{sM})^{k_u} r_M$, which is obtained by setting $\nu_{sb}(r) = \nu_s$ in equation (4), and which now increases with frequency. In both of these cases $r_{max} = r_u$, and so equation (11) gives

$$S_{ob\ s}(\nu_s) = \begin{cases} S_{ob\ s}(\nu_{sM})(\nu_s/\nu_{sM})^{-\alpha_{s1}} & \nu_{sM}(r_u/r_M)^{-k_m} \lesssim \nu_s \leq \nu_{sM} \\ S_{ob\ s}(\nu_{sM})(\nu_s/\nu_{sM})^{-\alpha_{s2}} & \nu_{sM} \leq \nu_s \lesssim \nu_{sM}(r_u/r_M)^{k_b}, \end{cases} \tag{12}$$

where, setting $k_s = (1 + \alpha_o)m + n - 3$,

$$S_{ob\ s}(\nu_{sM}) \approx 3 \times 10^4 \, [C_1(\alpha_o)/C_1(0.5)](1+z)^{1-\alpha_o} D_{\ell 9}^{-2} \mathcal{D}_j^{2+\alpha_o} \varphi^2$$

$$K_1 B_1^{1+\alpha_o} \nu_{sM}^{-\alpha_o} r_M^{-k_s/k_s} \qquad \text{Jy},$$

and where $\alpha_{s1} = (4 + m - 5k_m)/2k_m$ and $\alpha_{s2} = \alpha_o + k_s/k_b$. [It is assumed here that $r_M \geq r_\ell$; if $r_\ell \gg r_M$, then the spectrum between $\nu_{sm}(r_\ell)$ and $\gamma_{sb}(r_\ell)$ is dominated by emission with spectral index α_o from r_ℓ. In addition, it is assumed that k_s, as well as k_c and k_{cc} below, are positive numbers.] The spectral indices α_{s1} and α_{s2} represent the effect of the nonuniformity of the source in the optically-thick and optically-thin regimes, respectively [the flattening of the optically-thick spectrum in an inhomogeneous synchrotron source has previously been pointed out by Condon and Dressel (1973), de Bruyn (1976), and Marscher (1977)]. For $\nu_{sb}(r_u) \lesssim \nu_s \lesssim \nu_{su}(r_u)$, the spectrum is dominated by emission from near r_u with spectral index

$(\alpha_o + 0.5)$, whereas above $\nu_{su}(r_u)$ the emission comes predominantly from $r_{max}(\nu_s) = (\nu_s/\nu_{su}(r_u))^{-1/m} r_u$, and the spectral index is approximately $\alpha_{s3} = (m+2-n)/m$. The synchrotron spectrum terminates near $\nu_{su}(r_u)$. This description is only approximate, and the actual spectrum changes slope continuously over a wide range of frequencies. An example of a synchrotron spectrum calculated in this way is shown in Figure 2. It is seen that the nonuniformity of B and K can give rise to an integrated spectrum quite different from the underlying emission spectrum (cf. Fig. 1). In turn, it should in principle be possible to deduce the values of m and n (as well as of α_o) from the observed shape of the spectrum. (Note that this cannot be done in models where only the optically-thick spectrum is affected by the source inhomogeneity; cf. Marscher 1977.) For example, if $\alpha_o = 0.5$ and $\alpha_{s1} = 0$, then $n = (17-7m)/5$ and $\alpha_{s2} = (8m-3)/(15m-10)$. If the magnetic field is convected by the jet, then, in a conical geometry, m can vary between 1 and 2 (e.g., Blandford and Rees 1974). Correspondingly, in this example, n and α_{s2} lie in the ranges 2 to 0.6 and 1 to 0.65, respectively, and for $m = 1$ the magnetic and electron energy densities are in equipartition (this special case was considered in Paper I).

The synchrotron self-Compton spectrum is calculated on the assumption that the emission at radius r is due mainly to the scattering of photons produced within a distance $\sim (r\varphi)$ from the scattering site. Even though the optical-depth to Thomson scattering, $\tau_c \approx \mathcal{D}_j^{-1} \sigma_T K_e r \varphi \csc\theta \gamma_{e\,min}^{-2\alpha_e}/\alpha_e$ (for a line of sight passing through the jet at a distance r from the apex), is typically $\ll 1$, this assumption is valid for a sufficiently narrow jet ($\varphi \ll 1$). In this case, equations (7) and (9) for the local emissivities are applicable. The once-scattered photon spectrum lies in

the range $\nu_{cm}(r_u) \lesssim \nu_c \lesssim \min\{\nu_{cu}(r_M); \nu_{KN}\}$. In a manner similar to the synchrotron-spectrum calculation, one finds that the observed flux density just below $\nu_{cM} \equiv \nu_{cm}(r_M)$ is given by

$$S_{ob\ c}(\nu_c) = S_{ob\ c}(\nu_{cM})(\nu_c/\nu_{cM})^{-\alpha_{c1}}, \tag{13}$$

where, setting $k_c = k_s + n - 1$,

$$S_{ob\ c}(\nu_{cM}) \approx 0.03\ (k_m/k_c^2)[C_1(\alpha_o)/C_1(0.5)]$$
$$(1+z)^{1-\alpha_o} D_{\ell 9}^{-2} \mathcal{D}_j^{2+\alpha_o} \varphi^3 K_1^2 B_1^{1+\alpha_o} \nu_{cM}^{-\alpha_o} r_M^{-k_c}\ \text{Jy},$$

and where $\alpha_{c1} = \max\{-(k_c/k_m - \alpha_o); -1\}$. (An optically-thin inverse-Compton spectrum cannot rise faster than $S_{ob\ c} \propto \nu_c$; e.g., Blumenthal and Gould 1970.) For $\nu_{cM} \lesssim \nu_c \lesssim \nu_{cb}(r_M)$, the spectrum is dominated by emission from near r_M with spectral index α_o, whereas for $\nu_{cb}(r_M) \lesssim \nu_c \lesssim \nu_{cb}(r_u)$, the spectral index is approximately $\alpha_{c2} = \alpha_o + k_c/(2k_b + m)$. The spectral indices α_{c1} and α_{c2}, like α_{s1} and α_{s2} in the synchrotron spectrum, arise because of the inhomogeneity of the source. The once-scattered photon spectrum is also illustrated in Figure 2. The higher-order inverse-Compton spectra display similar behavior, but in the frequency range of interest they generally lie well below the once-scattered photon spectrum for typical radio-jet parameters. For example, the maximum observed flux density of the twice-scattered photon spectrum is given approximately by

$$S_{ob\ cc}(\nu_{ccM}) \approx 3 \times 10^{-8}\ (k_m^2/k_{cc}^3)[C_1(\alpha_o)/C_1(0.5)](1+z)^{1-\alpha_o}$$
$$D_{\ell 9}^{-2} \mathcal{D}_j^{2+\alpha_o} \varphi^4 K_1^3 B_1^{1+\alpha_o} \nu_{ccM}^{-\alpha_o} r_M^{-k_{cc}}\ \text{Jy}, \tag{14}$$

where $\nu_{ccM} \equiv \gamma_{e\ell}^{4}\nu_{sm}$ and $k_{cc} = k_c + n - 1$, which may be compared with the analogous expression for the once-scattered photon flux given by equation (13).

The inverse-Compton spectrum steepens once the Klein-Nishina regime is reached (cf. Fig. 2). The high-energy flux could in principle be attenuated also by collisions between once-scattered synchrotron photons of frequencies $\nu_c \gtrsim \sqrt{2}\,\mathcal{D}_j m_e c^2/(1+z)h$ and synchrotron photons of frequencies $\nu_s \approx 2(\mathcal{D}_j m_e c^2/(1+z)h)^2/\nu_c$, which produce e^+e^- pairs with cross section $\sigma_p \approx 10^{-25}$ cm^2 (e.g., Jelley 1966). However, the optical depth for this process, $\tau_p(\nu_c) \approx \mathcal{D}_j^{-1}(\varepsilon_s[2\mathcal{D}_j(m_e c^2/h)^2/(1+z)\nu_c]$ $r\varphi/hc)\ \sigma_p(2r\varphi \csc\theta)$, evaluated at $r_{min}(\nu_c)$, is typically much smaller than unity, so in practice the attenuation is negligible. Note that in this model most of the energy emitted from the jet is assumed to be synchrotron radiation [cf. the discussion following eq. (10)]. If the integrated synchrotron spectrum breaks near ν_s^* from $\alpha_s < 1$ to $\alpha_s > 1$, then most of the energy is emitted near ν_s^*. The precise value of ν_s^* depends of course on the parameters of the source, but in general it lies in the frequency range dominated by emission from the outer region of the jet.

The spectra displayed in Figure 2 are calculated for a representative beamed source. It is assumed in this calculation that $\mathcal{D}_j \approx \gamma_j \approx \csc\theta$, which for a source observed at a given angle θ is the combination which maximizes the Doppler factor $\mathcal{D}_j$. (In this case the apparent velocity β_{ob} is also $\approx \mathcal{D}_j$; cf. Paper I.) Those portions of the spectrum which arise essentially in the same region (e.g., near r_M or r_u) should show correlated

variability and could vary on a different timescale than the flux which is emitted from a different region [cf. eq. (10)]. Although some of the specific assumptions used in calculating the spectrum, such as constant φ and β_j, may not all apply in real sources, this model can nevertheless be used to account for various broad features of observed spectra, as is discussed in the next section.

III. APPLICATIONS

a) Spectra of BL Lac Objects

BL Lac objects have been interpreted as extreme cases of beamed sources, in which the Doppler boost is so large that a substantial portion of the observed optical spectrum is dominated by the nonthermal contribution from the jet (cf. Blandford and Rees 1978b, and Paper I). It is proposed here that the beamed component may in fact dominate most of the observed spectrum from radio frequencies through x-rays. In support of this hypothesis, it is shown that the model spectrum calculated in §IIb for an unresolved, inhomogeneous relativistic jet could account for various properties of the spectra measured in these sources. First, general features are outlined for the different spectral regimes, and then a particular source (Mrk 421) is discussed in greater detail.

i) Radio — The radio spectra typically are flat, and become optically-thin near or above $\sim 10^{11}$ Hz, which is higher than the average break frequency for flat-radio-spectrum QSO's (e.g., Condon 1978). The spectra may be interpreted in the inhomogeneous-jet model as corresponding to $\alpha_{s1} \approx 0$, and the higher break frequency is consistent, by equation (6) for ν_{sM}, with a higher degree of beaming (i.e., with a larger value of $\mathcal{D}_j$ or of $\csc \theta$).

ii) Optical — The high degree of variability and strong linear polarization displayed by BL Lac objects may be associated with the beamed emission from the jet, as discussed in Paper I. However, the optical spectrum of some sources, such as Mrk 421 and Mrk 501 (e.g., Ulrich et al. 1975, Maza, Martin, and Angel 1978), appears to contain also a contribution from the associated elliptical galaxy, and therefore cannot be compared with the model of §IIb.

iii) X-Rays — BL Lac objects have now been established also as a class of x-ray sources (e.g., Schwartz et al. 1979, Ku 1980). Present data indicate that below ~ 5 keV their spectra are generally soft ($\alpha \gtrsim 1$), but some sources, e.g., the Markarian galaxies 421 and 501 (Mushotzky et al. 1978b), and PKS 0548-322 (Riegler, Agrawal, and Mushotzky 1979), display a hard ($\alpha < 0.5$) component at higher energies. These two components could be interpreted as synchrotron radiation and once-scattered inverse-Compton radiation, respectively (cf. Margon, Jones, and Wardle 1978; Schwartz et al. 1978). In those sources where it was detected, the hard x-ray component has a flux density which is a fraction (a few) $\times 10^{-6}$ of the flat-spectrum radio flux density. This is consistent with the estimates of §IIb for a reasonable choice of parameters in equations (5), (6), (12), and (13), and suggests that the absence of a detectable hard x-ray component in sources like PKS 2155-304 (e.g., Griffiths et al. 1979) is due to the fact that they have a relatively high ($\gtrsim 10^{-5}$) ratio of x-ray to radio flux densities at the observed x-ray frequencies. In the present model it is predicted that all sources would display a hard x-ray component at sufficiently high energies, that this component would on the average show less linear polarization than the soft x-ray component (reflecting the difference between the emission mechanisms attributed to these com-

ponents), and that it would vary in correlation with the high-frequency ($\nu_s \lesssim \nu_{sM}$) radio flux density (since the bulk of the emission in both cases is assumed to come from the same region near r_M).

iv) γ-Rays — No BL Lac object has as yet been detected in high-energy γ-rays, but upper limits set by Bignami et al. (1979) for Mrk 421 and Mrk 501 indicate that the flux density must decrease by a factor $>10^2$ between 10 keV and 100 MeV. This means that the effective spectral index in this range exceeds 0.5, which is consistent with the behavior of the once-scattered photon spectrum in the present model, and implies that the hard x-ray component measured in these sources in the 2-30 keV range (e.g., Mushotzky et al. 1978b) must steepen at higher energies.

As a specific application of the model, consider the source Mrk 421. The high degree of variability measured in this object, particularly in the optical and x-rays, supports an association with a relativistic beamed source. However, because of the inherent variability and the incomplete spectral coverage, a steady-state spectrum which could be compared with the model spectrum of §IIb is still not well established. The observed radio spectrum is flat and shows no break below 90 GHz (cf. O'Dell et al. 1978), and so could conceivably join with the far-infrared spectrum, which is nonthermal with spectral index $\gtrsim 0.8$ (e.g., Ulrich et al. 1975, Maza, Martin, and Angel 1978). The UV spectrum measured by the IUE (Boksenberg et al. 1978) and the soft x-ray spectrum measured by Hearn, Marshall, and Jernigan (1979) below 6 keV have similar spectral indices (≈ 1), and may in fact join together. The hard x-ray component measured by Mushotzky et al. (1978b) at higher energies was not detected at a later measurement (Mushotzky et al. 1979), which also revealed a steepening of the soft component. It is possible to give a self-consistent interpreta-

tion of these observations in the inhomogeneous-jet model. The measured spectrum from the radio to soft x-rays, excluding the galactic optical contribution, may be modeled by a synchrotron spectrum with $\alpha_{s1} \approx 0$, $\alpha_{s2} \approx 0.8$, and $\alpha_o \approx 0.5$, and with the break frequencies ν_{sM}, $\nu_{sb}(r_u)$ and $\nu_{su}(r_u)$ being roughly 10^{12} Hz, 10^{15} Hz, and 10^{17} Hz, respectively. The soft x-ray component is then produced in the outer region of the jet near r_u, whereas the hard x-ray component, interpreted as once-scattered inverse-Compton emission, is produced in the inner region near r_M. It is therefore expected that the hard component would show a higher degree of variability, and the reported timescale of $\lesssim 1$ year is consistent with the cooling-time estimate of equation (10). Mrk 421 also displayed a strong x-ray outburst on a timescale of ~ 10 days (Ricketts, Cooke, and Pounds 1976), for which no direct evidence exists at optical wavelengths, but which was observed in the radio, with amplitude that increased with frequency and a variability timescale of a few months (Margon, Jones, and Wardle 1978). If the outburst was due to a change in the steady-state conditions near the origin of the jet, then these observations are consistent with the radio emission coming from progressively smaller radii as the frequency approaches ν_{sM}, and with the optical radiation being emitted at $r \gg r_M$. Alternatively, the outburst could be interpreted as emission from clouds or shock waves traveling in the jet, which at lower radio frequencies would be obscured by the optically-thick "core" of the jet (cf. Paper I).

b) Spectrum of 3C273

The archetypal quasar 3C273 has been observed at frequencies ranging from radio to high-energy γ-rays. It is associated with a core-jet radio source which is resolved by VLBI on a milliarcsecond scale (e.g., Readhead et al. 1979), and which shows evidence for relativistic motion in the form of apparent superluminal separation of radio components with $\beta_{ob} \approx 5.2$ (e.g., Cohen et al. 1979). The radio spectrum is flat and polarized (e.g., Rudnick et al. 1978), and could be accounted for by the inhomogeneous-jet model of §IIb, which is compatible with the observed morphology of the source. The absence of an observed counterjet may be another indication that the radio source is beamed (e.g., Readhead et al. 1978).

The radio spectrum breaks at $\sim$ 50 GHz, and could conceivably be extrapolated to the infrared regime with $\alpha \sim 0.8$ (cf. Elias et al. 1978); however, the infrared component is much steeper and, like the optical component, shows little variability (e.g., Neugebauer et al. 1979) and low polarization (e.g., Kemp et al. 1977). These components thus appear to be distinct from the radio component, a conclusion which is supported by the apparent lack of correlation between the infrared-optical and the radio regimes in quasars in general (cf. Neugebauer et al. 1979). The observed UV flux (e.g., Boksenberg et al. 1978) is consistent with the ionizing continuum required to produce the unbeamed H_β flux (e.g., Weedman 1976), and probably is also not associated with the jet.

X-ray spectral measurements of 3C273 have been obtained by Primini et al. (1979) and by Worrall et al. (1979). The best-fit spectral index is ≈ 0.4 in the range 2-60 keV, and ≈ 0.7 in the range 13-120 keV, with a change of slope indicated above $\sim$ 20 keV. The x-ray flux appears to vary by a factor $\lesssim 2$ on a timescale of months. Both the spectral shape and the degree of variability are similar to those of Seyfert 1 galaxies (e.g., Mushotzky et al. 1980), which are generally weak radio sources and do not show evidence for beaming (e.g., Weedman 1977). A similarity with Seyfert 1 spectra is indicated also by x-ray measurements of other quasars (e.g., Apparao et al. 1978), but more observations are required to determine whether it holds for quasars in general. The x-rays could in principle also be once-scattered synchrotron self-Compton photons (cf. Jones 1979). However, it is difficult to fit the observed x-rays with the model spectrum of §IIb given the constraints imposed by the radio spectrum and the apparent velocity.

As was mentioned in the Introduction, 3C273 is as yet the only quasar identified as a high-energy γ-ray source, with a possibly variable flux density of $\sim 2 \times 10^{-9}$ Jy around 100 MeV (Swanenburg et al. 1978). The γ-ray flux density is consistent with an extrapolation of the synchrotron spectrum with $\alpha \approx 1$ from the radio break frequency. (This spectrum would pass also through the observed x-ray regime, but is too steep to account for the observed x-ray spectrum.) However, the electron Lorentz

factors required to produce such high-energy synchrotron emission must be $\gtrsim 10^8$. If the synchrotron spectral index above the break frequency is in fact smaller (~ 0.7-0.8), then it is also possible to interpret the γ rays as once-scattered inverse-Compton radiation from the jet. For example, if $\alpha_o = 0.5$, the once-scattered spectrum would steepen near $\nu_{cb}(r_M) \approx 10^{15}$-$10^{16}$ Hz, where $S_{ob\ c} \approx 10^{-6}$-$10^{-5}$ Jy, from $\alpha_c \approx 0.5$ to $\alpha_c \approx 0.6$-0.7, and could extend up to the γ-ray region, passing below the observed x-ray spectrum. (Note that in the model of Jones (1979), the γ-rays are interpreted as twice-scattered synchrotron photons.)

To summarize, the radio emission in 3C273 is attributed to an inhomogeneous relativistic jet which could also produce the high-energy γ-rays, but other parts of the observed spectrum appear to be unbeamed. It is therefore likely that the Doppler factor associated with the beamed component is relatively small, implying that the angle θ between the jet axis and the observer direction is relatively large. However, the high observed velocity constrains θ to be $\leq 2\ \mathrm{ctn}^{-1}(\beta_{ob}) \approx 22^o$, and indicates a large β_j. The origin of the γ-ray flux in 3C273 is further discussed in §IV.

c) X-Ray Emission from Resolved Jets

The inhomogeneous-jet spectrum calculated in §IIb is based on a simple synchrotron spectrum, as described in §IIa. It is of interest to verify that the assumed local emission spectrum is in fact an adequate representation of the spectra observed in resolved jets. One suitable example is provided by the spectrum of the emission knot A in the jet of

M87 (e.g., Turland 1975; Redman 1978). The spectrum extends from $\sim 10^8$ Hz with $\alpha \approx 0.5$ and steepens above $\sim 10^{14}$ Hz to $\alpha \approx 1.3$. The recently discovered x-ray emission from this knot (e.g., Schreier et al. 1979b) is consistent with a linear extrapolation of this spectrum. The break at optical frequencies may be interpreted as due to synchrotron-radiation losses. (An increase in the spectral index by more than 0.5 could indicate that the reacceleration of relativistic electrons is not continuous; cf. Kellermann 1966.) It is then possible to estimate the magnetic field as a function of the size of the emission region and the velocity of the radiating material [cf. eq. (4)]. This was done for knot A by Blandford and Königl (1979a), who interpreted the emission as arising behind a shock wave traveling in the jet (see also Rees 1978).

X-ray emitting knots have also been detected in Cen A, where they lie within the inner NE radio lobe, and are aligned with the inner optical jet (e.g., Schreier et al. 1979a, Feigelson and Schreier 1979). A large knot located about 1' from the nucleus was measured by the Einstein HRI to have a diameter $d \sim 15''$ (≈ 0.4 kpc at a distance of 5 Mpc) and a surface brightness of $\sim 10^{-9}$ Jy arcsec^{-2} (0.3-3 keV). By analogy with knot A in M87, it is proposed here that the x-rays be interpreted as synchrotron radiation emitted above the break frequency. (Note that Schreier et al. (1979a) interpreted the x-ray emission as thermal in origin.) Using an injection spectral index $\alpha = 0.65$, which is compatible with the spectral index of both the radio and the x-ray emission from the nucleus (e.g., Mushotzky et al. 1978a), and a lower cutoff frequency of $\sim 10^8$ Hz, one can estimate the equipartition magnetic field in the emission region to be $B \approx 5 \times 10^{-6}\ (d/0.4)^{-2/7}$ G. (Note that emission due to inverse-Compton scattering of the microwave background will not exceed the synchrotron emission for as long as $B \gtrsim 3 \times 10^{-6}$ G; cf. Harris and Grindlay 1979.)

Unlike the case of the jet in M87, there is direct evidence in Cen A for radial motion of optical knots away from the nucleus (Osmer 1978, Dufour and van den Bergh 1978). The measured radial velocities are in the range $2.5\text{-}3.5 \times 10^7$ cm s^{-1} for knots lying at projected distances of 13 to 24 kpc from the nucleus. The relative uniformity of the velocity values supports the interpretation of the knots as clouds that have been accelerated by the jet. The terminal velocities of such clouds are generally expected to be smaller than the jet velocity (cf. Blandford and Königl 1979a) and, in addition, the jet velocity may be higher near the nucleus. The measured radial velocities thus provide only a lower limit on the velocity v_j of the jet at the position of the large x-ray knot. Assuming that the emission arises behind a strong shock, as is in fact indicated by the optical spectra of three of the knots observed by Osmer (1978), one can estimate the break frequency in the x-ray knot to be $\nu_b \approx 5 \times 10^{12}\ (d/0.4)^{-8/7}\ (v_j/10^8)^2$ Hz. Now, the x-ray knot is located within the radio ridge which appears in the 1.4 GHz ($\sim$ 1' resolution) map of Christiansen et al. (1977) between the nucleus and the inner NE lobe. In order not to exceed the radio surface brightness estimated from this map ($\approx 10^{-3}$ Jy arcsec^{-2}), the break frequency must be $\gtrsim 10^{15}$ Hz (for $\alpha \approx 0.65$). This could be reconciled with the above estimate if either $d \ll 15''$ or $v_j \gg 10^8$ cm s^{-1}. The first possibility is consistent with the visual diameters of the moving knots measured by Osmer (1978), which are $\sim$ 1" (e.g., Blanco et al. 1975), especially in view of the fact that accelerated clouds would expand as they move downstream in the jet (cf. Blandford and Königl 1979a). As was discussed by Blandford and Königl (1979a and Paper I), the knots could be either interstellar clouds (which may form in the inner optical jet of Cen A by a thermal instability; cf. Schreier et al. 1979a), planetary nebulae, or supernova remnants. They might also be portions of the jet's wall which were torn

off near the origin of the jet by hydrodynamical instabilities. High-resolution radio observations and sensitive spectroscopic measurements should be able to determine the actual sizes of the x-ray emitting knots, their velocities, and their origin.

IV. DISCUSSION

As was mentioned in the Introduction, recent x-ray observations suggest that a large fraction of quasars and BL Lac objects are also x-ray sources. Although the sample is still incomplete, there are indications that BL Lac objects and optically-violent variable quasars have a higher ratio of x-ray to optical luminosity than radio-quiet QSO's (e.g., Ku and Helfand 1980). This is manifested in the value of the effective optical-to-x-ray spectral index α_{ox} (defined, e.g., by Tananbaum et al. 1979), which is ~ 1.25 for blazars and ~ 1.5 for radio-quiet QSO's. These spectral indices could be interpreted as corresponding, respectively, to the beamed and isotropic emission spectra in quasars. In fact, the deduced value of α_{ox} for blazars is consistent with the soft x-ray component measured in several BL Lac objects, as discussed in §IIIa. Alternatively, the larger average x-ray luminosity in blazars could reflect an increase in the relative contribution of the beamed component in these sources on going from optical to x-ray frequencies. Ku and Helfand (1980) analyzed the statistical properties of a sample of active galactic nuclei, and found a good correlation between the x-ray (2 keV) and optical (2500 Å) fluxes, but no correlation between the x-ray flux and the radio flux at 1.4 GHz. These properties are consistent with the x-rays being associated with the isotropic optical component rather than with the beamed radio emission (cf. §IIIb). However, according to the inhomogeneous-jet model

discussed in the previous sections, the flux densities at 2 keV and 1.4 GHz could be emitted from widely separated regions in the jet, and so need not be well correlated even in strongly beamed sources. In some of these sources, moreover, the low-frequency radio emission could be associated with an observed steep-spectrum halo (cf. Ku and Helfand 1980), which may correspond to an outer radio lobe seen head on (e.g., Paper I).

It has been suggested, on the basis of their observed x-ray luminosities and apparently strong cosmological evolution, that quasars account for most of the diffuse x-ray background in the few-keV range (e.g., Setti and Woltjer 1979, Tananbaum et al. 1979). However, Schwartz et al. (1978) estimated that, in the absence of density evolution, BL Lac objects contribute only a few percent of the background in that energy range. Of course, this estimate could be revised if BL Lac objects are shown to evolve, or if their volume emissivity is larger than that assumed by Schwartz et al. According to the beaming hypothesis, radio-loud quasars (which are usually associated with cD galaxies) and BL Lac objects (generally associated with giant elliptical galaxies) are the intrinsically faint sources which are brightened by the relativistic Doppler effect. If the Lorentz factors associated with the beamed components in these two types of sources are comparable, then the fraction of radio-loud quasars among optically-selected QSO's ($\approx$ 5%, e.g., Sramek and Weedman 1978) is expected to be of the same order as the fraction of BL Lac objects among giant elliptical galaxies. This in fact is consistent with the current space-density estimates of BL Lac objects ($\approx 10^2$ Gpc^{-3}; e.g., Setti 1978) and of giant elliptical galaxies ($\approx 10^4$ Gpc^{-3}; e.g., Schmidt 1966). However, at least some BL Lac objects

appear to be associated with elliptical galaxies at the top of the luminosity function (e.g., Kinman 1978, Griffith et al. 1979), suggesting that there may be many more faint BL Lac objects which have not yet been identified. Setti and Woltjer (1979) noted that if quasars account for much of the observed x-ray background, then only 5% of quasars could have the same ratio of x-ray to γ-ray flux densities as 3C273 if the diffuse high-energy γ-ray background is not to be exceeded. If 3C273 is a typical quasar, then this fact may have important consequences when interpreted in the context of the beaming hypothesis. It could suggest the existence of a correspondence between radio-loud and γ-ray-loud quasars, implying that both the radio and the γ-ray emission in 3C273 originate in the beamed jet. Such correspondence would also imply that the diffuse background at high ($\gtrsim$ 100 MeV) energies is dominated by radiation from beamed sources. Of course, these inferences are merely suggestive, and could only be checked after additional extragalactic high-energy γ-ray sources are detected. Note that if the ratios of γ-ray to x-ray flux density in BL Lac objects are comparable to that in 3C273, then Lacertids would contribute a substantial fraction of the diffuse γ-ray background even without evolution. If most of the high-energy background is produced by beamed sources with similar spectra, then the observed spectrum of the background at these energies (e.g., Fichtel, Simpson, and Thompson 1978) should reflect the shape of the individual spectra. In addition, improved limits on the isotropy of the background could constrain the number density of these sources (cf. Schwartz and Gursky 1974).

V. SUMMARY

This paper considered the radio-through-γ-ray emission from relativistic jets associated with bright compact radio sources. A simple local synchrotron emission spectrum was adopted, with an assumed break frequency determined by equating the synchrotron cooling time to the expansion time. This spectrum was applied to the interpretation of emission knots in the jets of M87 and of Cen A, and to the calculation of a synchrotron and inverse-Compton spectra for an unresolved inhomogeneous jet. In this calculation it was shown how the nonuniformity of the magnetic field and relativistic-electron density in the source could give rise to an integrated spectrum which is quite different from the local emission spectrum in both the optically-thick and the optically-thin regimes. It was pointed out which parts of the integrated spectrum are emitted from the same region of the jet, and would therefore be expected to show correlated variability. The inhomogeneous-jet model was applied to the interpretation of the spectra of BL Lac objects. In particular, it could account for the flat radio spectrum and the relatively high break frequency, as well as for the soft component and the more highly variable hard component observed in x-rays. On the basis of this model, it was predicted that a hard spectral component would be detected in all BL Lac objects at sufficiently high energies, that it would be less strongly polarized than the soft x-ray component, and that it would vary in correlation with the high-frequency radio emission. In the case of 3C273, it was concluded that the infrared-through-x-ray spectrum is probably unbeamed, but that the radio flux and possibly also the high-energy γ-rays could be attributed to the relativistic inner radio jet. Finally, the distinguishing properties of blazars as a class of x-ray sources were considered in

the context of the jet model, and it was pointed out that beamed sources could contribute a major fraction of the diffuse high-energy γ-ray background.

I thank Roger Blandford and David Payne for valuable suggestions and encouragement.

TABLE 1

LOCAL RELATIVISTIC ELECTRON DISTRIBUTION AND OPTICALLY-THIN SYNCHROTRON SPECTRUM IN THE JET

K_e	α_e	$\gamma_{e\ min}$	$\gamma_{e\ max}$	ε_s	α_s	$\nu_{s\ min}$	$\nu_{s\ max}$
K	α_o	$\gamma_{e\ell}$	γ_{eb}	const. $\nu_s^{-\alpha_o}$	α_o	ν_{sm}	ν_{sb}
K γ_{eb}	$\alpha_o + 0.5$	γ_{eb}	γ_{eu}	const. $(\nu_s/\nu_{sb})^{-0.5}\nu_s^{-\alpha_o}$	$\alpha_o + 0.5$	ν_{sb}	ν_{su}

REFERENCES

Angel, J. R. P., and Stockman, H. S. 1980, to be published in Ann. Rev. Astr. Ap., Vol. 18.

Apparao, K. M. V., Bignami, G. F., Maraschi, L., Helmken, H., Margon, B., Hjellming, R., Bradt, H. V., and Dower, R. G. 1978, Nature, 273, 450.

Bignami, G. F., Fichtel, C. E., Hartman, R. C., and Thompson, D. J. 1979, Ap. J., 232, 649.

Blanco, V. M., Graham, J. A., Lasker, B. M., and Osmer, P. S. 1975, Ap. J. (Letters), 198, L63.

Blandford, R. D., and Königl, A. 1979a, Ap. Letters, 20, 15.

_____. 1979b, Ap. J., 232, 34 (Paper I).

Blandford, R. D., and Rees, M. J. 1974, M.N.R.A.S., 169, 395.

_____. 1978a, Physica Scripta, 17, 265.

_____. 1978b, in Pittsburgh Conference on BL Lac Objects, ed. A. M. Wolfe (Pittsburgh: University of Pittsburgh), p. 328.

Blumenthal, G. R., and Gould, R. J. 1970, Rev. Mod. Phys., 42, 237.

Boksenberg, A., et al. 1978, Nature, 275, 404.

Christiansen, W. N., Frater, R. H., Watkinson, A., O'Sullivan, J. D., and Lockhart, I. A. 1977, M.N.R.A.S., 181, 183.

Cohen, M. H., Pearson, T. J., Readhead, A. C. S., Seielstad, G. A., Simon, R. S., and Walker, R. C. 1979, Ap. J., 231, 293.

Condon, J. J. 1978, in Pittsburgh Conference on BL Lac Objects, ed. A. M. Wolfe (Pittsburgh: University of Pittsburgh), p. 21.

Condon, J. J., and Dressel, L. L. 1973, Ap. Letters, 15, 203.

de Bruyn, A. G. 1976, Astr. Ap., 52, 439.

Dufour, R. J., and van den Bergh, S. 1978, Ap. J. (Letters), 226, L73.

Elias, J. H., et al. 1978, Ap. J., 220, 25.

Feigelson, E., and Schreier, E. 1979, Bull. AAS, 11, 792.

Fichtel, C. E., Simpson, G. A., and Thompson, D. J. 1978, Ap. J., 222, 833.

Griffiths, R. E., Tapia, S., Briel, V., and Chaisson, L. 1979, Ap. J., 234, 810.

Harris, D. E., and Grindlay, J. E. 1979, M.N.R.A.S., 188, 25.

Hearn, D. R., Marshall, F. J., and Jernigan, J. G. 1979, Ap. J. (Letters), 227, L63.

Jelley, J. V. 1966, Nature, 211, 472.

Jones, T. W. 1979, Ap. J., 233, 796.

Kellermann, K. I. 1966, Ap. J., 146, 621.

Kemp, J. C., Rieke, G. H., Lebofsky, M. J., and Coyne, G. V. 1977, Ap. J. (Letters), 215, L107.

Kinman, T. D. 1978, in Pittsburgh Conference on BL Lac Objects, ed. A. M. Wolfe (Pittsburgh: University of Pittsburgh), p. 82.

Ku, W. H. M. 1980, to be published in Highlights in Astronomy.

Ku, W. H. M., and Helfand, D. J. 1980 (preprint).

Margon, B., Jones, T. W., and Wardle, J. F. C. 1978, A. J., 83, 1021.

Marscher, A. P. 1977, Ap. J., 216, 244.

Maza, J., Martin, P. G., and Angel, J. R. P. 1978, Ap. J., 224, 368.

Mushotzky, R. F., Boldt, E. A., Holt, S. S., Pravdo, S. H., Serlemitsos, P. J., Swank, J. H., and Rothschild, R. H. 1978b, Ap. J. (Letters), 226, L65.

Mushotzky, R. F., Boldt, E. A., Holt, S. S., and Serlemitsos, P. J. 1979, Ap. J. (Letters), 232, L17.

Mushotzky, R. F., Marshall, F. E., Boldt, E. A., Holt, S. S., and Serlemitsos, P. J. 1980, Ap. J., 235, 377.

Mushotzky, R. F., Serlemitsos, P. J., Becker, R. H., Boldt, E. A., and Holt, S. S. 1978a, Ap. J., 220, 790.

Neugebauer, G., Oke, J. B., Becklin, E. E., and Mathews, K. 1979, Ap. J., 230, 79.

O'Dell, S. L., Puschell, J. J., Stein, W. A., Owen, F., Porcas, R. W., Mufson, S., Moffett, T. J., and Ulrich, M. H. 1978, Ap. J., 224, 22.

Osmer, P. S. 1978, Ap. J. (Letters), 226, L79.

Primini, F. A., et al. 1979, Nature, 278, 234.

Readhead, A. C. S., Cohen, M. H., Pearson, T. J., and Wilkinson, P. N. 1978, Nature, 276, 768.

Readhead, A. C. S., Pearson, T. J., Cohen, M. H., Ewing, M. S., and Moffet, A. T. 1979, Ap. J., 231, 299.

Redman, R. O. 1978 (preprint).

Rees, M. J. 1978, M.N.R.A.S., 184, 61.

Ricketts, M. J., Cooke, B. A., and Pounds, K. A. 1976, Nature, 259, 546.

Riegler, G. R., Agrawal, P. C., and Mushotzky, R. F. 1979, Ap. J. (Letters), 233, L47.

Rieke, G. H., and Weekes, T. C. 1969, Ap. J., 155, 429.

Rudnick, L., Owen, F. N., Jones, T. W., Puschell, J. J., and Stein, W. A. 1978, Ap. J. (Letters), 225, L5.

Scheuer, P. A. G., and Readhead, A. C. S. 1979, Nature, 277, 182.

Schmidt, M. 1966, Ap. J., 146, 7.

Schreier, E. J., Feigelson, E., Delvaille, J., Giacconi, R., Grindlay, J., and Schwartz, D. A. 1979a, Ap. J. (Letters), 234, L39.

Schreier, E., Feigelson, E., Fabricant, D., and Gorenstein, P. 1979b, Bull. AAS, 11, 791.

Schwartz, D. A., Bradt, H. V., Doxsey, R. E., Griffiths, R. E., Gursky, H., Johnston, M. D., and Schwarz, J. 1978, Ap. J. (Letters), 224, L103.

Schwartz, D. A., Doxsey, R. E., Griffiths, R. E., Johnston, M. D., and Schwarz, J. 1979, Ap. J. (Letters), 229, L53.

Schwartz, D., and Gursky, H. 1974, in X-Ray Astronomy, ed. R. Giacconi and H. Gursky (Dordrecht: Reidel), p. 359.

Setti, G. 1978, in Pittsburgh Conference on BL Lac Objects, ed. A. M. Wolfe (Pittsburgh: University of Pittsburgh), p. 385.

Setti, G., and Woltjer, L. 1979, Astr. Ap., 76, L1.

Sramek, R. A., and Weedman, D. W. 1978, Ap. J., 221, 468.

Swanenburg, B. N., et al. 1978, Nature, 275, 298.

Tananbaum, H., et al. 1979, Ap. J. (Letters), 234, L9.

Turland, B. D. 1975, M.N.R.A.S., 170, 281.

Ulrich, M. H., Kinman, T. D., Lynds, C. R., Rieke, G. H., and Ekers, R. D. 1975, Ap. J., 198, 261.

Weedman, D. W. 1976, Ap. J., 208, 30.

_____. 1977, Ann. Rev. Astr. Ap., 15, 69.

Worrall, D. M., Mushotzky, R. F., Boldt, E. A., Holt, S. S., and Serlemitsos, P. J. 1979, Ap. J., 232, 683.

FIGURE CAPTIONS

FIG. 1. The local emission spectra in the jet. The model synchrotron spectrum (labeled S) has an injection spectral index $\alpha_o = 0.5$. The once-scattered inverse-Compton spectrum (labeled C) was calculated for this model spectrum using equations (7) and (9). The spectra displayed in this figure represent the local emission spectra at a distance of 1 pc from the origin in the inhomogeneous-jet model described in the caption of Fig. 2. All the frequencies marked in the figure are defined in the text.

FIG. 2. The synchrotron and inverse-Compton spectra for an unresolved inhomogeneous jet. This example corresponds to a relativistic conical jet with $D_{\ell 9} = 0.5$, $\mathcal{D}_j = \gamma_j = \csc\theta = 5$ and $\varphi = 0.1$, and a synchrotron spectrum with $\nu_{sm}(r_u) = 10^9$Hz, $\nu_{sM} = 5 \times 10^{11}$ Hz, $S_{ob\ s}(\nu_{sM}) = 1.0 J_y$, $\alpha_o = 0.5$, $\alpha_{s1} = 0$, and $\alpha_{s2} = 0.8$. (All the quantities referred to in the caption or marked in the figure are defined in the text.) Using these observable parameters in eqs. (5), (6), and (12), one obtains m = 1.25, n = 1.65, $K_1 = 1.7 \times 10^2$ cm^{-3}, $B_1 = 2.9 \times 10^{-2}$G, $r_M = 2.3 \times 10^{-2}$ pc and $r_u/r_M = 3.7 \times 10^2$. These values, as well as $\gamma_{e\ell} = 50$ and $\gamma_{eu} = 5 \times 10^6$, were used in eqs. (2), (7), (9), and (11) to generate the synchrotron spectrum (labeled S) and the once-scattered inverse-Compton spectrum (labeled C) which are shown here. Note that in this example $\alpha_{s3} = 1.28$, $\alpha_{c1} = 0.62$, and $\alpha_{c2} = 0.75$. The local emission spectra in this jet at a distance of 1 pc from the origin are displayed in Fig. 1.

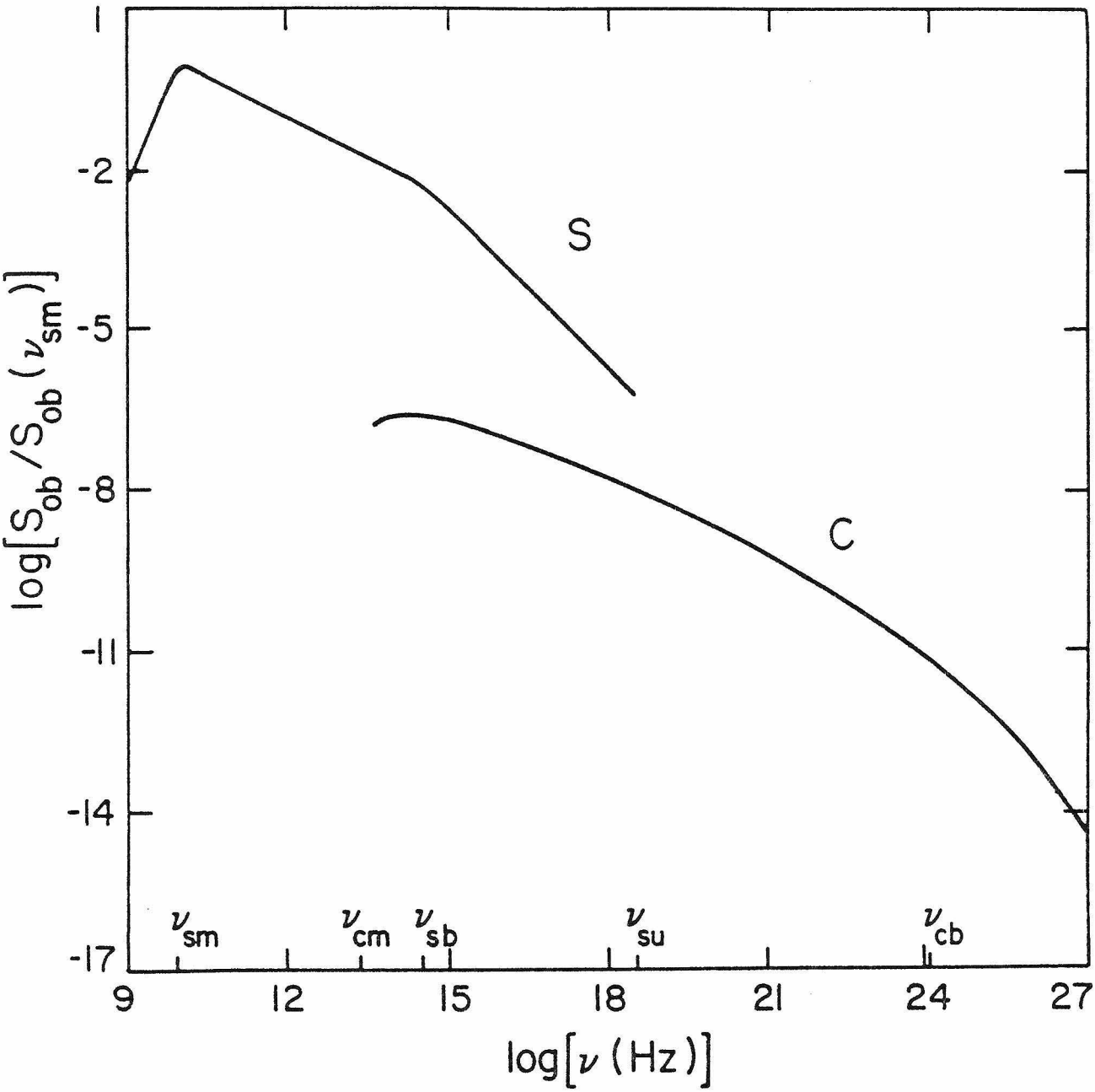
1
-2
-5
-8
-11
-14
-17
9
12
15
18
21
24
27
S
C
ν_{sm}
ν_{cm}
ν_{sb}
ν_{su}
ν_{cb}
$\log[S_{ob}/S_{ob}(\nu_{sm})]$
$\log[\nu\,(Hz)]$

Fig. 1

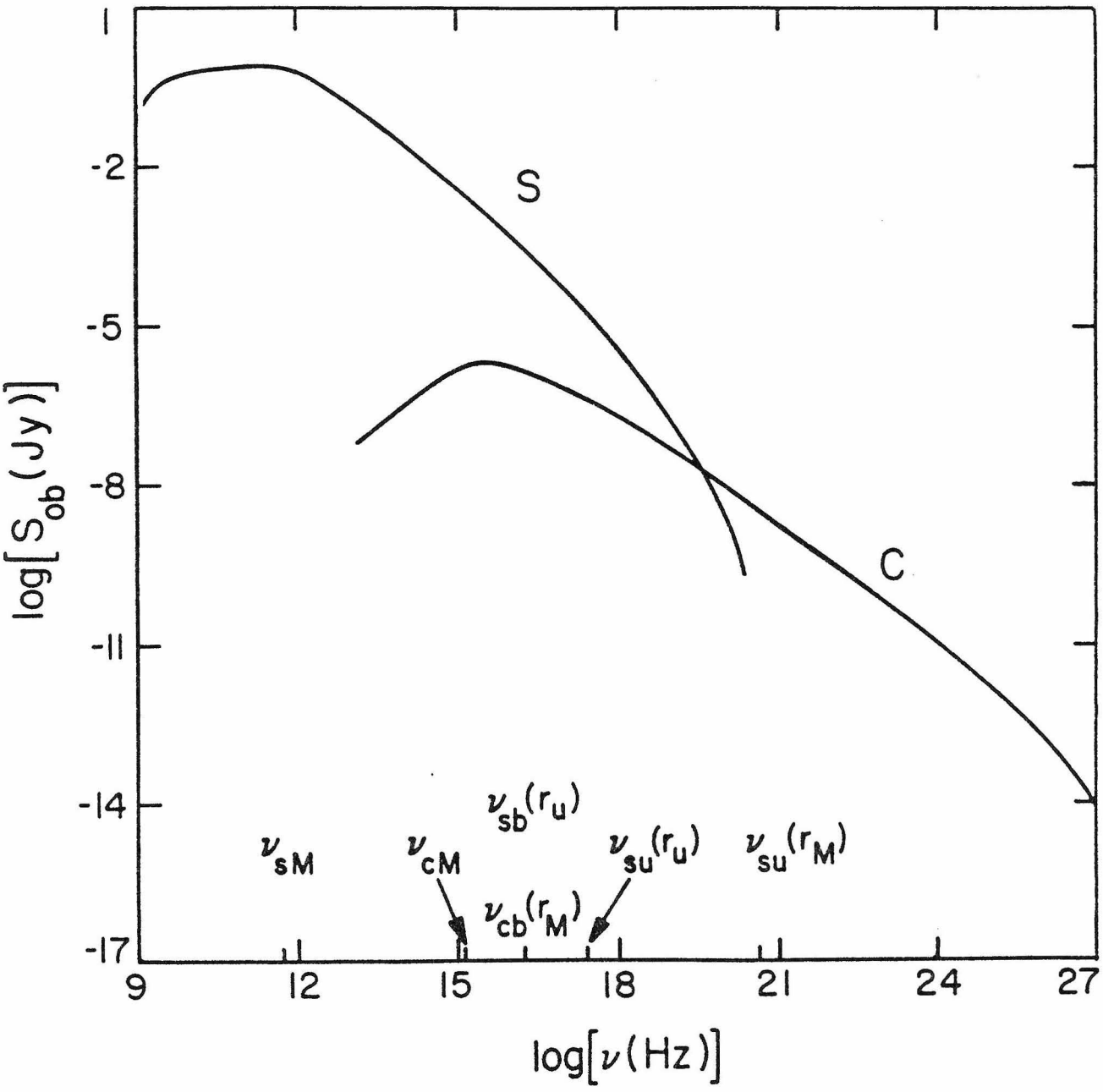
1
-2
-5
-8
-11
-14
-17
9
12
15
18
21
24
27
log[S_ob(Jy)]
log[ν(Hz)]
S
C
ν_sb(r_u)
ν_sM
ν_cM
ν_su(r_u)
ν_su(r_M)
ν_cb(r_M)

Fig. 2

PAPER 5

RELATIVISTIC GAS DYNAMICS IN TWO DIMENSIONS

I. INTRODUCTION

Relativistic gas dynamics is the study of the equations of gas motion when either the macroscopic velocity (associated with bulk motion) or the average microscopic velocity (associated with temperature) is of the order of the speed of light. In the absence of gravitational effects, this study is carried out within the framework of special-relativity theory. Most of the work in this field to date has been on problems of motion in one dimension[1-6]; the treatment of two-dimensional gas flow has not been as extensive, probably because it was not considered necessary to the analysis of actual physical phenomena. However, very-long-baseline interferometric observations over the past few years[7] have revealed that many extra-galactic radio sources are associated with plasma jets emanating from a central component and show evidence for relativistic bulk motions. These discoveries provide one motivation for a study of relativistic gas dynamics in two dimensions, with application to such problems as the structure of the jet and the refraction of shock waves at the interface between the jet and the surrounding medium. Two-dimensional relativistic flows may arise also in cosmology (e.g., in the context of galaxy formation from fluctuations in the early universe[8]) and in nuclear physics (e.g., in collisions of energetic heavy ions with heavy nuclei[9]).

The present paper considers steady flow of an ideal compressible fluid in two dimensions. In studying relativistic gas dynamics, one is confronted with the task of transforming coordinate-independent relationships which describe the flow in four-dimensional space-time into more useful expressions which describe the ordinary three-dimensional flow as

it appears in some particular frame of reference. One approach to this problem[10,11] consists of transforming the special-relativistic equations of motion into an equivalent Newtonian form by means of a suitable change of variables (see Sec. IIC). Although the results of the Newtonian theory can then be taken over directly, the transformed quantities are usually not the ones which occur in practical applications, and besides, it is not always possible to apply this transformation also to the equation of state of the gas (cf. Sec. IVA). In the present paper we take an alternative approach, one which affords a greater insight into the nature of the relativistic results. Starting with the covariant equations of motion, we manipulate them in a manner analogous to the Newtonian derivation, with the aim of obtaining simple generalizations of the Newtonian results. In particular, we attempt to derive useful analytical expressions which can be applied to the solution of specific flow problems. We consider only special-relativistic flows, since the covariant expressions become much more complicated when space-time is not flat; however, all the results that we derive in the local rest-frame of a wave which propagates in the fluid (Secs. IVA and V) also remain valid in the presence of external gravitational fields.

The plan of this paper is as follows: Section II describes the basic equations and the assumptions which are used in the derivations. Section III deals with continuous irrotational flow. In Sec. IV we consider oblique plane shock waves and the problem of shock refraction at a gas interface. In Sec. V we derive the proper magnetosonic wave speeds. A summary of our results is given in Sec. VI.

II. BASIC EQUATIONS

A. Thermodynamic Relations and Conservation Laws[6, 12, 13]

In the following, thermodynamic quantities are measured in the local rest-frame of the fluid, densities are referred to a unit proper volume, and velocities are measured in units of the speed of light c.

The thermodynamic quantities which characterize a fluid are: the rest-mass density mn (where n is the number density of particles and m is the average rest-mass per particle), the pressure p, the internal energy density e, the absolute temperature T, and the entropy per particle $\mathcal{S}$. In general, only two of these quantities are independent. The total mass-energy density of the fluid, ρ, can be expressed as $\rho = mnc^2 + e$. The speed of sound relative to the fluid is $\beta_s = [(\partial p/\partial \rho)_{\mathcal{S}}]^{1/2}$, which is required to be < 1. The adiabatic index of the fluid is given by $\Gamma = (\partial \ln p/\partial \ln n)_{\mathcal{S}}$. We shall refer to the quantity $\hat{\Gamma} \equiv \gamma_s \Gamma$, where $\gamma_s = (1 - \beta_s^2)^{-1/2}$, as the generalized adiabatic index; clearly, $\hat{\Gamma}$ reduces to Γ in the non-relativistic limit ($\beta_s << 1$).

In a frame of reference where the fluid moves with 3-velocity $\underset{\sim}{\beta} = (\beta_x, \beta_y, \beta_z)$, the 4-velocity of the fluid is given by $u^\alpha = \gamma(1, \beta_x, \beta_y, \beta_z)$, where $\gamma = (1 - \beta^2)^{-1/2}$ is the Lorentz factor. [A Greek index stands for t, x, y, z.] In this frame, the Mach number of the flow is $M = \beta/\beta_s$. We also introduce the proper Mach number $\mathcal{M} \equiv u/u_s$, where $u = \gamma\beta$ is the proper speed of the fluid and $u_s = \gamma_s \beta_s$ is the proper speed of sound relative to the fluid. In the Newtonian limit (β_s and $\beta << 1$), $\mathcal{M}$ and M become equal and reduce to $M_N = \beta c/[(\partial p_N/\partial \rho_N)_{\mathcal{S}_N}]^{1/2}$, where ρ_N is the Newtonian mass density. [The subscript N denotes the Newtonian limit.]

The first law of thermodynamics can be written in the form

$$d\rho = \frac{\omega}{n}\, dn + nTd\mathcal{S}\,, \tag{1}$$

where $\omega = \rho + p$ is the enthalpy density. From this relation and the definitions of β_s and Γ it follows that $\beta_s = (\Gamma p/\omega)^{1/2}$.

The stress-energy tensor for an ideal fluid (no viscosity or heat conduction) is given by

$$T_{\alpha\beta} = \omega u_\alpha u_\beta + p g_{\alpha\beta}, \tag{2}$$

where $g_{\alpha\beta}$ is the metric tensor, whose non-zero components are $g_{tt} = -1$, $g_{xx} = g_{yy} = g_{zz} = 1$. The conservation laws for energy and momentum are given by the vanishing of the 4-divergence of the stress-energy tensor

$$(T_{\alpha}{}^{\beta})_{;\beta} = 0 \ , \tag{3}$$

where repeated indices imply summation and where the covariant derivative (semi-colon) reduces in rectangular coordinates to a partial derivative (comma). Similarly, the conservation law for the number of particles is given by

$$(nu^{\alpha})_{;\alpha} = 0 \ . \tag{4}$$

Specifically, for a steady ($\partial/\partial t = 0$) plane flow in the x direction, the continuity of the energy flux, the x-momentum flux, the y-momentum flux, and the particle flux is expressed by $T_{xt} = \text{const}$, $T_{xx} = \text{const}$, $T_{xy} = \text{const}$, and $nu_x = \text{const}$, respectively. Equations (1)-(4) imply

$$\Omega_{\alpha\beta} u^{\beta} = -T\delta_{,\alpha} \ , \tag{5}$$

where $\Omega_{\alpha\beta} = (\omega u_{\beta}/n)_{;\alpha} - (\omega u_{\alpha}/n)_{;\beta}$. A relativistic potential flow is an isentropic ($\delta = \text{const}$) flow for which $\Omega_{\alpha\beta} = 0$. A steady potential flow satisfies the relativistic Bernoulli's equation

$$\gamma\mu = \mu_o \ , \tag{6}$$

where $\mu = \omega/n$, and where the subscript o denotes the stagnation point ($\beta = o$). Such a flow is therefore irrotational in the Newtonian sense ($\underset{\sim}{\nabla} \times \underset{\sim}{\beta} = 0$).

B. Equation of State

At those stages of our calculation where the nature of the fluid has to be specified, we assume that it is a perfect gas, described by $p = knT$ (where k is Boltzmann's constant). In addition, we assume that the adiabatic index Γ is constant. [As was shown by Taub,[1] Γ must lie in the range $4/3 \leq \Gamma \leq 5/3$, which in turn implies that the speed of sound and the speeds of shock waves are less than the speed of light.] This is not in general true for a monatomic perfect gas, since Γ decreases with increasing

effective temperature $\tau = kT/mc^2$, most noticeably near $\tau \sim 1$.[14] However, this assumption holds in the non-relativistic limit, roughly $\tau < 10^{-2}$, where $\Gamma = 5/3$; in the extreme-relativistic limit, roughly $\tau > 10$, where the material gas is equivalent to a photon gas with $\Gamma = 4/3$; and for a mixture of two perfect gases, one with a non-relativistic and the other with an extreme-relativistic equation of state, which are in thermal equilibrium with each other (e.g., protons and electrons at $T \sim 10^{11}\ ^{o}K$). The adiabatic index for such a mixture, in which the number of non-relativistic particles is a fraction r of the total number of particles in the gas, is given by $\Gamma = (4 - 3/2\ r)/(3 - 3/2\ r)$, which lies in the same range as Γ for a one-component relativistic gas. [This relation does not apply when the number of particles is not conserved; e.g., when the mixture consists of material gas and black-body radiation, or when pairs are created.] For a perfect gas with Γ = const, $p = (\Gamma - 1)e$, and the enthalpy density can be expressed as

$$\omega = mnc^2 + \Gamma p/(\Gamma - 1). \tag{7}$$

C. Transformation of Variables

The relativistic conservation equations and thermodynamic relations for an ideal fluid in a steady flow can be transformed into an equivalent Newtonian form by substituting the following analogs of Newtonian variables (labeled by tildes):[10,11]

$$\begin{aligned}
\tilde{\beta} &= \alpha u && [\beta u] \quad , \\
\tilde{n} &= n/\alpha && [\omega/\beta^2] \quad , \\
\tilde{\mu} &= \tfrac{1}{2}\,\alpha\mu && [\tfrac{1}{2}\,\beta^2] \quad , \\
\tilde{T} &= \alpha T && [\beta T] \quad , \\
\tilde{p} &= p, \\
\tilde{s} &= s;
\end{aligned} \tag{8}$$

where $\alpha \equiv \mu/mc^2$, $\beta \equiv (p/p_o)^{(\Gamma - 1)/\Gamma}$, and where the expressions in square

brackets correspond to the exteme-relativistic limit ($\omega = \Gamma p/(\Gamma - 1)$). The transformation of other quantities can be deduced from these definitions; for example,

$$\tilde{e} = \tilde{\mu}\tilde{n} - \tilde{p} \quad ; \quad \tilde{M} = \tilde{\beta}/\tilde{\beta}_s = u/u_s \equiv \mathcal{M} \quad ; \quad \tilde{\Gamma} = \left(\frac{\partial \ell n \tilde{p}}{\partial \ell n \tilde{n}}\right)_{\tilde{s}} = \gamma_s^2 \Gamma \equiv \hat{\Gamma}.$$

III. STEADY POTENTIAL FLOW

A. Characteristics

The method of characteristics is applicable to the analysis of the flow whenever the equations of motion are quasi-linear partial differential equations of the hyperbolic type. In Newtonian gas dynamics this is the case for unsteady one-dimensional flow and for steady supersonic two-dimensional flow (cf. Sec. 96 and Sec. 109 in Ref. 12). The former case was first generalized to relativistic gas dynamics by Taub,[1] and the second case by Chiu,[11] who applied the transformation of variables (8) to the corresponding Newtonian expressions.

In order to derive the equation for the characteristics in a steady potential flow directly from the relativistic equations of motion (3), we first take their scalar product with the operator $P_{\alpha\beta} = g_{\alpha\beta} + u_\alpha u_\beta$, which projects them along a direction perpendicular to the 4-velocity u^α.[12,13] The three space components of the resulting equation are the relativistic Euler's equation which, for a steady flow, becomes

$$\gamma\omega\, \underset{\sim}{\beta} \cdot \underset{\sim}{\nabla}(\gamma\underset{\sim}{\beta}) = - \underset{\sim}{\nabla} p - \gamma^2 (\underset{\sim}{\beta} \cdot \underset{\sim}{\nabla} p)\, \underset{\sim}{\beta} \,. \tag{9}$$

Scalar-multiplying $\underset{\sim}{\beta}$ into Eq. (9), we get

$$\gamma\omega\, \underset{\sim}{\beta} \cdot [\underset{\sim}{\beta} \cdot \underset{\sim}{\nabla}(\gamma\underset{\sim}{\beta})] = - \gamma^2\, \underset{\sim}{\beta} \cdot \underset{\sim}{\nabla} p = - \gamma^2 \beta_s^2\, \underset{\sim}{\beta} \cdot \underset{\sim}{\nabla} \rho \,, \tag{10}$$

where the last step holds for an isentropic flow. We next take the scalar product of Eq. (3) with u^{α}. Since $u^{\alpha}u_{\alpha} = -1$, $u^{\alpha}u_{\alpha;\beta} = 0$, and we get, for a steady flow,

$$\gamma\underset{\sim}{\beta} \cdot \underset{\sim}{\nabla}\rho = -\omega \underset{\sim}{\nabla} \cdot (\gamma\underset{\sim}{\beta}) \, . \tag{11}$$

Equations (10) and (11) combine to give

$$\frac{1}{\beta_s^2} \underset{\sim}{\beta} \cdot [\underset{\sim}{\beta} \cdot \underset{\sim}{\nabla} (\gamma\underset{\sim}{\beta})] = \underset{\sim}{\nabla} \cdot (\gamma\underset{\sim}{\beta}) \, . \tag{12}$$

In addition, a steady potential flow is irrotational (see Sec. II A),

$$\underset{\sim}{\nabla} \times \underset{\sim}{\beta} = 0. \tag{13}$$

We now specialize Eqs. (12) and (13) to a two-dimensional flow (rectangular coordinates x-y):

$$(\mathcal{M}_x^2 - 1) \frac{\partial \beta_x}{\partial x} + \mathcal{M}_x \mathcal{M}_y \frac{\partial \beta_x}{\partial y} + \mathcal{M}_x \mathcal{M}_y \frac{\partial \beta_y}{\partial x} + (\mathcal{M}_y^2 - 1) \frac{\partial \beta_y}{\partial y} = 0, \tag{14a}$$

$$- \frac{\partial \beta_x}{\partial y} + \frac{\partial \beta_y}{\partial x} = 0. \tag{14b}$$

The equation for the x-y characteristics of this system of equations is

$$(\mathcal{M}_x^2 - 1) \left(\frac{dy}{dx}\right)^2 - 2\mathcal{M}_x \mathcal{M}_y \left(\frac{dy}{dx}\right) + (\mathcal{M}_y^2 - 1) = 0, \tag{15}$$

whose discriminant is given by $\Delta = 4(\mathcal{M}^2 - 1)$. When $\mathcal{M}$ is greater than 1, the system of equations (14) is of the hyperbolic type ($\Delta > 0$) and has two families of characteristics in the physical (x-y) plane, the C_+ and C_- characteristics, given by[11]

$$\left(\frac{dy}{dx}\right)_{C_\pm} = \frac{-\mathcal{M}_x \mathcal{M}_y \mp (\mathcal{M}^2 - 1)^{\frac{1}{2}}}{1 - \mathcal{M}_x^2} . \tag{16}$$

This fact has led Chiu[11] to identify $\mathcal{M}$ (which he obtained by means of the transformation of variables described in Sec. II C) as the appropriate Mach number for the flow.

The changes in β_x and β_y along the physical characteristics are related by the "compatibility relations,"[15] which determine the equation of the corresponding hodograph $(\beta_x - \beta_y)$-plane characteristics Γ_+ and Γ_-:

$$\left(\frac{d\beta_y}{d\beta_x}\right)_{\Gamma_\pm} = \frac{\mathcal{M}_x \mathcal{M}_y \pm (\mathcal{M}^2 - 1)^{\frac{1}{2}}}{1 - \mathcal{M}_y^2} . \tag{17}$$

Equation (17) does not involve the independent variables x and y, which means that the hodograph characteristics are fixed and do not depend on the initial conditions of a particular flow problem. This property is a consequence of the homogeneity of the system of equations (14), and does not hold for an axisymmetric (i.e., quasi-two-dimensional) flow. Introducing cylindrical coordinates (r, φ, z) and making the correspondence $r \leftrightarrow y$, $z \leftrightarrow x$, we find that Eq. (16) is still valid for an axisymmetric flow with $\beta_\varphi = 0$, but that an additional term, $-[\beta_r / r(1 - \mathcal{M}_r^2)](dr/d\beta_z)$, appears on the right-hand side of Eq. (17) in this case.

From Eqs. (16) and (17) we deduce the orthogonality relations between the C_+ and Γ_- and between the C_- and Γ_+ families of characteristics,

$$\left(\frac{dy}{dx}\right)_{C_\pm} \left(\frac{d\beta_y}{d\beta_x}\right)_{\Gamma_\mp} = -1. \tag{18}$$

If we adopt polar coordinates in the hodograph plane ($\beta_x = \beta \cos\Theta$, $\beta_y = \beta \sin\Theta$), and define the relativistic Mach angle ν by $\sin\nu \equiv 1/\mathcal{M}$, then Eq. (16) becomes

$$\left(\frac{dy}{dx}\right)_{C_\pm} = \tan(\Theta \pm \nu). \tag{19}$$

From this equation and the orthogonality relations (18) it follows that the normal to the Γ_- (Γ_+) characteristic lies at an angle $+\nu$ ($-\nu$) to the velocity vector $\underline{\beta}$.

B. Relativistic Mach Angle

We observe that the Newtonian counterparts of Eqs. (14)-(19)[12,15] can be obtained by simply replacing the proper Mach number $\mathcal{M} = u/u_s$ and the corresponding Mach angle $\nu = \sin^{-1}(1/\mathcal{M})$ by M_N and $\nu_N = \sin^{-1}(1/M_N)$, respectively. This suggests that the relativistic Mach angle ν also has the same physical meaning as ν_N in Newtonian gas dynamics, which we now verify. We assume that in the laboratory frame the fluid flows along the z axis with speed β which is greater than β_s, the speed of sound measured in the local rest-frame of the fluid. If in the fluid rest-frame the vector $\underset{\sim}{\beta}_s$ makes an angle Θ' with the $z' = z$ axis, then in the laboratory frame this angle is measured as Θ, with $\tan\Theta = \beta_s \sin\Theta'/[\gamma(\beta_s \cos\Theta' + \beta)]$. Setting $d\tan\Theta/d\Theta' = 0$, we find that Θ attains a maximum, ν, when $\cos\Theta' = -\beta_s/\beta$, and that $\sin\nu = 1/\mathcal{M}$. Thus ν, like ν_N in the Newtonian theory, is the generating angle of the cone within which disturbances can propagate downstream in a supersonic flow. The fact that this angle is based on the proper Mach number $\mathcal{M}$, rather than on the ordinary Mach number $M = \beta/\beta_s$, reinforces the interpretation of $\mathcal{M}$ as the relativistic generalization of the Newtonian Mach number M_N. Note, however, that the condition $\mathcal{M} > 1$ for a supersonic flow is equivalent to the condition $M > 1$.

C. Simple Waves

Equation (17), written in terms of polar coordinates, becomes

$$d\Theta\Big|_{\Gamma_\pm} = \pm \frac{d\beta}{\beta}\,(\mathcal{M}^2 - 1)^{\frac{1}{2}} \,. \tag{20}$$

Now, for a given equation of state, β_s can be expressed as a function of β by means of the relativistic Bernoulli's equation (6). Hence, Eq. (20) gives the relation between β and Θ along the hodograph characteristics.

This type of flow, in which the velocity is a function only of its direction, characterizes steady simple waves.

For the equation of state (7), β_s is given as a function of γ by

$$\beta_s(\gamma) = [(\Gamma - 1)(1 - (mc^2/\mu_o)\gamma)]^{\frac{1}{2}} . \tag{21}$$

In this case it is possible to integrate Eq. (20) in closed form only in the Newtonian ($\mu_o \approx mc^2$, $\beta << 1$; $\Gamma = 5/3$) and the extreme-relativistic ($\mu_o >> mc^2$; $\Gamma = 4/3$) limits, when Eq. (21) reduces to

$$\beta_s^2 = \begin{cases} \beta_{so}^2 - 1/3\ \beta^2 \\ 1/3 \end{cases} , \tag{22}$$

where β_{so} is the speed of sound at the stagnation point. Equation (20) can then be written in terms of the proper Mach number $\mathcal{M}$ in a form which is valid in both limits:

$$d\theta\Big|_{\Gamma_\pm} = \pm \frac{(\mathcal{M}^2 - 1)^{\frac{1}{2}}\, d\mathcal{M}}{\mathcal{M}(1 + \frac{1}{2}(\hat{\Gamma} - 1)\mathcal{M}^2)} \quad , \text{ where } \hat{\Gamma} \equiv \gamma_s^2 \Gamma = \begin{cases} 5/3 \\ 2 \end{cases} \tag{23}$$

(Newtonian and extreme-relativistic limits only).

The integral of Eq. (23) is[11]

$$J_\pm = \theta \mp \varepsilon(\mathcal{M}) , \quad \text{where}$$

$$\varepsilon(\mathcal{M}) = [(\hat{\Gamma} + 1)/(\hat{\Gamma} - 1)]^{\frac{1}{2}} \arctan \{[(\hat{\Gamma} - 1)/(\hat{\Gamma} + 1)](\mathcal{M}^2 - 1)\}^{\frac{1}{2}} - \arctan (\mathcal{M}^2 - 1)^{\frac{1}{2}} . \tag{24}$$

[This expression is valid only in the Newtonian and the extreme-relativistic limits. Outside these limits, $\varepsilon(\mathcal{M})$ provides a lower bound to the exact integral for a mixture of non-relativistic and extreme-relativistic gases described by Eq. (7).] J_+ and J_-, the Riemann invariants, remain constant along the $C_+(\Gamma_+)$ and $C_-(\Gamma_-)$ characteristics, respectively, and correspond to the value of θ at $\mathcal{M} = 1$ (they are not Lorentz scalars). The integral of Eq. (20) gives the shape of the hodograph characteristics; in the two limits given by Eq. (24)

they form a family of epicycloids occupying the space between the circles of radii $\beta = \beta_s^*$ and $\beta = [(\hat{\Gamma}+1)/(\hat{\Gamma}-1)]^{\frac{1}{2}}\beta_s^*$, where β_s^*, the speed at which $\beta = \beta_s$, is given by

$$\beta_s^* = \begin{cases} \sqrt{3}/2 \ \beta_{so} \\ 1/\sqrt{3} \end{cases} . \tag{25}$$

The hodograph characteristics are useful for studying such problems as the wave pattern formed in a supersonic flow along a curved wall, or the structure of a supersonic jet emerging from a duct into a region of different pressure.[15]

In analyzing steady simple waves, which may be either compression or rarefaction waves, one is usually interested in the deflection angle of the streamlines, δ, between the upstream and downstream regions of the wave, where the proper Mach numbers are $\mathcal{M}_1$ and $\mathcal{M}_2$, respectively. This angle is given, according to Eq. (24), by

$$\delta = \varepsilon(\mathcal{M}_2) - \varepsilon(\mathcal{M}_1) . \tag{26}$$

$\mathcal{M}_2$ can be expressed in terms of $\mathcal{M}_1$ and the pressure ratio $\xi = p_2/p_1$ across the wave by combining Eqs. (6) and (7) with the adiabatic relation $p \propto n^{\Gamma}$;

$$\mathcal{M}_2 = \left(\frac{1}{(\hat{\Gamma}-1)} \left\{ \left[(\hat{\Gamma}-1)\mathcal{M}_1^2 + 2 \right] \xi^{(1/\hat{\Gamma}-1)} - 2 \right\} \right)^{\frac{1}{2}} \tag{27}$$

(Newtonian and extreme-relativistic limits only).

It is often convenient to study such waves graphically by plotting the image of the corresponding Γ characteristic in the $\{\delta,\xi\}$ plane. This method is applied in Sec. IV B.

D. Relativistic Chaplygin's Equation

Chaplygin's equation is the equivalent second-order partial differential equation (with β and θ as the independent variables) for the system of equations (14). Since a steady potential flow is irrotational [Eq. (14b)], we can define a velocity potential $\varphi(x,y)$ such that $\underset{\sim}{\beta} = \nabla\varphi$, and then proceed, as in the Newtonian derivation (Ref. 12, Sec. 108), to define the function $\Phi(\beta,\theta)$, which satisfies $\varphi = -\Phi + \beta\, \partial\Phi/\partial\beta$. The procedure for obtaining the equation for Φ follows the Newtonian steps, except that the particle conservation equation (4) replaces the Newtonian continuity equation, so that (γn) is substituted for the Newtonian mass density ρ_N. The result is

$$\frac{d(\gamma n\beta)}{d\beta}\ \frac{\partial\Phi}{\partial\beta} + \frac{1}{\beta}\frac{\partial^2\Phi}{\partial\theta^2} + \gamma n\beta\,\frac{\partial^2\Phi}{\partial\beta^2} = 0\ ,$$

where (γn) is a function of β alone. In fact, by Eq. (1), $(dn/d\beta)_\delta = n/\omega\ (d\rho/d\beta)_\delta$ which, together with Euler's equation (10) along a streamline, implies

$$\left(\frac{d(\gamma n)}{d\beta}\right)_\delta = -\gamma^3\,\beta\, n/\gamma_s^2\,\beta_s^2\ , \tag{28}$$

in which β_s is again a given function of β [cf. Eq. (21)]. We thus obtain the relativistic Chaplygin's equation

$$\frac{\partial^2\Phi}{\partial\theta^2} + \frac{\beta^2}{1-\mathcal{M}^2}\,\frac{\partial^2\Phi}{\partial\beta^2} + \beta\,\frac{\partial\Phi}{\partial\beta} = 0, \tag{29}$$

which is identical to the Newtonian expression,[12] except that $\mathcal{M}$ replaces M_N.

E. Relativistic Euler-Tricomi Equation

In the region where $\mathcal{M} \sim 1$, Chaplygin's equation reduces to the Euler-Tricomi equation, which is useful for the study of transonic flow. We are interested in the form of $\beta^2/(1-\mathcal{M}^2)$, which appears in the second term of Eq. (29), near $\beta = \beta_s = \beta_s^*$. In this limit $\beta_s - \beta = (\beta_s^* - \beta)[1 - (d\beta_s/d\beta)_{\beta=\beta_s^*}]$. Now,

$$\left(\frac{d\beta_s}{d\beta}\right)_{\beta=\beta_s^*} = \left(\frac{d(\gamma n)}{d\beta}\right)_{\beta=\beta_s^*}\left(\frac{d\beta_s}{d(\gamma n)}\right)_{\beta=\beta_s^*} = -\left[\frac{\gamma n}{\beta}\left(\frac{d\beta_s}{d(\gamma n)}\right)\right]_{\beta=\beta_s^*},$$

where the last step follows from Eq. (28). Hence,

$$\beta_s - \beta = (\beta_s^* - \beta)\left(\frac{1}{\beta}\frac{d(\gamma n \beta_s)}{d(\gamma n)}\right)_{\beta=\beta_s^*} = (\alpha^*/\gamma_s^{*2})(\beta_s^* - \beta), \tag{30}$$

where $\gamma_s^* = (1 - \beta_s^{*2})^{-1/2}$ and $\alpha^* \equiv \left\{(\gamma^2/\beta)\,[d(\gamma n \beta_s)/d(\gamma n)]_{\mathcal{S}}\right\}_{\beta=\beta_s^*}$. [$\alpha^*$ generalizes the Newtonian parameter $\alpha_N^* = \left\{(1/\beta)[d(\beta_{s_N}\rho_N)/d\rho_N]_{\mathcal{S}_N}\right\}_{\beta=\beta_{s_N}^*}$, from which it may be obtained directly by means of the transformation of variables (8).] When β_s is given by Eq. (21), α^* becomes

$$\alpha^* = \gamma_s^{*2}\{1 - [\beta_s^{*2} - (\Gamma - 1)]\,\gamma_s^{*2}/2\}, \tag{31}$$

which has constant values, $(\hat{\Gamma}+1)/2 = 4/3$ and $3/2$, in the Newtonian and extreme-relativistic limits, respectively. Thus, using Eq. (30),

$$\frac{\beta^2}{1-\mathcal{M}^2} = \frac{\beta^2}{\gamma^2(1-M^2)} \approx \frac{\beta_s^{*2}}{2\gamma_s^{*2}(1-\beta/\beta_s)} \approx \frac{\beta_s^{*2}}{2\alpha^*(1-\beta/\beta_s^*)}.$$

The last term in Chaplygin's equation is small in comparison with the

second term when $\mathcal{M} \to 1$, and can be neglected. Finally, we replace β by a new variable $\eta \equiv (2\alpha^*)^{1/3} (\beta - \beta_s^*)/\beta_s^*$, which changes sign at $\mathcal{M} = 1$. Equation (29) then simplifies to

$$\frac{\partial^2 \Phi}{\partial \eta^2} - \eta \frac{\partial^2 \Phi}{\partial \theta^2} = 0, \tag{32}$$

which is just the Newtonian Euler-Tricomi equation.[12] The only difference between Newtonian and relativistic transonic flows is in the value of the constant α^*, which, in fact, contains the entire dependence of the flow on the properties of the gas.

IV. STEADY PLANE SHOCK WAVES

A. Oblique Shock Waves

Figure 1 describes the flow configuration in the local rest-frame of a shock front, idealized here as the plane x = 0. [The upstream and downstream regions of the front are denoted by 1 and 2, respectively.] We assume that the fluid is a perfect gas with a constant adiabatic index Γ, and that the following variables are initially known: the upstream proper Mach number $\mathcal{M}_1$, the upstream generalized adiabatic index $\hat{\Gamma}_1$, and the pressure ratio across the shock $\xi = p_2/p_1$. Our purpose is to express the other flow variables in terms of these initial values. At any given instant in the local rest-frame of the shock, the conservation equations (2)-(4) take the steady-state form

$$\omega_1 \gamma_1^2 \beta_{1x} = \omega_2 \gamma_2^2 \beta_{2x} \qquad \text{(energy)}, \tag{33a}$$

$$\omega_1 \gamma_1^2 \beta_{1x}^2 + p_1 = \omega_2 \gamma_2^2 \beta_{2x}^2 + p_2 \qquad \text{(x momentum)}, \tag{33b}$$

$$\omega_1 \gamma_1^2 \beta_{1x} \beta_{1y} = \omega_2 \gamma_2^2 \beta_{2x} \beta_{2y} \qquad \text{(y momentum)}, \tag{33c}$$

$$n_1\gamma_1\beta_{1x} = n_2\gamma_2\beta_{2x} \qquad \text{(particles)}. \tag{33d}$$

From Eqs. (33a) and (33c) it follows that, for any equation of state, $\beta_{1y} = \beta_{2y} \equiv \beta_y$, and hence that $\tan\psi_1 = \chi \tan\psi_2$, where $\chi \equiv \beta_{2x}/\beta_{1x}$. Specializing to the equation of state (7), we solve Eq. (33a) for p_2,

$$p_2 = \left(\frac{(\Gamma - 1)}{\Gamma}\right)\left(\frac{1}{\gamma_2^2\beta_{2x}}\right)(mn_1c^2\gamma_1^2\beta_{1x} - mn_2c^2\gamma_2^2\beta_{2x} + \frac{\Gamma}{\Gamma - 1}\gamma_1^2\beta_{1x}p_1),$$

which we substitute into Eq. (33b), together with $n_2 = (\gamma_1\beta_{1x}/\gamma_2\beta_{2x})\,n_1$ from Eq. (33d). Equation (33b) then becomes

$$\left(\frac{\Gamma}{(\Gamma - 1)}\right)u_{1x}^2(1 - \chi) - \frac{\gamma_1^2}{\gamma_2^2}\frac{1}{\chi} + 1 = \left(\frac{mn_1c^2}{\Gamma p_1}\right)\left[\Gamma u_{1x}^2\,(\chi - 1) + (\Gamma - 1)\left(\frac{\gamma_1^2}{\gamma_2^2} - \frac{\gamma_1}{\gamma_2}\right)\frac{1}{\chi}\right].$$

Now,

$$\gamma_1^2/\gamma_2^2 = 1 + u_{1x}^2(1 - \chi^2), \tag{34}$$

and $(mn_1c^2/\Gamma p_1) = (1/\beta_{s_1}^2) - 1/(\Gamma - 1)$. Hence, we obtain the following equation for χ in terms of the upstream variables

$$\begin{aligned}(u_{1x}^2/\beta_{s_1}^2)\chi^2 - (1 + \Gamma u_{1x}^2/\beta_{s_1}^2)\chi + \left[(\Gamma - 1)/\beta_{s_1}^2\right](1 + u_{1x}^2) - \\ - \left[(\Gamma - 1)/\beta_{s_1}^2 - 1\right]\left[1 + u_{1x}^2(1 - \chi^2)\right]^{\frac{1}{2}} = 0,\end{aligned} \tag{35}$$

where, for real shock waves, $u_{1x} > u_{s_1}$ and $\chi < 1$.[3] Equation (35) can be solved analytically in the following two cases:

(i) The second term in Eq. (34), $u_{1x}^2(1 - \chi^2)$, is $\ll 1$, so the square root in Eq. (35) can be expanded as $1 + \frac{1}{2}u_{1x}^2(1 - \chi^2)$. This condition is satisfied either when $1 - \chi^2 \ll 1$ (weak-shock limit) or when $u_{1x}^2 \ll 1$

(in which case $u_{s_1}^2$ must also be << 1).

(ii) The equation of state is extreme-relativistic [$\omega = \Gamma p/(\Gamma - 1)$]. In this case $\beta_s^2 = (\Gamma - 1)$ [Eq. (22)], and the last term in Eq. (35) vanishes. In both of these cases Eq. (35) reduces to a quadratic equation, whose non-trivial root is given by

$$\chi = \left[2 + (\hat{\Gamma}_1 - 1)\mathcal{M}_{1x}^2\right] \left[(\hat{\Gamma}_1 + 1)\mathcal{M}_{1x}^2\right]^{-1}. \tag{36}$$

[In all other cases, Eq. (36) provides an upper limit to the exact root of Eq. (35) when $\beta_{s_1}^2$ is given by Eq. (21).] By combining Eqs. (33), (34), and (36) we may now express every flow variable in terms of any three other variables. In particular, in terms of $\mathcal{M}_1$, $\hat{\Gamma}_1$, and ξ,

$$\cos^2\psi_1 = (\beta_{1x}/\beta_1)^2 = \left[(\hat{\Gamma}_1 + 1)/2\hat{\Gamma}_1\mathcal{M}_1^2\right]\left[\xi + (\hat{\Gamma}_1 - 1)/(\hat{\Gamma}_1 + 1)\right], \tag{37a}$$

$$\chi = \beta_{2x}/\beta_{1x} = \left[(\hat{\Gamma}_1 - 1)\xi + (\hat{\Gamma}_1 + 1)\right]\left[(\hat{\Gamma}_1 + 1)\xi + (\hat{\Gamma}_1 - 1)\right]^{-1}, \tag{37b}$$

$$\mathcal{M}_2^2 = u_2^2/u_{s_2}^2 = \left[2/(\hat{\Gamma}_1 - 1)\right]\left\{\left[(\hat{\Gamma}_1 + 1)/(\hat{\Gamma}_1 - 1) + 1/\xi\right]\left[(\hat{\Gamma}_1 + 1)/(\hat{\Gamma}_1 - 1) + \xi\right]^{-1}\left[1 + \tfrac{1}{2}(\hat{\Gamma}_1 - 1)\mathcal{M}_1^2\right] - 1\right\}, \tag{37c}$$

$$\tan\delta = \tan(\psi_2 - \psi_1) = \pm\left[(\xi - 1)/(1 + \hat{\Gamma}_1\mathcal{M}_1^2 - \xi)\right]\left\{\left[2\hat{\Gamma}\mathcal{M}_1^2/(\hat{\Gamma} + 1) - (\hat{\Gamma}_1 - 1)/(\hat{\Gamma}_1 + 1) - \xi\right]\left[(\hat{\Gamma}_1 - 1)/(\hat{\Gamma}_1 + 1) + \xi\right]^{-1}\right\}^{1/2}. \tag{37d}$$

[These expressions are valid only in the limits (i) and (ii).] The variable $\hat{\Gamma}_2 = \gamma_{s_2}^2\Gamma$ can be obtained from Eqs. (37) and the relation $\hat{\Gamma}_2/\hat{\Gamma}_1 = \chi\mathcal{M}_{1x}^2/\xi\mathcal{M}_{2x}^2$, which follows from Eq. (33a); it is equal to $\hat{\Gamma}_1$ in the Newtonian ($\hat{\Gamma} = 5/3$) and the extreme-relativistic ($\hat{\Gamma} = 2$) limits. Equations (36) and (37) have the

same form as the corresponding Newtonian expressions,[12,16] with $\mathcal{M}$ replacing M_N and $\hat{\Gamma}_1$ replacing Γ. These replacements are consistent with the transformation of variables described in Sec. IIC; however, Eqs. (36)-(37) cannot be derived by transforming the variables in the Newtonian conservation equations for a perfect gas, where $p_N/(\Gamma - 1)$ is substituted for e_N, because this substitution is not valid for the transformed quantities (except in the extreme-relativistic limit).

Equation (37d) describes the shock polar in the $\{\delta,\xi\}$ plane which, for given values of $\mathcal{M}_1$ and $\hat{\Gamma}_1$, is a "heart-shaped" curve (a strophoid). For a fixed value of $\mathcal{M}_1$, the maximum pressure ratio ξ_{max} (corresponding to $\delta = 0$) is larger and the maximum deflection angle $|\delta_{max}|$ is smaller in the extreme-relativistic limit than in the Newtonian limit (cf. Fig. 3). In fact, the upper limit on $|\delta_{max}|$, corresponding to $\mathcal{M}_1 = \infty$, is given by $\sin^{-1}(1/\hat{\Gamma}_1)$, which is 30° for $\hat{\Gamma}_1 = 2$ and 36.87° for $\hat{\Gamma}_1 = 5/3$. [Note that the value of the deflection angle varies according to the frame of reference in which it is measured; for example, in a frame in which the shock front moves along the x axis with Lorentz factor γ', this angle is given by $\tan \delta' = \gamma' \tan \delta$.]

B. Refraction of Shock Waves at a Gas Interface

As an application of our results, we now consider the refraction of a plane shock wave incident at an arbitrary angle on an interface between two gaseous media. The interface forms a tangential discontinuity, where the pressure and the normal component of the velocity are continuous, but where other variables may be discontinuous. In a regular refraction, the incident shock wave is reflected as either a shock wave or a centered rarefaction wave, and another shock wave is transmitted into the second medium. Figure 2 describes the stationary wave pattern seen in a frame which moves with the point of intersection O of the three waves (the wave frame). A physically realizable configuration satisfies

$$\delta_t = \delta_i + \delta_r \ , \tag{38a}$$

$$\xi_t = \xi_i \, \xi_r \ , \tag{38b}$$

$$\xi_i, \xi_t > 1 \ , \tag{38c}$$

$$\mathcal{M}_r > 1 \ , \tag{38d}$$

where the subscripts i, t, r refer to the incident, transmitted, and reflected waves, respectively. Equations (38a,b) are just the continuity conditions across the interface, Eq. (38c) expresses the fact that the incident and transmitted waves are shocks,[3] and Eq. (38d) is the requirement that the flow behind the incident shock be supersonic. The reflected wave is a shock or a rarefaction depending on whether ξ_r is greater than or less than unity. The possible wave patterns can be analyzed in the $\{\delta,\xi\}$ plane (Fig. 3) for given values of $\mathcal{M}_i$, $\hat{\Gamma}_i$, $\mathcal{M}_t$, $\hat{\Gamma}_t$, and ξ_i.[16, 17] One first plots the shock polars I and II, corresponding to the incident and transmitted shocks, respectively. Then, starting at the point ξ_i on polar I, one constructs the polar III, corresponding to a reflected shock, and if this point lies inside polar II, also the image of a hodograph characteristic Γ corresponding to a reflected rarefaction wave. The intersection points of the curves III and Γ with polar II represent the realizable configurations for the given initial conditions.

In the case of shock refraction at the interface between an extreme-relativistic and a non-relativistic medium, it is possible to carry out the analysis using the explicit expressions derived in Sec. IIIC and Sec. IVA. As an illustration, we consider the refraction of a shock wave incident in the extreme-relativistic medium when $\mathcal{M}_i = \mathcal{M}_t$ (i.e., when the wave-frame proper Mach number is the same for the incident and the transmitted shocks), and when $\mathcal{M}$ reduces to M_N in the non-relativistic medium.

From the polar diagram in Fig. 3 it follows that this problem may have as many as three distinct solutions: two in which the reflected wave is a shock, and one in which it is a rarefaction. Which of these solutions is realized in practice is determined by the boundary conditions; for example, in the absence of strong disturbances downstream from the refraction site, the relevant solution is probably the one with the smallest value of ξ_r, i.e., the reflected-rarefaction-wave solution.[17] The wave patterns corresponding to different initial conditions can be found in a similar manner.

An interesting situation occurs when the two media are extreme-relativistic ($\hat{\Gamma}_i = \hat{\Gamma}_t = 2$) and at rest with respect to each other. In contrast to the analogous Newtonian situation, the shock polars in this case coincide, even though the two gases may have different particle number densities and therefore be separated by a tangential discontinuity. This situation arises because the fluid equations of motion in the extreme-relativistic limit are independent of n. The problem of shock refraction thus reduces to that of the splitting of a shock wave,[16, 18] and so the reflected wave can only be a shock (cf. Sec. 102 in Ref. 12).

V. HYDROMAGNETIC WAVE SPEEDS

In the previous sections we saw that $\mathcal{M} = u/u_s$ plays the same role in relativistic gas dynamics as $M_N = \beta/\beta_{s_N}$ in the Newtonian theory. In this section we further illustrate the analogy between β_{s_N} and u_s by considering the propagation speeds of magnetosonic waves (the small-amplitude limit of hydromagnetic shock waves) in a compressible, non-viscous, and perfectly conducting relativistic plasma. These speeds were derived by various authors, and are reviewed, e.g., in Ref. 19. Here, we give a direct generalization of the method used by de Hoffmann and Teller,[20]

who were the first to derive these speeds in the Newtonian case. Figure 4 shows the velocity and magnetic field configurations for a hydromagnetic shock wave, in the local rest-frame of the shock front. [The upstream and downstream regions are again denoted by 1 and 2, respectively.] In the derivation of de Hoffmann and Teller, the velocity was parallel to the magnetic field on both sides of the shock, so that no electric fields appeared in the shock frame. However, a transformation to such a frame is not always possible in the relativistic case, since it may involve velocities greater than c.[21] An electric field is thus present on either side of the shock, and is given by the perfect-conductivity condition

$$E_z = \beta_y B_x - \beta_x B_y, \tag{39}$$

where all quantities are measured in the shock frame. Maxwell's equations $\underset{\sim}{\nabla} \times \underset{\sim}{E} = 0$ and $\underset{\sim}{\nabla} \cdot \underset{\sim}{B} = 0$ imply that E_z and B_x are continuous at the shock front. In addition, Eqs. (4) and (3) imply that (nu_x) as well as T_{xt}, T_{xx}, and T_{xy} are continuous there, where now $T_{\alpha\beta} = T^{M}_{\alpha\beta} + T^{E.M.}_{\alpha\beta}$,[13] with $T^{M}_{\alpha\beta}$ given by Eq. (2) and with

$$\begin{aligned} T^{E.M.}_{xt} &= \left(\frac{1}{4\pi}\right) E_z B_y \ , \\ T^{E.M.}_{xx} &= \left(\frac{1}{4\pi}\right)\left[- B_x^{\,2} + \tfrac{1}{2}\,(B_x^{\,2} + B_y^{\,2}) + \tfrac{1}{2}\, E_z^{\,2}\right] , \\ T^{E.M.}_{xy} &= - \left(\frac{1}{4\pi}\right) B_x B_y \ . \end{aligned} \tag{40}$$

In the limit when the shock reduces to a magnetosonic wave, the continuity conditions can be expressed as derivatives with respect to a single parameter (e.g., u_x), which are evaluated at the upstream side of the wave front.[20] Specifically:

$$\left(\frac{dE_z}{du_x}\right)_1 = \left(B_x \frac{d\beta_y}{du_x} - B_y \frac{d\beta_x}{du_x} - \beta_x \frac{dB_y}{du_x}\right)_1 = 0 \quad , \tag{41a}$$

$$\left(\frac{dT_{xy}}{du_x}\right)_1 = \left[\beta_y \frac{d(\omega\gamma u_x)}{du_x} + \omega\gamma u_x \frac{d\beta_y}{du_x} - \left(\frac{B_x}{4\pi}\right)\frac{dB_y}{du_x}\right]_1 = 0 \quad , \tag{41b}$$

$$\left(\frac{dT_{xt}}{du_x}\right)_1 = \left[-\frac{d}{du_x}(\omega\gamma u_x) + \left(\frac{E_z}{4\pi}\right)\frac{dB_y}{du_x}\right]_1 = 0 \quad , \tag{41c}$$

$$\left(\frac{dT_{xx}}{du_x}\right)_1 = \left[\frac{d}{du_x}(\omega u_x^2 + p + B_y^2/8\pi)\right]_1 = 0. \tag{41d}$$

Equations (41a-b) imply

$$\left(\frac{d(B_y^2/8\pi)}{du_x}\right)_1 = \frac{(B_{1y}'^2/4\pi)u_1}{B_x'^2/4\pi - u_1^2} \quad , \tag{42}$$

where $B_x' = B_x$ and $B_{1y}' = B_{1y}/\gamma$ are the fields measured in the local rest-frame of the upstream fluid. Furthermore, across a sound wave $dS = 0$, and so Eq. (1) becomes $d\rho = (\omega/n)dn$ which, together with $d(nu_x) = 0$, gives

$$\frac{d}{du_x} = -\frac{\omega}{u_x}\frac{d}{d\rho} \quad . \tag{43}$$

Using Eqs. (39), (41c), (42), and (43) in Eq. (41d), and substituting β_s^2 for $(dp/d\rho)$, we obtain a quadratic equation for u^2,

$$u^4 - [u_s^2 + (\gamma_s^2 B_y'^2 + B_x'^2)/4\pi\omega]u^2 + u_s^2 B_x'^2/4\pi\omega = 0 \quad , \tag{44}$$

where all the quantities are evaluated upstream. [This equation can also be derived by using the transformation of variables (8); see Ref. 19.] The roots of this equation represent the proper speeds of propagation (in the x direction) of the fast (+) and slow (-) magnetosonic waves.

They are given by

$$u_{\pm} = \tfrac{1}{2}\left[u_s^2 + (\gamma_s^2 B_y'^2 + B_x'^2)/4\pi\omega \pm \{[u_s^2 + (\gamma_s^2 B_y'^2 + B_x'^2)/4\pi\omega]^2 - 4(B_x'^2/4\pi\omega)u_s^2\}^{\frac{1}{2}}\right], \tag{45}$$

which closely resemble the analogous Newtonian expressions,[20] to which they of course reduce in the limit $\tau, B'^2/4\pi mnc^2 \ll 1$. When $B_y' \to 0$, u_- reduces to $B_x'/(4\pi\omega)^{1/2}$, the proper phase velocity (in the x direction) of an Alfvén wave,[19] which has the same form as the corresponding Newtonian velocity $B_x'/(4\pi\rho_N c^2)^{1/2}$. This formal similarity with the Newtonian results, which is much less pronounced in the expressions for the ordinary (coordinate) speeds, is another example of the analogy between Newtonian sound speeds and the corresponding relativistic proper speeds.

VI. SUMMARY

We have investigated various aspects of steady two-dimensional flow in relativistic gas dynamics. We found that it is possible to carry out a step-by-step generalization of the Newtonian derivation, and that the resulting expressions often reduce to the Newtonian form when written in terms of proper quantities (i.e., quantities which are measured in the local rest-frame of the fluid). In particular, $\mathcal{M} = u/u_s$ plays the role of Mach number in these expressions, and we verified that it has the same properties as $M_N = \beta/\beta_{s_N}$ in the Newtonian theory; we also showed that the analogy between β_{s_N} and u_s extends to the expressions for hydromagnetic

wave speeds. We found that the equations which describe general continuous flow can always be cast in the Newtonian form, but that expressions pertaining to a particular equation of state can be generalized only in certain limits and when the equation of state has a simple form. In our examples we considered a perfect gas with constant adiabatic index. We discovered that the Newtonian results for this equation of state can always be generalized in the extreme-relativistic limit and, in the case of oblique plane shock waves, also in certain other limits, where, in particular, the method of transformation of variables (Sec. IIC) is not applicable. These expressions, too, can be written in the Newtonian form, with $\hat{\Gamma} \equiv \gamma_s^2 \Gamma$ generalizing the adiabatic index in the corresponding Newtonian results; it is then possible to study specific flow problems using the methods of Newtonian gas dynamics. Although in most cases these expressions are exact only in the Newtonian and the extreme-relativistic limits, they are nevertheless useful for interpolating between these two limits.

ACKNOWLEDGMENTS

I thank Roger Blandford for valuable suggestions and encouragement. This work was supported in part by the National Science Foundation [AST78-05484, AST76-80801].

REFERENCES

1. A.H. Taub, Phys. Rev. 74, 328 (1948).
2. M.H. Johnson and C.F. McKee, Phys. Rev. D3, 858 (1971).
3. K.S. Thorne, Astrophys. J. 179, 897 (1973).
4. R.D. Blandford and C.F. McKee, Phys. Fluids 19, 1130 (1976).
5. E.P.T. Liang, Astrophys. J. 211, 361 (1977).
6. A.H. Taub, in Annual Reviews of Fluid Mechanics (Annual Reviews, Palo Alto, California, 1978), Vol. 10, p. 301.
7. M.H. Cohen, K.I. Kellermann, D.B. Shaffer, R.P. Linfield, A.T. Moffet, J.D. Romney, G.A. Seielstad, I.I.K. Paulin-Toth, E. Preuss, A. Witzel, R.T. Schilizzi and B.J. Geldzahler, Nature 268, 405 (1977).
8. B.J.T. Jones, Rev. Mod. Phys. 48, 107 (1976).
9. A.S. Goldhaber and H.H. Heckmann, Ann. Rev. Nucl. Part. Sci. 28, 161 (1978).
10. I.S. Shikin, Dokl. Akad. Nauk SSSR 142, 296 (1962) [Sov. Phys.-Dokl. 7, 13 (1962)].
11. H.H. Chiu, Phys. Fluids 16, 825 (1973).
12. L.D. Landau and E.M. Lifshitz, Fluid Mechanics (Pergamon, Oxford, 1958), Chaps. IX, XI, XII, and XV.
13. C.W. Misner, K.S. Thorne, and J.A. Wheeler, Gravitation (Freeman, San Francisco, 1973), Chap. 22.
14. J.L. Synge, The Relativistic Gas (North Holland, Amsterdam, 1957), Chap. VI.
15. J.A. Owczarek, Fundamentals of Gas Dynamics (International Textbook Co., Scranton, 1964), Chap. 9.
16. R. Courant and K.O. Friedrichs, Supersonic Flow and Shock Waves (Interscience, New York, 1948), Chap. IV.
17. L.F. Henderson, J. Fluid Mech. 26, 607 (1966).
18. L.F. Henderson, Aero. Quart. 15, 181 (1964).

19. I.S. Shikin, Annals de l'Institute Henri Poincaré A11, 343 (1969).

20. F. de Hoffmann and E. Teller, Phys. Rev. 80, 692 (1950).

21. P.D. Hudson, Mon. Not. R. Astron. Soc. 131, 23 (1965).

FIGURE CAPTIONS

Fig. 1. The flow configuration in the local rest-frame of a shock front.

Fig. 2. Regular refraction pattern of a shock wave at the interface AOB between two gaseous media, as seen in a frame in which the point O is stationary. The incident shock, the transmitted shock, and the reflected wave, which can be either a shock or a centered rarefaction wave, are denoted by i, t, and r, respectively. The direction of the flow is indicated by arrows.

Fig. 3. Graphical solution in the $\{\delta,\xi\}$ plane for the regular refraction patterns of a shock wave incident in an extreme-relativistic gas on a boundary with a non-relativistic gas. The extreme-relativistic and non-relativistic media are represented by continuous and dashed lines, respectively. The polars I, II, and III correspond to the incident, transmitted, and reflected shocks, respectively, and Γ denotes the image of a hodograph characteristic. In this example $\mathcal{M}_i^2 = M_{Nt}^2 = 10$ and $\xi_i = 5$. The solutions are indicated by asterisks.

Fig. 4. The flow and magnetic field configurations in the local rest-frame of a hydromagnetic shock front.

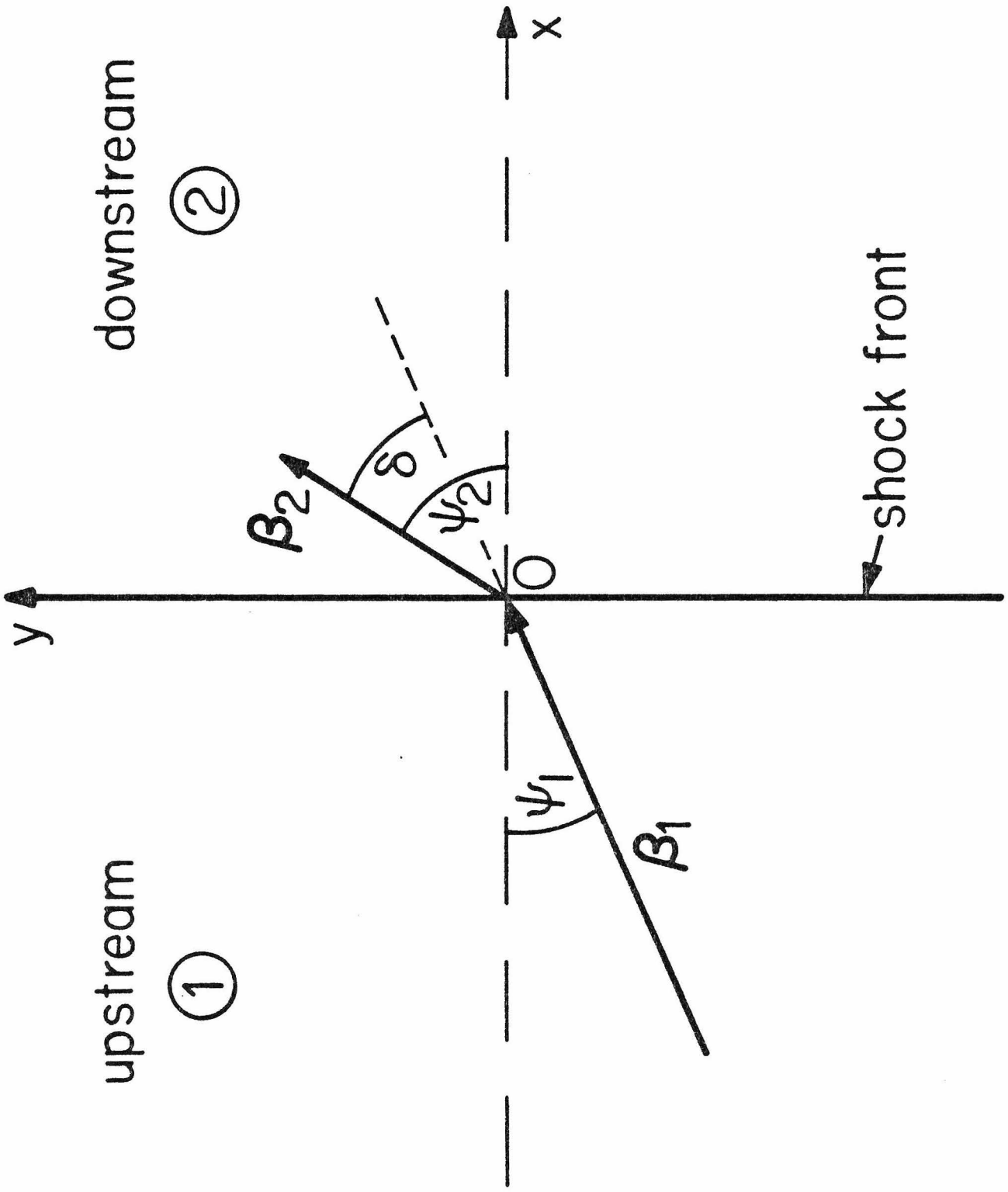
upstream
①
downstream
②
x
y
O
shock front
β_1
β_2
ψ_1
ψ_2
δ

Fig. 1

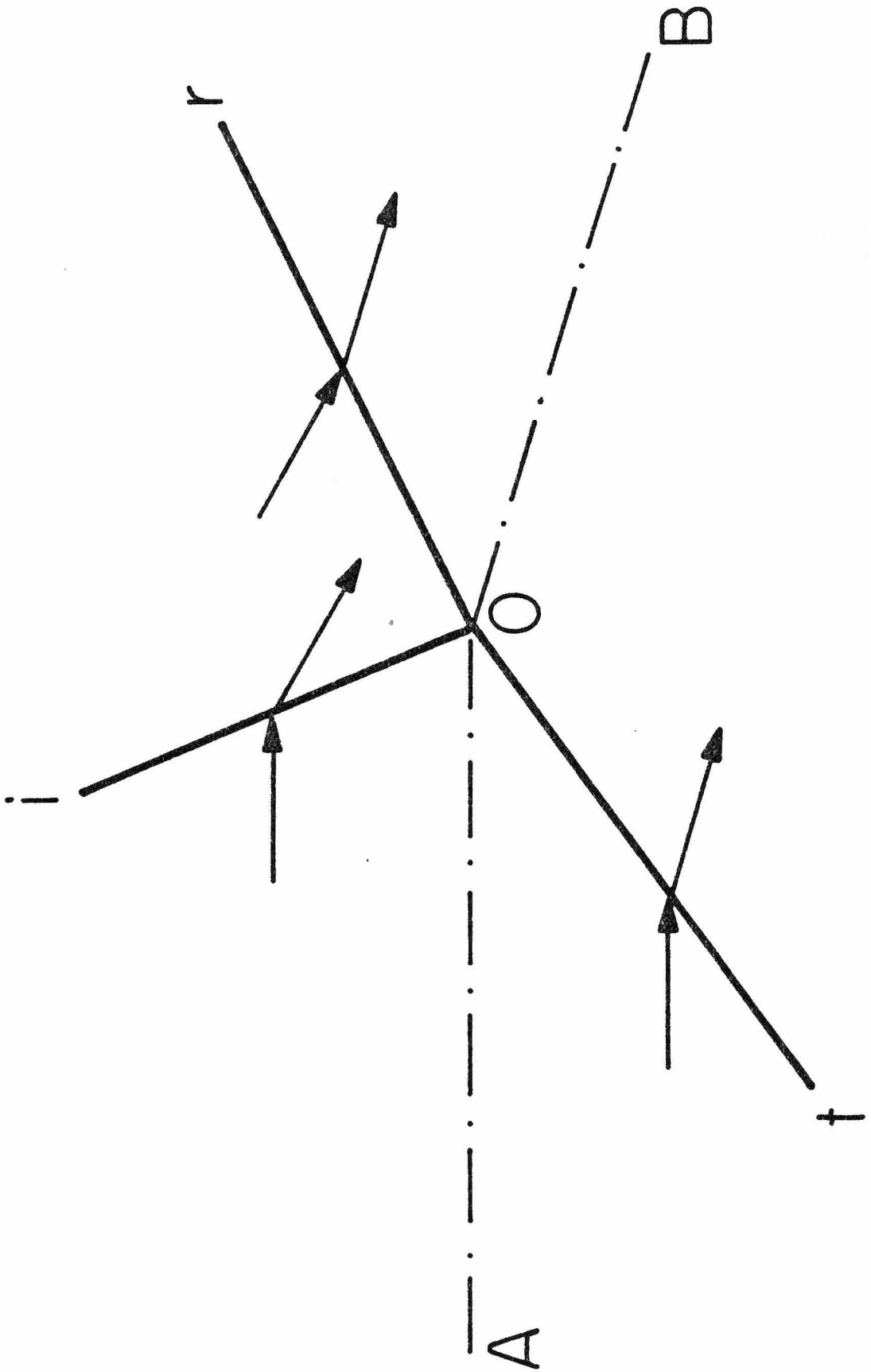

Fig. 2

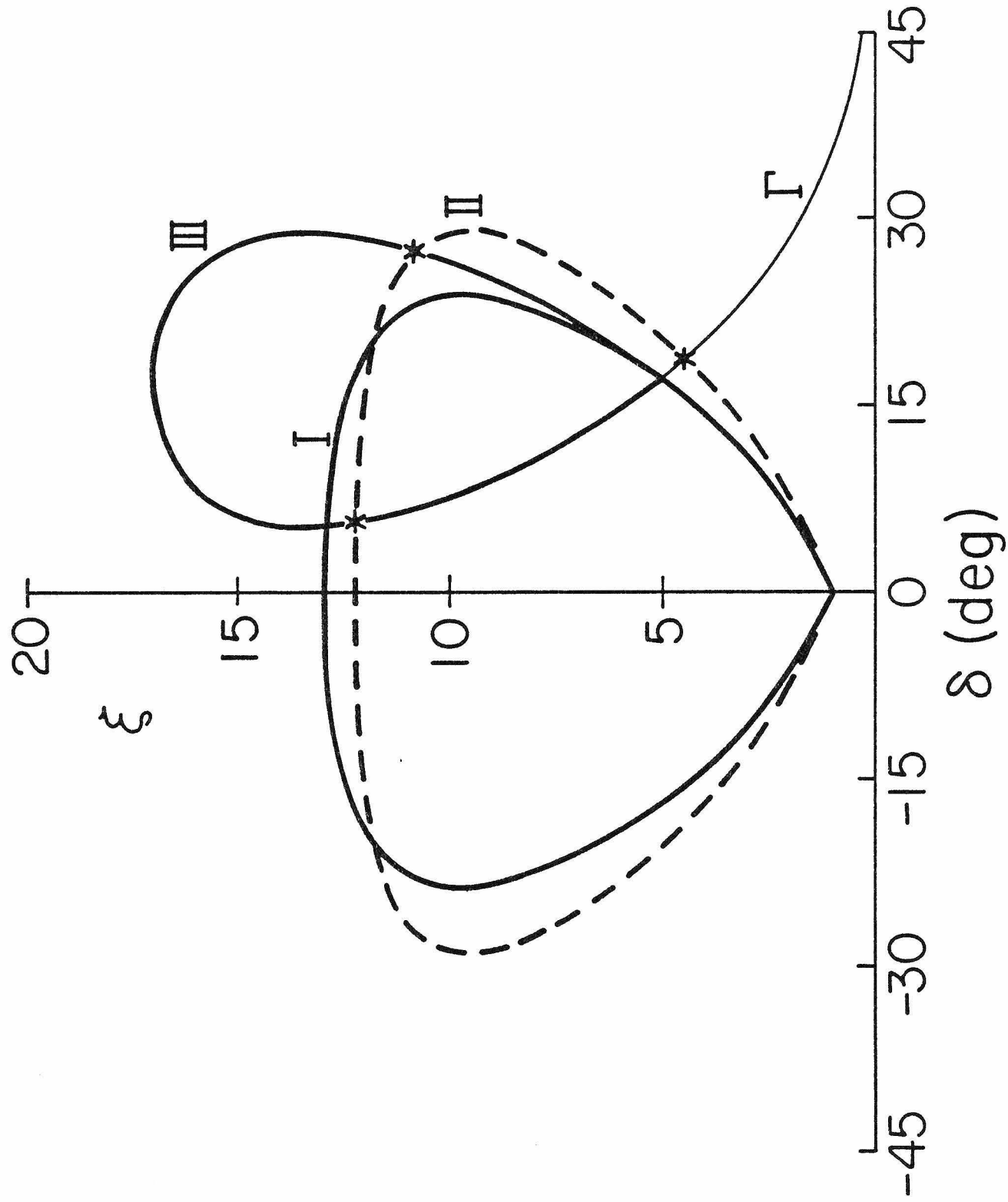

Fig. 3

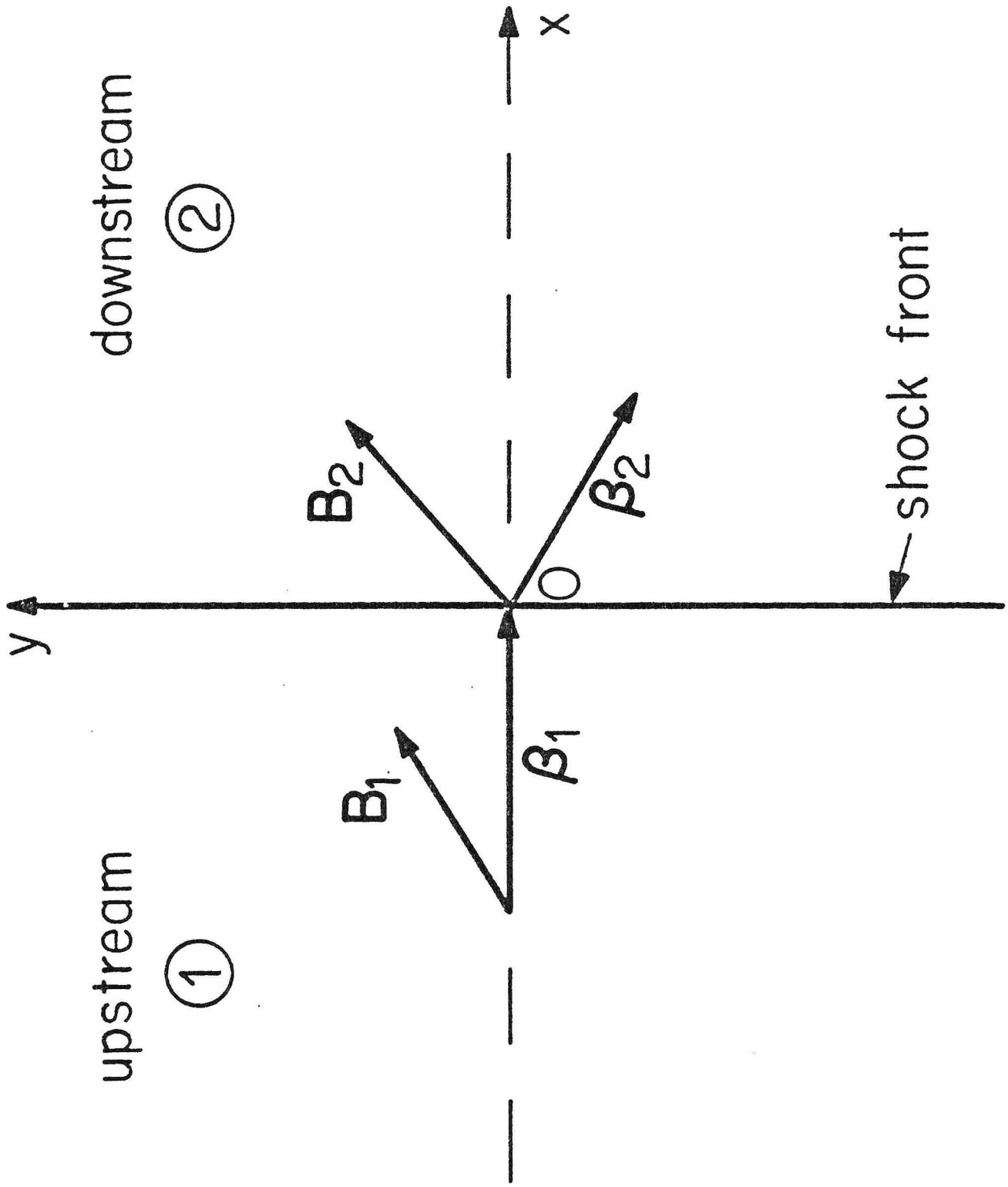

Fig. 4